J Mater Sci (2020) 55:13490–13542

Review

Roll-to-roll printing of polymer and perovskite solar cells: compatible materials and processes

Abhay Gusain[1,*], Aparna Thankappan[2], and Sabu Thomas[2]

[1] *Instituto de Física de São Carlos, Universidade de São Paulo, CP 369, São Carlos, SP 13566-590, Brazil*
[2] *Mahatma Gandhi University, Kottayam, Kerala 686 560, India*

Received: 27 February 2020
Accepted: 27 May 2020
Published online: 25 June 2020

ABSTRACT

The exploration and harnessing of the renewable sources of energy, in addition to that of the conventional sources, has become significantly prominent with the increasing global energy demands for the continuous production of the energy for world consumption. Among these sources, for different applications, the approach of harnessing of the solar energy using the solar cells based on organic materials has already been envisaged as an alternative to that of using the solar cells based on silicon, with much of focus on the polymer based solar cells, and more recently perovskite solar cells. Such applications require the unique property of flexibility of the solar cells based on solution processable active materials. In addition, as the required area of the solar cells for these applications can be very large, the upscaling of the manufacturing rate and the size of these solar cells requires the manufacturing of these solar cells with faster techniques of roll-to-roll printing, which allow the faster and massive commercial scale for production. This review gives a detailed account of the recent progress and the development of the roll-to-roll printing technology for the polymer and perovskite solar cells, including the roll-to-roll-compatible materials and processes, over few years.

Address correspondence to E-mail: agusain@usp.br

https://doi.org/10.1007/s10853-020-04883-1

GRAPHIC ABSTRACT

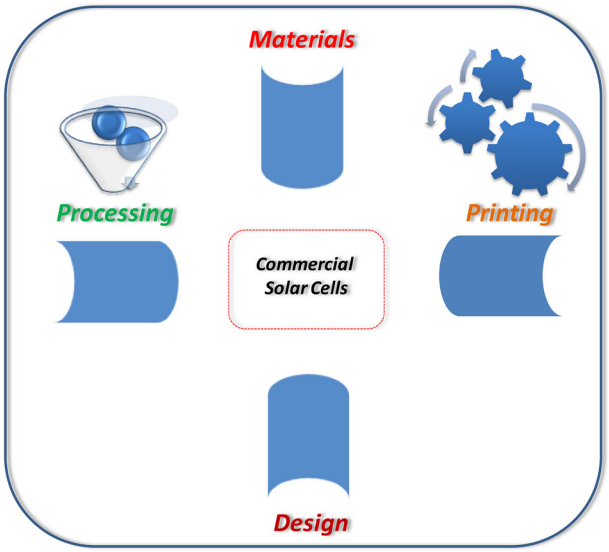

Abbreviations

P1	Poly[4,8-bis(2-ethylhexyloxy)benzo(1,2-b:4,5-b′)dithiophene-alt-5,6-bis(octyloxy)-4,7-di(thiophen-2-yl)(2,1,3-benzothiadiazole)-5,50-diyl]
P2	Poly[(4,40-bis(2-ethylhexyl)dithieno[3,2-b:20,30-d]silole)-2,6-diyl-alt-(2,1,3-benzothiadiazole)-4,7-diyl]
P3	Poly[2,3-bis-(3-octyloxyphenyl)quinoxaline-5,8-diyl-alt-thiophene-2,5-diyl]
P3HT	(Poly(3-hexyl)thiophene)
PCDTBT	Poly[N-9′-heptadecanyl-2,7-carbazole-alt-5,5-(4′,7′-di-2-thienyl-2′,1′,3′-benzothiadiazole)]
$PC_{61}BM$	([6,6]-Phenyl C_{61} butyric methyl ester)
PII2T-PS	Polyisoindigobithiophene-polystyrene
PPDIT	Perylene diimide
PDTSTTz	Poly[(4,4′-bis(2-ethylhexyl)dithieno[3,2-b:2′,3′-d]silole)-5,5′-(3,6-bis[4-(2-ethylhexyl)thienyl-2-yl]-stetrazine)
CH_3NH_3I	Methylammonium iodide
$CH_3NH_3PbI_3$	Methylammonium lead halide
PTB7-Th	Poly[4,8-bis(5-(2-ethylhexyl)thiophen-2-yl)benzo[1,2-b:4,5-b′]dithiophene-co-3-fluorothieno[3,4-b]thiophene-2-carboxylate]
$MAPbI_3$	Methylammonium lead iodide
F4TCNQ	2,3,5,6-Tetrafluoro-7,7,8,8-tetracyanoquinodimethane
PEN	Polyethylene naphthalate
SDS	Sodium dodecyl sulphate
ITO	Indium tin oxide
PEDOT:PSS	Poly(3,4-ethylenedioxythiophene):polystyrene sulfonate
ZnO	Zinc oxide
BHJ	Bulk heterojunction
V_2O_5	Vanadium pentoxide
BPE	*o*-xylene/benzyl phenyl ether
HTL	Hole transport layer
ETL	Electron transport layer
R2R	Roll-to-roll
PCEs	Power conversion efficiencies
PDMS	Poly(dimethylsiloxane)
SiO_2	Silicon dioxide
FTEs	Flexible transparent electrodes
MAI	Methylammonium iodide

LBIC	Light beam-induced current
BDT	Benzo[1,2-b:4,5-b′]dithiophene
IDT	Indacenodithiophene
FTQ	Mono-fluorodithienobenzoquinoxaline
DTS	Dithieno[3,2-b:2′,3′-d]silole
TTz	Dithienylthiazolo[5,4-d]thiazole
BDT-TT	Benzodithiophene-co-thieno[3,4-b]thiophene
DIO	1,8-Diiodooctane
DMSO	Dimethylsulfoxide
PNDIT	Naphthalene diimide
PPDIT	Perylene diimide
PEI	Polyethyleneimine
PBTI3T	[*N*-(2-hexyldodecyl)-2,2-bithiophene-3,3-dicarboximide-alt-5,5-(2,5-bis(3-decylthiophen-2-yl)-thiophene)]
P3MHOCT	Poly-(3-(2-methylhexan-2-yl)-oxy-carbonyldithiophene)

Introduction

The polymer solar cells have become an attractive alternative to the silicon-based solar cells, with more focused and continuous research since last decade toward significant improvements in their reported efficiencies [1–22]. Such improvements have only become possible with—the continuous research on new types of materials which include the low-bandgap polymers, fullerene derivatives and non-fullerene small molecule acceptors, research toward improvements in the different properties of the current materials like the solubility and bandgap of the fullerenes, improvements in the device architecture, application of new buffer layers in the conventional architecture and application of novel approaches like thermal and solvent annealing among others [12–26]. Apart from the efficiency, the research on other aspects of the device performance like the stability and degradation of the polymer solar cells during the period of their operation has also been well undertaken [20–30]. The recent research on these devices is also focused toward large-scale manufacturing of the flexible solar cells using roll-to-roll printing techniques. In addition to the polymer-based solar cells, the roll-to-roll printing technology has been employed for the perovskite solar cells, and the studies on the manufacturing of the stable perovskite solar cells through roll-to-roll coating as well as scalable organic–inorganic hybrid perovskite solar cells have also been explored [31, 52, 153–165]. These studies are discussed in various sections of this review. Although the perovskite-based solar cells have recently emerged as effective extensions to the polymer-based solar cells, there are many challenges to address in the area of these solar cells.

The various developments achieved in this research area are ultimately required to be transformed into fully fledged commercial level technology for different applications. Not only this, this commercial technology is required to be achieved on a massive scale so that the technology should be available for global level consumption around the world. Such transformation of research in this area to a commercial level technology brings the technology of roll-to-roll printing into picture and ultimately makes it an important element of this transformation. The technology of the roll-to-roll printing simply consists of the manufacturing techniques which involve continuous and faster material processing on a flexible substrate as it is transferred between moving rolls of material. It involves the application of various solution processable materials and constituent printing techniques in order to scale up the production of the solar cells at a much faster pace. The advantages of the roll-to-roll solution-processed polymer solar cells have already been well demonstrated in terms of volume, robustness and reproducibility [32]. It has been shown that even a simple laboratory roll-to-roll machine can enable the robust manufacture of large area of foil with solar cell modules over a short duration [32]. This ultra-high-speed manufacture of large-area modules of solar cells with very little energy and materials clearly demonstrates the edge this technology may offer over all other known energy technologies. In addition, at the full scale commercial application of these solar cells, some of the important requirements, apart from flexibility, to be fulfilled by these solar cells are low environmental impact and low cost.

The roll-to-roll technology has been envisaged as the means to fulfill the large-scale commercialization, and this technology in its current state is preceded by rigorous efforts made in developing, optimizing and upscaling the laboratory-scale techniques. Some of these laboratory-scale techniques include the deposition of several thin layers of the active materials on the flexible substrates, the development of roll-to-roll printing compatible materials as well as other aspects

of upscaling the manufacturing of the solar cells. Earlier attempts have already shown the manufacturing of the small area solar cells with area varying from few mm^2 to around 1 cm^2 and with efficiencies reaching up to 8–9% [33, 34]. Despite this, the challenge for the large-area production of the flexible solar cells using a high-throughput process still remains to be addressed more effectively. The large-scale production of the flexible solar cells simply differs from the laboratory-scale fabrication which uses the common fabrication steps of the spin coating and high vacuum thermal evaporation. These fabrication steps are incompatible with the high-throughput process, and therefore are replaced by the faster and advanced techniques of the roll-to-roll printing technology. However, translation from laboratory-scale solution processing deposition techniques to large-scale roll-to-roll methods has typically led to reduced photovoltaic performance.

Table 1 gives a detailed account of the some of the several types of active materials used, compatible architectures and parameters like bandgap and efficiency that have been achieved by various groups with the roll-to-roll-compatible/printing technology. The table clearly depicts the improvements in these parameters with different types of the materials used as well as the differences in the roll-to-roll-compatible/printing technology over the course of their history of recent developments in this technology.

However, the compatibility of the various materials, architectures and the fabrication techniques, as reported in these studies, may ideally indicate the reproducibility of the performance of the flexible solar cells manufactured through roll-to-roll printing using the same materials. This reported compatibility of these materials is important factor in case of the roll-to-roll printing of the solar cells, as many earlier reported materials with high performance at the laboratory scale have not been shown to be compatible with the roll-to-roll printing technology [68]. Nonetheless, the technology is still improving in its current stage of development and rigorous efforts made in this research area have shown a tremendous potential of the developed techniques in order to boost up this technology further.

Table 1 Summary of recently reported parameters of the roll-to-roll-compatible/printed devices

S. no.	Donor polymer/acceptor material or active material	Deposition/printing technique for donor polymer/acceptor material or active material	Bandgap of donor polymer (eV)	Efficiency (%)	Year	References
1.	P3HT:$PC_{61}BM$	Slot-die coating	2.1	0.3	2009	[35]
2.	P3HT:$PC_{61}BM$	Gravure printing	2.1	2.8	2010	[36]
3.	P1:$PC_{61}BM$, P2:$PC_{61}BM$ P3:$PC_{61}BM$	Slot-die coating	1.8, 1.5, 1.8	0.07, 0.55, 0.15	2011	[37]
4.	P3HT:$PC_{60}BM$	Slot-die coating/spin coating	2.1	0.5	2011	[38]
5.	P3HT:$PC_{61}BM$	Gravure printing	2.1	1.92	2011	[39]
6.	P3HT:$PC_{61}BM$	Slot-die coating	2.1	1.5	2013	[40]
7.	P3HT:$PC_{61}BM$	Slot-die coating	2.1	1.33	2013	[41]
8.	P3HT:$PC_{61}BM$	Spin coating	2.1	1.96	2013	[42]
9.	P3HT:$PC_{61}BM$	Gravure printing	2.1	1.0	2013	[43]
10.	PDTSTTz-4:$PC_{61}BM$	Slot-die coating	1.76	3.35	2013	[44]
11.	PCDTBT:$PC_{71}BM$	Spin coating	1.8	5.58	2014	[45]
12.	P3HT:$PC_{61}BM$	Inkjet printing/spin coating	2.1	0.98	2015	[46]
13.	CH_3NH_3I/doped P3HT	Slot-die coating	2.1	10.14	2015	[47]
14.	P3HT:$PC_{61}BM$	Gravure printing	2.1	1.26	2015	[48]
15.	P3HT:$PC_{61}BM$/PTB7-Th:$PC_{71}BM$	Spin coating	1.6	2.40	2015	[49]
16.	PII2T-PS:PPDIT	Slot-die coating	–	3.71	2017	[50]
17.	$CH_3NH_3PbI_3$/$PC_{61}BM$	Slot-die coating	–	12.52	2017	[51]
18.	CH_3NH_3I/PbI_2	Slot-die coating	–	11	2017	[52]
19.	PTB7-Th:$PC_{71}BM$	Slot-die coating	1.6	6.61	2017	[53]
20.	$MAPbI_3$	Slot-die coating/all-blade-coated	1.71	14.1	2018	[54]
21.	$MAPbI_3$:F4TCNQ	Doctor-blading	1.71	20	2018	[55]
22.	$CH_3NH_3PbI_3$/C_{60}/$PC_{61}BM$	Slot-die coating	–	8.3	2018	[56]

Although several reviews on the given subject have been reported earlier, with each describing the subject from different perspectives, the current review focuses on organizing the details and progress made in this vast area into appropriate, effective and comprehensive way. Earlier reviews on this subject have clearly mentioned different areas like solution-processed perovskite solar cells for their commercialization, application of materials like graphene in this area, techniques like inkjet printing for commercialization and, flexibility and stability issues of the solar cells and modules during their manufacturing etc. [57–67]. However, this review comprehensively covers and critically analyzes the different aspects of this area in an organized way. These aspects are organized in following way—(1) roll-to-roll compatible as well as potentially commercial deposition/printing techniques—the basics of various R2R-compatible deposition/printing techniques, (2) roll-to-roll compatible materials used—the various types of R2R-compatible materials for active layers and electrodes, including the environmental and process stable materials, (3) the various types of roll-to-roll compatible processing techniques for these materials and (4) and finally, roll-to-roll manufactured photovoltaic modules and the characterization techniques for performance and stability assessment of such modules. The different existing problems and challenges within each of these aspects and how these have been addressed, have been discussed in the review. In fact, optimizing the performance of the devices while addressing one of these aspects, and how such optimization affects the other aspect has also been presented in a critical way in the review. Therefore, this review presents these important aspects of the R2R technology in an organized way, focusing on the important progress made in this area. The review presented here also gives a detailed account of the research undertaken to achieve the current state of the art of the roll-to-roll printing technology, the gaps that exist in this technology and the methods that have been developed to try to overcome these gaps.

Roll-to-roll printing: technique basics

The roll-to-roll printing is an important class of substrate-based manufacturing processes in which structures can be built in a continuous manner using additive and subtractive processes. It comprises many combined technologies which can produce rolls of finished material continuously in an efficient and cost-effective manner with the benefits of high production rates on large scale. These high throughput and low cost are the factors which differentiate the roll-to-roll manufacturing from slower and higher-cost conventional manufacturing due to the multiple steps involved. The technology of the roll-to-roll printing simply consists of the manufacturing techniques which involve continuous processing of materials on a flexible substrate as it is transferred between moving rolls of material. It involves the application of various solution processable materials and constituent printing techniques in order to scale up the production of the solar cells at much faster pace [68]. As discussed earlier, the methods of spin coating and thermal evaporation for electrode deposition are not compatible with high-throughput production of the devices through this technology in which the production is a continuous process [68]. Therefore, the constituent methods for this technique are different from the general methods employed for device fabrication at the lower scale. These methods of the roll-to-roll printing technology are discussed below in detail.

Film and device preparation methods

The basic roll-to-roll printing technique for the film preparation on the substrate is simply transferring the material/ink onto the substrate using another object in a well-controlled and optimized manner at a faster rate. The films of the different active materials can be deposited on the substrate with multiple layers using a wide variety of techniques [68, 69]. Such deposition of the active material has been tested on laboratory scale on rigid as well as flexible substrates to develop rigid and flexible modules [68]. However, the throughput speed in case of the flexible modules can be much higher as compared to the rigid modules [68]. In addition, the performance of the developed module is governed by a wide range of parameters like the processing method, solvents, additives, drying process, active layer materials, substrate and a control of these parameters [68, 69]. Also, the processing conditions for the new setting of the roll-to-roll technology need to be continuously developed and improved, especially considering the boundary conditions of speed, temperature, drying process, multilayer processing, solvents and materials involved in fast roll-to-roll processing [68]. Further, it

has also been reported that a single deposition technique cannot be considered to be the best choice for each layer in the polymer solar cell consisting of stack of multiple layers and therefore, different film deposition techniques optimal for each layer in the stack need to be developed [68].

Printing techniques

As discussed above, the basic roll-to-roll printing technique for the film preparation on the substrate is simply transferring the material/ink onto the substrate using another object in a well-controlled and optimized manner at a faster rate. The ink formulations are the solutions of the different materials, in a required ratio, processed in the appropriate solvents with the required viscosity needed to be deposited on the substrate through the printing techniques. Such ink formulations can be the solutions for the active layer, the interlayers and the charge transporting layers. The active layer consists of the materials which generate and then separate the charge carriers after absorption of the light photons. In a BHJ solar cell, an ultrathin active layer, consisting of a nanostructured blend of a conjugated polymer and an electronegative molecule, forms the photon absorbing component. The mechanism of conversion of the energy of an absorbed photon into electrical energy occurs in a semiconductor with an electronic gap equal to or smaller than the energy of the absorbed photon. After photon absorption, the generation of an electron–hole pair occurs, and due to an internal field generated by the work function difference of the electrodes, the free charge carriers are conducted to the respective electrodes where they are captured. The interlayers establish ohmic contact and determine different device parameters such as the internal electric field, film morphology and carrier recombination rate, which are important for the device performance. The charge transporting layers effectively separate the charges generated by light absorption and selectively transfer the separated electrons and holes.

A wide variety of printing methods like gravure, flexographic, screen and rotary screen printing, shown in Fig. 1, have been developed and utilized for the deposition of the layers of the active materials on the substrates [68, 69].

Gravure printing This is a very common printing method, shown in Fig. 1a, and consists of transferring of the ink from patterned cavities, which are engraved on the gravure cylinder, to the web or substrate. This process utilizes the surface tension developed due to the contact between the web and the cylinder, as they are brought together through a pressurized soft cylinder having impressions [68–70]. The shape and thickness of the print are determined by the cavity patterns and their depths in the cylinder [68, 69]. This printing technique has found its suitability for less viscosity inks at high reported speeds of 15 m/s, with the quality of the print being determined by the parameters like speed of the web and cylinder pressure [68, 69].

Flexographic printing Flexographic printing is a relatively new technique in comparison with gravure printing with the difference that the transferring of the ink is performed through a relief rather than the patterns [68, 69]. This technique (Fig. 1a) consists of fountain rollers allowing a steady transfer of ink to the ceramic anilox roller. This roller consists of microshaped cavities embedded into its outer part, which allows the collection of ink. The ink is then further transferred to the relief on a cylinder, which ultimately transfers the ink to the web [68, 69]. This technique has been reported to be used for various applications like wetting agent processing on the active layer surface and the conducting grid patterning [68, 69].

Screen printing This technique is useful for printing the films with high conductivity, as the films printed through this technique are thick, with around 10–500 μm thickness [68, 69]. The technique has been further classified into two types—flat bed screen and rotary screen printing. The flat bed method consists of a squeegee which moves on the top of a flat bed screen and, thus forces out the ink paste through the mesh mouth, giving the required motif. In case of rotary screen printing, the squeegee moves relative to the rotary screen and forces the ink paste through the opening of the mesh, giving the desired motif. The difference in both techniques is that flat bed screen printing employs low-cost mask, produces single print and provides possibility of large-area applications on the m^2 scale, while rotary screen method employs expensive mask but provides higher throughput speed and better resolution [68, 69].

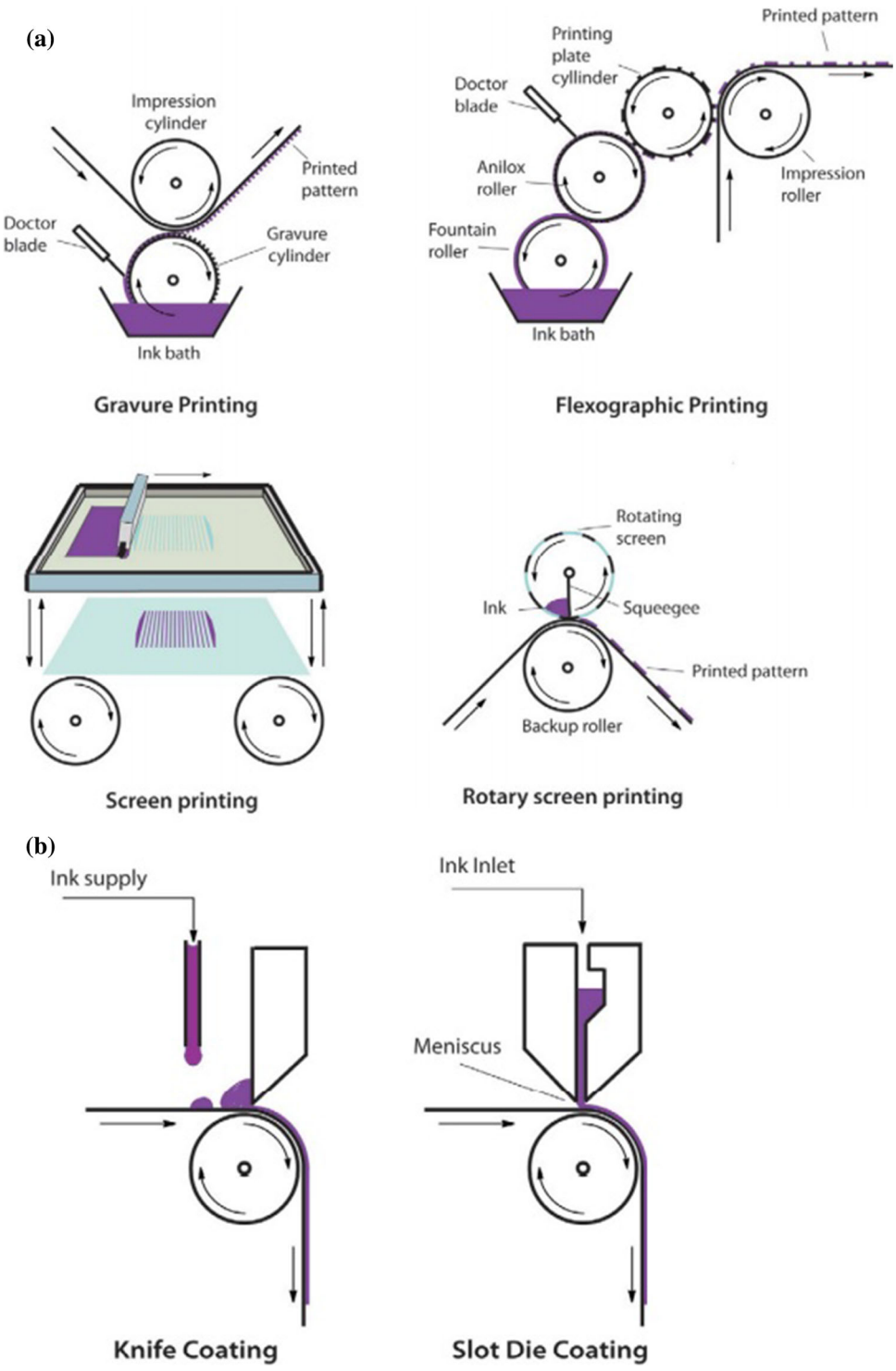

Figure 1 **a** Illustrations of the principles behind the four printing techniques—gravure printing, flexographic printing, screen printing and rotary screen printing. **b** A schematic illustration of knife coating where excess ink is kept ahead of the knife that is in close proximity to the web. Slot-die coating relies on the ink kept between ink supply feeder with a slot from which ink is supplied, thus forming a continuous (or striped) wet film. Reproduced with permission from Elsevier (Ref. [68]).

Inkjet printing This is a contact less deposition method without any mask with potential for developing prototypes and fabricating polymer solar cells from digital images [71]. Inkjet printing offers important advantages with its non-contact operation and ability to give patterned films directly from digital images with lateral resolution better than 10 μm at potentially very high speeds for uniform bigger area deposition, higher than unit cm^2 [46, 72, 73]. It can be used for the deposition of a range of functional materials, e.g., inorganic/metal

nanoparticles, polymeric/small molecules or dispersion solutions [74].

The operating principle of inkjet printing is based on the ejecting of fixed quantity ink in the of small droplet forms from nozzles, deposited on the substrate surface [74]. Based on how droplets form, two types of inkjet systems exist—continuous inkjet and drop-on-demand inkjet printing system [74].

In continuous inkjet printing system, shown in Fig. 2, a steady pressurized stream is used to produce the printed materials, ejecting through a tiny nozzle at a voltage relative to the ground. The stream breaks into smaller droplets, and the gravitational force makes these droplets to move toward the substrate. The descending droplets are then charged by the electrodes, kept below the nozzle, as they pass through space between the electrodes. These charged droplets are then deflected by the deflection plates by a length as controlled by the electric field input signal. These droplets are then deposited on a fixed/moving substrate. The application of a piezoelectric transducer is used to cause the synchronization of liquid droplet formation to minor pressure fluctuations [74].

In contrast, in drop-on-demand inkjet printing system, shown in Fig. 2, a single drop is generated when required. In this system, either the movement of the ink supply feeder is accurately controlled, thus allowing the droplets to accurately settle on the desired location, or the substrate is kept in motion during deposition. The control of printing material ejection is achieved through a steady pressurized pulse in the printing nozzles, produced by a sudden contracting of the ink chamber volume, which then ejects the ink out from the nozzles. This pulse is produced by two mechanisms—the mechanical deforming of a piezoelectric transducer or the thermal bubble collapsing due to local resistive heating in the chamber [74].

The inkjet printing systems offer the advantage that the nozzle is not in the physical contact with the substrate, which makes it potential technique for printing on rough/curved or pressure sensitive surfaces. Further, the method is also suitable for printing any sufficiently conductive fluid material or any solute that is soluble in a conductive fluid vehicle. However, the inkjet printing systems also result in the wastage of material during deposition [74].

The coating techniques

The coating technique is employed to coat a steady wet layer along the web length with no contact between the ink supply feeder and web, with a difference that no pattern formation is done through this technique [68, 69]. This is in contrast with the printing technique which allows for lateral two-dimension printing only through physical contact. However, the control of the wet thickness obtained through coating technique is superior as compared to any of the

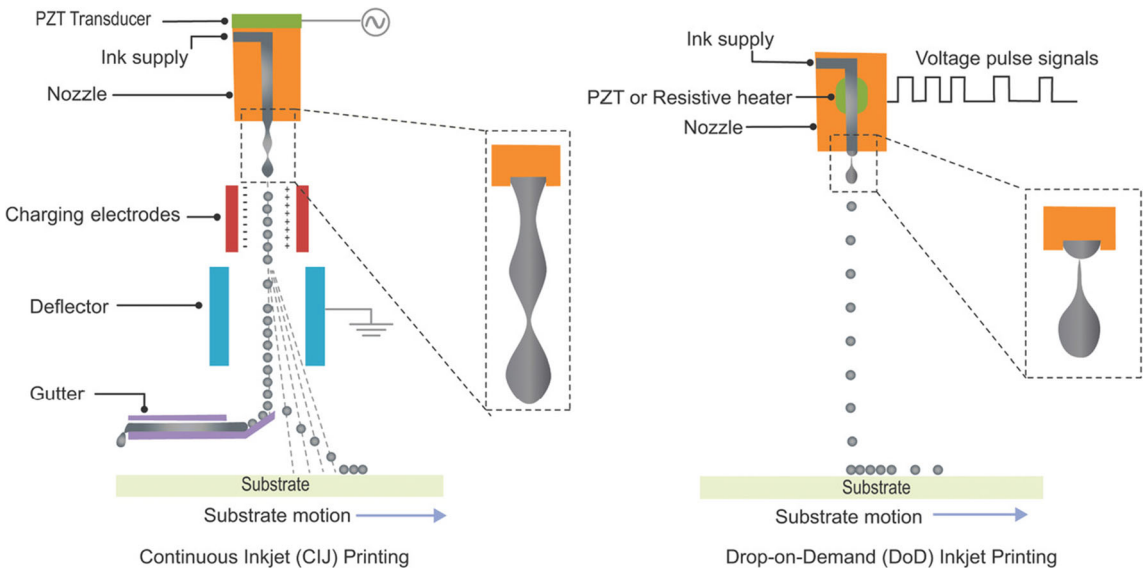

Figure 2 Schematic diagram of inkjet printing methods. Reference [74] Copyright Wiley–VCH Verlag GmbH & Co. KGaA. Reproduced with permission.

printing techniques [68, 69]. The two different types of coating techniques, shown in Fig. 1b, that have been widely used, are knife coating and slot-die coating [68, 69]. The knife coating procedure consists of an ink supply before a knife. The ink is slowly deposited behind the knife with the relative movement of the web to the knife [68]. In slot-die coating, the ink is supplied using a slot and a pump, which gives a possibility of adjustment of the layer thickness though the control of web speed or ink supply [68]. With the slot-die coating techniques, recent efficiencies on the polymer solar cells up to 13.5% have been reported [75].

In addition, the other important type of the coating technique that is widely used is spray coating which has been demonstrated for the deposition of photoactive material layer, polymeric interfacial layers, nanowire materials, alternative transparent/metal electrodes [76–80].

There are several methods, with some common working mechanisms, through which the spray coating method can be used to deposit the layers of the materials on the substrate. Two such types of spray coating techniques are—concurrently pumped single-pass spray and ultrasonic spray coating method [76, 79].

In concurrently pumped method, shown in Fig. 3a, two separate ink solutions are separately pumped through a coaxially connected tube system by using an ultrasonically vibrational nozzle tip. In order for atomization of the liquid, the ink spreading over the tip surface is allowed, after which a micron-scale liquid droplet ejection occurs. A low-pressure N_2 is then used for guiding spray toward the substrate. In case of single-pass method, with a combination of high ink flow rate and lower substrate temperature, merging of a single droplet into a single wet layer is allowed before drying. This leads to complete wet layer formation rather than the quick droplet evaporation occurring during multi-pass deposition, which otherwise will lead to the problems in obtaining a thin uniform layer [76].

In ultrasonic spray coating technique, shown in Fig. 3b, the sizes of the sprayed droplets are moderated through precisely controlled ultrasonic drop formation, which creates a narrow distribution of drop sizes. The drop sizes are comparable or even smaller than the drop sizes of inkjet drops. A clean gas stream is used to direct the atomized solution onto a substrate. The deposited films are optimized by varying solution flow rate, carrier gas flow and substrate temperature. This technique is well suited for large-area processing of the devices and the deposition through this technique clogs less readily as compared to the inkjet printing and, therefore, allows the use of lower boiling point solvents and

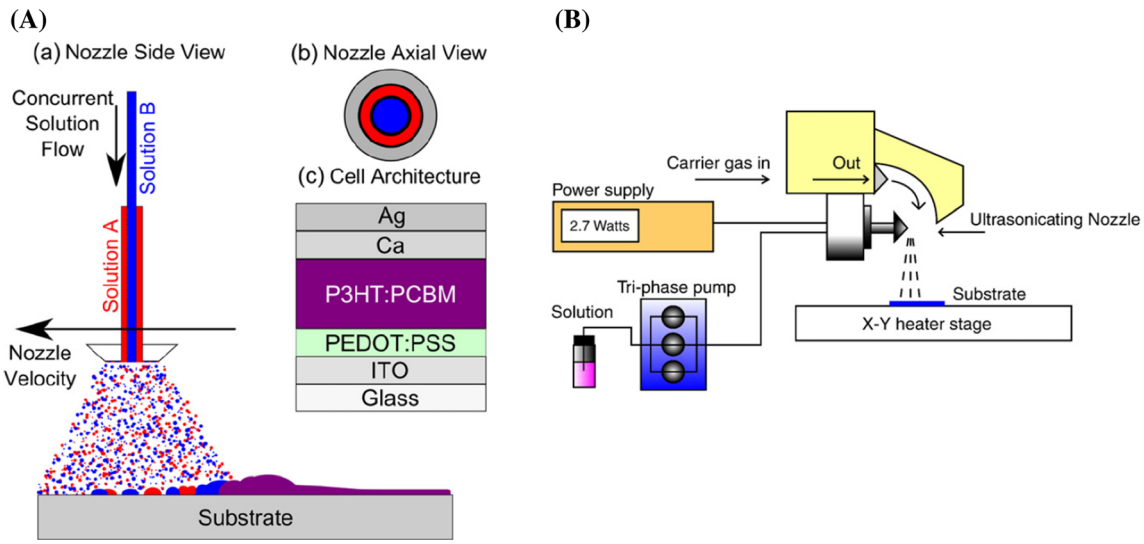

Figure 3 Schematic diagram of **a** concurrently pumped single-pass spray coating, showing separate solutions being sprayed, mixing on the substrate and drying into a thin and uniform film. An axial schematic view of the spray coating nozzle as seen from below. The schematic representation of the conventional polymer solar cell architecture fabricated using the spray coating method. **b** Schematic of ultrasonic spray deposition system. The ultrasonic nozzle mediates a narrow drop size distribution, while the tri-phase pump maintains regular flow. Reproduced with permission from Elsevier (Refs. [76, 79]).

higher solution concentrations. The upper viscosity limits in this technique are also similar to inkjet printing, of the order of 50×10^{-3} Pa s. Further, this technique also easily allows the deposition of the thick films after the optimization of solution properties, substrate temperature and desired surface treatment [79].

A typical example of the full developed flexible R2R printed solar cell with a stack of multiple layers of different materials is shown in Fig. 4e [35]. It has an inverted device geometry, and the initial four layers are deposited by slot-die coating. It consists of layers of materials, with a bottom electrode comprising silver nanoparticles deposited at a web speed of 0.9 m per min (Fig. 4d) on a 130-micron-thick PEN substrate. Further, an ETL of ZnO nanoparticles is coated at a web speed of 0.7 m per min (Fig. 4a), followed by an active layer of P3HT:PCBM coated at a web speed of 0.4 m per min (Fig. 4b) and a hole transporting layer of PEDOT:PSS coated at a web speed of 0.2 m per min (Fig. 4c). The top electrode is deposited by screen printing of a grid-like structure that allows for 80% light transmission. The materials are patterned into stripes that allow for the forming of a unit cell device and serially connected modules having 2, 3 and 8 stripes [35].

A part of typical setup for the roll-to-roll processing methods for the printing of a stack of multiple layers of solar cell, as described above, is shown in Fig. 5 [35]. It is used for slot-die coating silver nanoparticles in order to develop a highly reflecting smooth/non-transparent silver back electrode. A similar setup for the roll-to-roll processing methods has been also been reported [178]. It consists of a mini-roll coater which makes it possible to eliminate the potential sources of error resulting from the boundary conditions implied in the full R2R processing. The mini-roll coater allows for multilayer

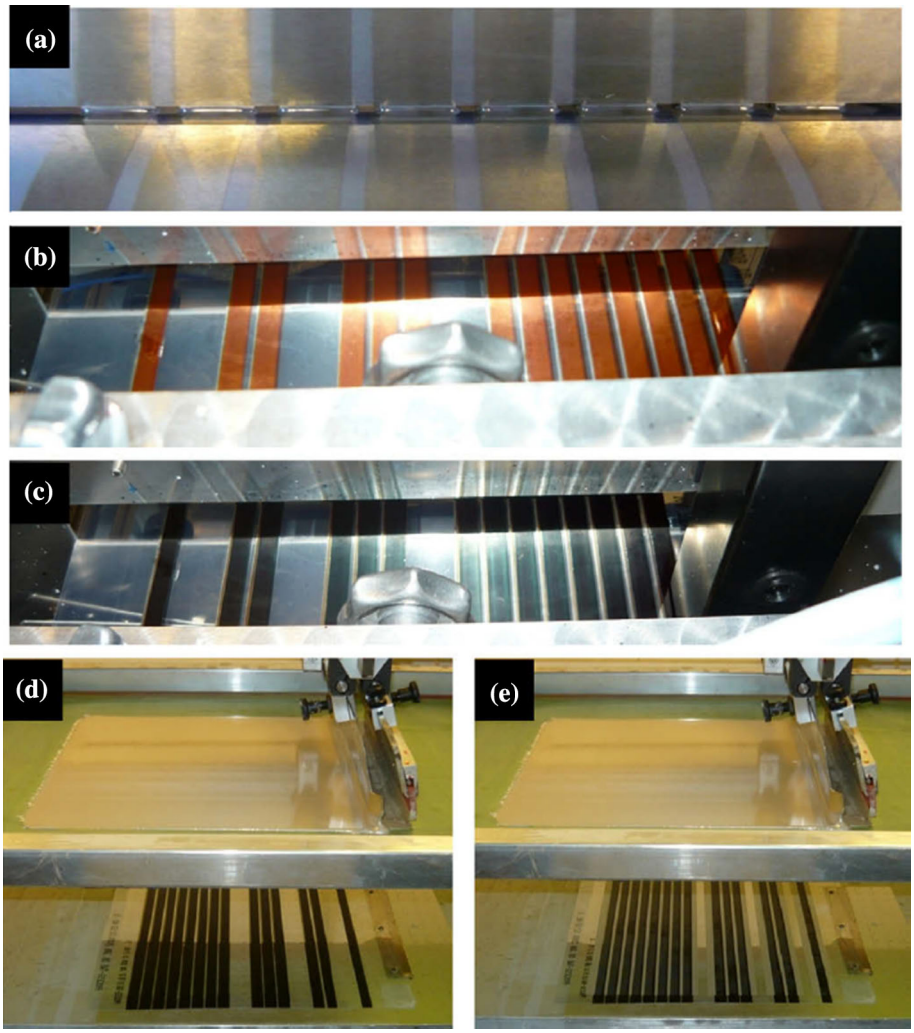

Figure 4 The menisci during slot-die coating of ZnO (**a**). The ZnO stripes are shifted 1 mm to the right with respect to the underlying silver pattern (top). The wet layer during coating of P3HT-PCBM (**b**) and PEDOT:PSS (**c**). Sheet-fed screen printing of the silver front electrode grid before (**d**) and after the printing (**e**). Reproduced with permission from Elsevier (Ref. [35]).

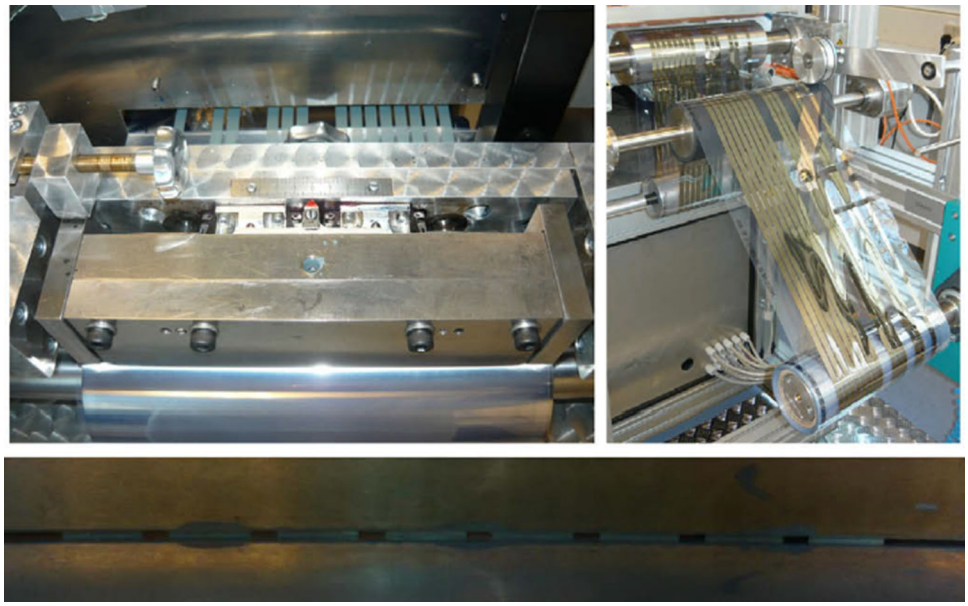

Figure 5 Slot-die coating of the silver back electrode onto PEN. The wet print that has an opaque green color (top right). The dried and highly reflective silver back electrode is shown on the rewinding side (top right). The menisci during coating of the eight stripe module are also shown. Reproduced with permission from Elsevier (Ref. [35]).

stack formation, with the advantages of no contact to the foil surface, no web tension, large bending radius and use of the flexless foil throughout full experiment. Further, in order to study the structural growth of a printed/deposited layer, the method of GISAXS was shown to be used [178]. Table 2 gives a summarized account of the printing/deposition techniques used for the roll-to-roll-compatible/printing technology.

However, the above discussed printing/deposition methods are some of the processing methods used in the roll-to-roll printing technology. The advanced processing methods and their evolution through the research have been discussed in detail in sections below.

Roll-to-roll printing: technology advancements

The development of large-area devices at high throughput requires developing or scaling up the low-throughput technology. The materials and processes used in such low-scale technology are usually not compatible for high-throughput production of the devices. In addition, there are certain important conditions that should be fulfilled, while the different kinds of materials and techniques are developed. For example, the processing of polymer photovoltaics on the gigawatt scale does not leave any scope for the use of any solvents other than environmental friendly solvents like water and some alcohols. Therefore, the application of the environmentally degrading chlorinated/aromatic organic solvents in the research on the roll-to-roll processing methods has been avoided. Further, by avoiding the application of the rare

Table 2 Summary of reported deposition/printing techniques for the fabrication of the roll-to-roll-printed/compatible devices

S. no.	Deposition/printing technique for donor polymer/acceptor material or active material		
1.	Printing	Gravure printing	
		Flexographic printing	
		Screen printing	
		Inkjet printing	Continuous inkjet printing
			Drop-on-demand inkjet printing
2.	Coating	Knife coating	
		Slot-die coating	
		Spray coating method	Concurrently pumped single-pass spray coating method
			Ultrasonic spray coating method

materials like indium and by avoiding vacuum processing, shorter energy payback times have been demonstrated to be possible [81]. A significant research has led to the development and optimization of different materials and methods suitable for a large-scale production of the large-area devices, as discussed below.

Material processing

For employing the roll-to-roll printing technique for the large-area scale solar cells, it is important to either use new types of R2R-compatible materials or mold the properties of the existing active layer materials formulations as per the requirements of the technique in order to obtain high-throughput production of the devices. Some of the requirements posed in the roll-to-roll printing techniques are—(1) environmental compatibility of the materials, (2) application of inexpensive materials, e.g., for electrodes, (3) avoiding the use of vacuum processing and (4) environmental and processing stability of the materials. Several studies have been done in order to develop or tune the material formulations for such requirements. This optimization of the materials and the processes is important, as the materials and processes which might suit up for the development of the devices at the laboratory scale and low throughput might not be well suited for high-throughput device production. Therefore, the research in this area has been focused keeping these requirements in view and these studies have been accordingly discussed below.

Environmental-compatible materials

The polymers used in solar cell devices are usually processed in the environmentally harmful solvents such as chlorobenzene and 1,2-dichlorobenzene. Also, with the state-of-the-art technology based on ProcessOne, the use of approximately 16 million liters of chlorobenzene for the production of 1 GWp of the polymer solar cell has been estimated [30, 82]. In addition, other concerns include the severe effects of the choice of the inefficient processing methods and the processing materials on the energy payback time, when the total energy needed for raw material production is also considered [30]. However, the life cycle analysis has shown that aqueous processing of the water-soluble polymers is the most beneficial, with less electrical energy input for production [83]. Therefore, the manufacturing of the solar cells on gigawatt scale with environmental-compatible materials requires the processing of the polymers to be replaced from the organic solvents-based process to aqueous process [37, 88]. The solubility of the polymers in water is achieved by methods such as synthesizing a tertiary ester side chain, containing polyether units as well as free alcohol groups, and by the addition of hydroxyl groups [84, 88]. In order to add the hydroxyl groups, a cost-effective and environmental-friendly method using the oxidants of ferrous chloride ($FeCl_2$) and hydrogen peroxide (H_2O_2) has been demonstrated to prepare water-soluble PPy NPs [88]. The soluble PPy was shown to contain some hydroxyl groups [88]. The introduction of sulfonic acid salts at the end of the side chains has also been reported to provide the water solubility, and water-soluble polymers using different ions such as sulfonium, pyridinium or ammonium salts and with varying chain lengths have also been reported [85–88]. Such aqueous processing in the manufacture of the solar cells necessitates certain requirements to be fulfilled. The major differences between the processing techniques of the polymer solar cells using the laboratory-scale fabrication techniques and that of the high-throughput processing, along with the differences in the fulfilling of the ultimate requirements by these solar cells, are outlined in Fig. 6. Currently, almost all the steps of the processing of the polymer solar cells are done in an inert atmosphere (e.g., N_2 atmosphere) maintained inside a glovebox, while these devices are supposed to operate for long durations in the ambient environment. Not only this, except the aqueous processing of the PEDOT:PSS, other processing steps like solution processing of the active layer are done using the environmentally harmful toxic organic solvents, while the thermal evaporation of the metallic electrodes like LiF and aluminum is not compatible with high-throughput methods (Fig. 6a). Comparing this scenario with the all aqueous processable steps of the high-throughput methods reveals the fulfillment of the objectives of the environmental compatibility as well as high-throughput production of the devices through the aqueous processing (Fig. 6b).

Therefore, this requirement of the processing using water of the multiple stacked layers in the solar cell necessitates the conjugated and active material aqueous solubilization for roll-to-roll printing [37, 88]. In order to fulfill this, the designing of the

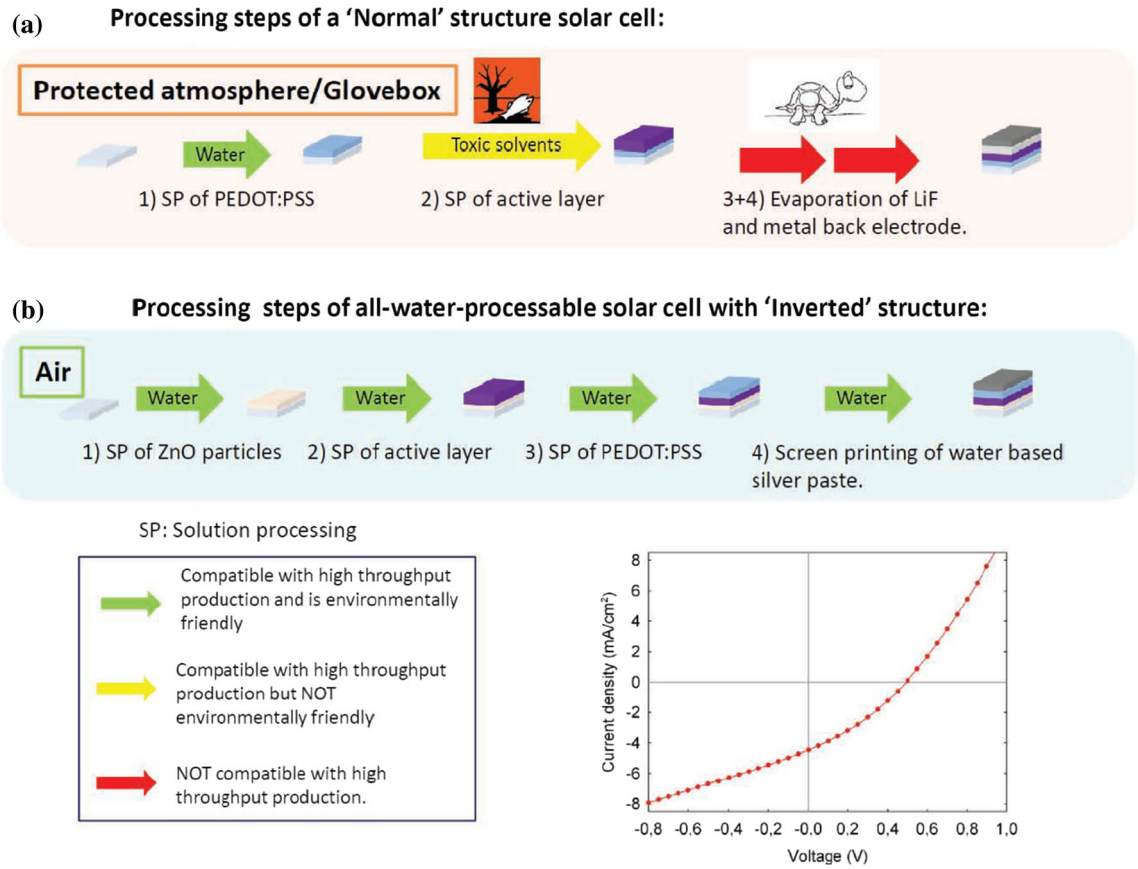

Figure 6 Comparison of the potential for high-throughput production using the standard laboratory buildup of a solar cell, which involves both **a** the use of toxic solvents and the slow metal deposition by evaporation and **b** the all-water-processable method where all steps are processed from aqueous solution, which makes it compatible with high-throughput processing like roll-to-roll coating. Furthermore, the use of water-based solutions guarantees a minimal impact on the environment (middle). The environmental compatibility of the processing steps is shown (lower left) along with an IV curve for a device prepared using the aqueous processing of all layers described here (lower right). Reference [88] Copyright Wiley-VCH Verlag GmbH & Co. KGaA. Reproduced with permission.

inks for the ETL of ZnO ink, HTL of PEDOT:PSS and metallic back electrode layer (silver ink) using the aqueous solution (Fig. 7a) has been demonstrated in one of the studies [88]. The technique of the screen printing, shown in Fig. 7b, c, was used to deposit the multiple layers of these materials. However, for such multiple layer formation, the previous deposited layers were converted into the insoluble state to prevent the interaction of the subsequent layer with the previous layer. This was achieved by using temperature-cleavable materials to turn off the polymeric solubility through side chain removal after film was processed. The study has reported efficiencies in the range of 0.4–0.7% with the device areas of 0.5 cm^2 [88].

Further, the aqueous nanoparticle dispersions of a series of three low-band-gap polymers P1 (1.8 eV), P2 (1.5 eV) and P3 (1.8 eV) were made using ultrasonic treatment of a chloroform solution of the polymeric/PCBM mixture with an aqueous solution of SDS [37]. Such aqueous dispersions have been demonstrated to be important for the formation of films of solar cell devices, in addition to the significant advantages of lower release of chlorinated/aromatic solvent into the environment due to containment and reuse of solvents in the preparation of these nanoparticle dispersions [37]. The deposition of the thin films using the formulated ink of these nanoparticle dispersions, for a device area of 4 cm^2, was achieved through both spin coating and R2R coating at higher web speed of 8 m per min with 80 °C roller temperature. These deposition techniques have been shown to influence the deposited thin-film morphology. In case of the spin-coated samples, as shown in Fig. 8a–

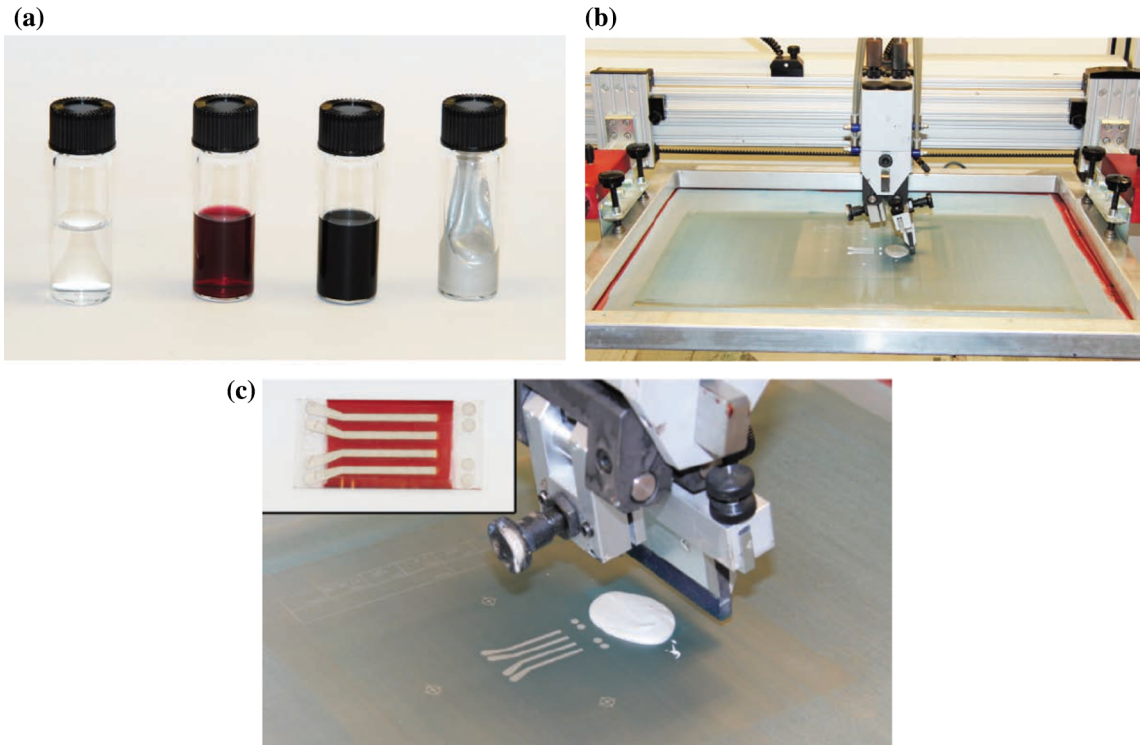

Figure 7 The picture of the inks involved in the 'all-water-based processing.' **a** From left to right: aqueous ZnO precursor solution, aqueous solution of polymer 1 (diluted in order to show color), aqueous PEDOT:PSS with isopropanol and aqueous silver paste. **b** The picture of the screen printing machinery. **c** The close-up of the screen printing process. The silver paste has been applied and is ready to be pushed though the pattern of the mask by sweeping the squeegee across the steel mesh screen. Insert shows a picture of the final device after encapsulation. Reference [88] Copyright Wiley-VCH Verlag GmbH & Co. KGaA. Reproduced with permission.

c, the single nanoparticle shapes can be observed, except in case of P1 with agglomerations of smaller particles. In contrast, the nanoparticles in roll-to-roll-coated films cannot be further clearly differentiated and have merged in places, as shown in Fig. 8d–f. The efficiency obtained for each of the materials in the study was reported to be 0.07, 0.55 and 0.15% for P1, P2 and P3, respectively [37]. Previous studies have shown different approaches of the aqueous conjugated/active material solubilization which include solubilization through ionic side chains like sulfonic or carboxylic acid or ammonium, hydrophobic polymeric nanoparticle aqueous dispersions, nonionic alcohol and glycol side chains [86, 88–90]. With the approach of solubilization through these side chains, the power conversion efficiency up to 0.7% has been obtained on ITO substrates with aqueously processed four subsequent layers in the solar cell stack along with printed metal back electrode [88].

The aqueous processing in the manufacturing of the large-area tandem polymeric solar cells has also been demonstrated [91]. Although the processing using other different solvents like alcohols and chlorobenzene has also been reported in this study, the application of an aqueous ink for the processing of the back-BHJ was demonstrated to address the morphology issues in the large-area tandem polymer solar cells [91]. For example, one of the challenges presented in the manufacturing of the tandem polymer solar cells during the roll-to-roll technology is the coating of the multilayers on top of each other with no adverse influence of subsequent coating steps on previously coated layers. The study has demonstrated the manufacturing of a roll-to-roll-compatible tandem polymer solar cell with a structure consisting of a multilayer stack with the composition—PET/ITO/ZnO/front-BHJ/V_2O_5/ZnO/back-BHJ/PEDOT:PSS/Ag, where PET is the substrate, ITO is transparent front electrode, ZnO is the ETL, front-BHJ and back-BHJ consist of two active

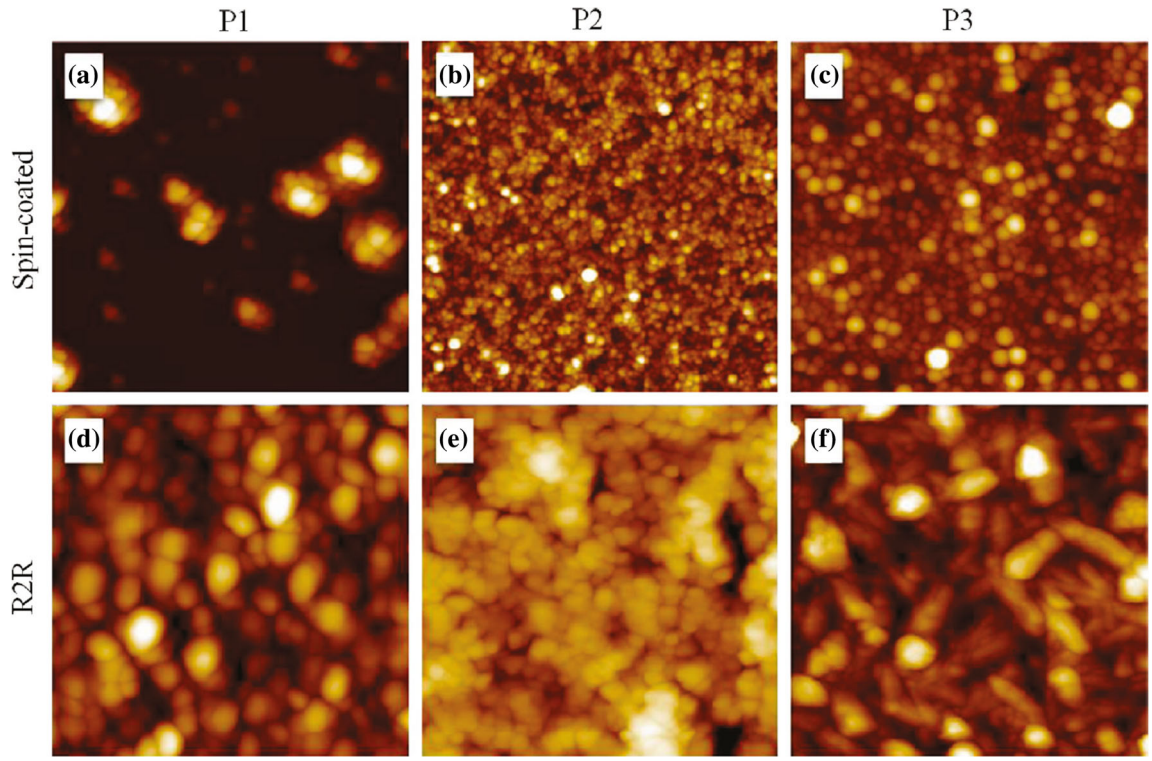

Figure 8 The AFM topography images of spin-coated (**a**–**c**) and R2R (**d**–**f**) prepared samples of P1, P2 and P3. All the images have been taken at 5 × 5 μm^2. Reprinted with permission from Ref. [37]. Copyright (2011) American Chemical Society.

layers—P3HT:$PC_{60}BM$ and TQ-1:$PC_{60}BM$, V_2O_5/ZnO is the recombination layer, PEDOT:PSS is the HTL and Ag is the back electrode [91]. The study revealed the presence of cracks in the V_2O_5 part of the recombination layer, formed during the processing of V_2O_5 layer either due to the thermal annealing or due to the substrate bending when passing through the R2R instrument. However, the application of an aqueous ink for the back-BHJ processing was demonstrated to address this issue. For the roll-to-roll manufactured tandem polymer solar cell, an efficiency of 0.10% was also reported [91].

In addition to the aqueous processing, in order to ensure the environmental compatibility of the materials used, the application of the halogen-free solvents has also been explored in several studies [46, 92, 93]. However, among these, not all studies have demonstrated the application of the materials or techniques that are compatible with the roll-to-roll processing. For example, the non-halogenated solvent system *o*-xylene/benzylphenylether (BPE) has been utilized to fabricate polymer solar cells using both spin-coating and spray-coating techniques [92]. Therefore, the solar cells fabricated using spray coating from non-halogenated solvents *o*-xylene/BPE can also be fabricated with roll-to-roll techniques, and have been shown to achieve a high efficiency of 7.74% [92]. The application of a mixture of halogen-free solvents, consisting of *o*-xylene, indan and tetraline for the processing of the solar cells has also been reported [46]. For the photoactive layer, an ink was formulated using *o*-xylene, indan and tetraline (1:1:1) along with a P3HT/PCBM in 1.3 wt% concentration. This mixture of halogen-free solvents was used for achieving an optimum ink's viscosity of 1.8 mPa.s for the print-jet technique, and a surface tension of 32 mN/m was achieved to ensure a good surface wetting of printed ZnO layer. This ZnO layer, in combination with highly conducting PEDOT printed layer, was used as ETL. Such optimum viscosity and surface tension are important for both stability of the ink at the room temperature as well as good contact line pinning after deposition [46]. The technique of inkjet printing was also demonstrated for the sequential deposition of multiple layers of active materials, as it provides versatility and flexibility in the sequential deposition of these materials [46]. An efficiency of 0.98% was achieved for a four-

inkjet-printed-layer device module with an area of 92 cm^2 [46]. The study also demonstrated the introduction of the industrial print-jets with printing width of 3.5 cm, in contrast with earlier printing equipments with limited number of nozzles which causes artifacts in the printing and leads to slow printing of larger areas [46]. The printing of the large areas in an individual passing with processing speeds compatible with roll-to-roll speeds was also demonstrated [46].

However, most semiconducting polymer/fullerene blends show a limited solubility in non-halogenated solvents, which results in ink compositions having less viscosities, and therefore posing the limitations on the application of R2R-compatible processes such as inkjet printing [94]. This challenge of low viscosity, while simultaneously using the non-halogenated solvents, has been addressed in a study. In order to overcome the limitation of low viscosity, the application of polystyrene as a rheological modifier to enhance the viscosity of BHJ non-halogenated inks has been reported [94]. The study has demonstrated that the addition of 1 wt% polystyrene increases the viscosity, with the largest viscosity reported with the polymer having the highest molecular weight. However, it was reported that such addition of polystyrene resulted in the occupation of 20 vol% of the layer by the inactive material. Further, a significant portion of the interface of the BHJ and the evaporated back electrode was shown to be occupied by the non-conducting polystyrene. This resulted in the decrease in the device performance by 20% [94].

The application of aqueous particle-less ink compositions for the deposition of the silver back electrode in inverted devices at low annealing temperatures has also been demonstrated [48]. It has been reported that the deposition of the back electrode is difficult as it is performed during the last step of the multilayer stack formation; thus, this process leaves some major technology considerations [48]. Firstly, in order to achieve higher morphological stability of the underlying material layers and compatibility with flexible substrates such as PET, relatively less annealing temperatures are needed [95]. In addition, the possible diffusion of ink through the buffer HTL can lead to unwanted interaction between the solvent used in the ink composition and the underlying material, leading to inefficient device performance [42]. Further, the ink compositions typically used for the formation of the back electrode are based on micro/nanosized metal particles, usually dispersed in an organic medium, and usually sintering temperatures in 120–140 °C range are needed for higher conducting values in these inks [80, 96]. Therefore, in order to address these problems, an aqueous-based silver ink composition was developed and demonstrated as a fabrication precursor for the metal back electrode in inverted flexible P3HT:PCBM devices [48]. It was shown that in such solution-processed particle-less reactive ink, the lowering of a diamminesilver (I) complex in water medium leads to the formation of a highly conducting film at low annealing temperatures, which significantly limits the morphology/thermal degradation of the deposited layers. Different back-electrode configurations, with different coverage areas, were developed by flexography-printing of the aqueous-based solution-processed ink composition on top of the PEDOT:PSS layer at the speed of 30 m/min and subsequent sintering for 15 min at 90 °C. It was also shown from the morphology assessment of the vertical stack of layers that the coverage area of the back electrode determines the amount of ink passing through the HTL layer into the layers beneath. This process of ink passing through the HTL layer leads to shunt problems and thus poor device performance. In case of the back-electrode configuration with the larger coverage area, the amount of silver ink penetration was shown to be higher, and therefore, the device performance was lower for such back-electrode configuration (Fig. 9). In addition, the thickness of the PEDOT:PSS buffer layer was also shown to affect the functional performance. The shunt resistance was reported to increase with increase in HTL thickness, possibly resulting from decreased ink diffusion in the devices with thick HTLs. Therefore, better device performance was achieved for devices with higher HTL thickness (Fig. 9).

Application of inexpensive materials for electrodes

One of the important materials that need to be addressed is ITO, which is used as an electrode material in the solar cells. The solar cells in the roll-to-roll printing modules have the electrodes consisting of ITO, which offers several disadvantages. Firstly, more than 80% of the cost and up to 90% of the embedded energy results from the use of ITO, and due to the scarcity of indium, this problem may further become more severe [97, 118, 119]. Secondly, the

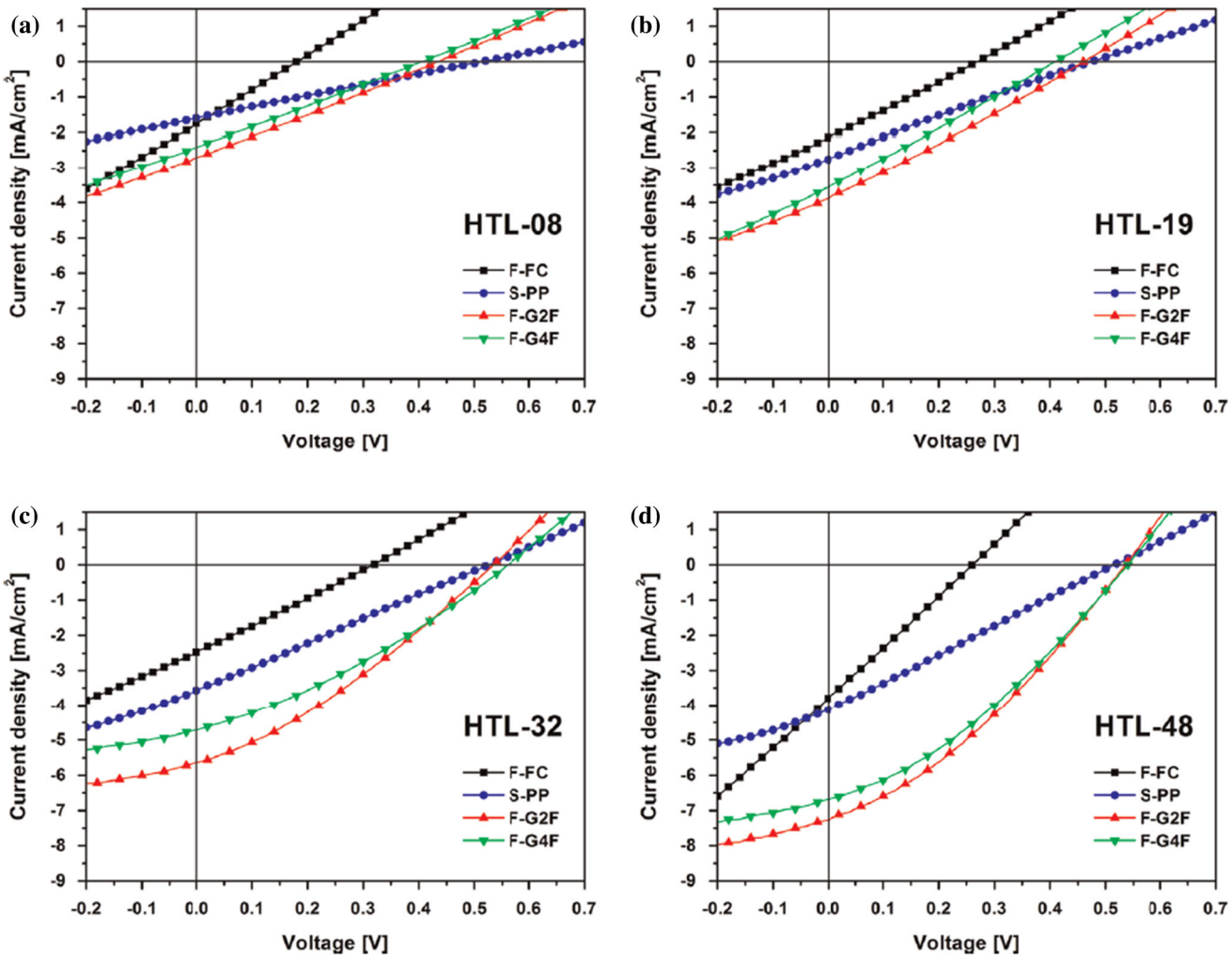

Figure 9 *J–V* characteristics of PSC devices with different back-electrode architectures measured at different PEDOT:PSS thicknesses: **a** 0.8 μm (HTL-08), **b** 1.9 μm (HTL-19), **c** 3.2 μm (HTL-32) and **d** 4.8 μm (HTL-48). Reproduced with permission from Elsevier (Ref. [48]).

preparation of the ITO involves vacuum deposition, and further, photolithography or laser scribing is required to make the conducting pattern of ITO for electrodes. In addition, ITO is a brittle material and even with capability of bending to a certain extent during manufacturing, its purpose is limited to integration with a final rigid product [97]. These requirements, thus, necessitate the manufacturing of the electrodes which are free from ITO, for their suitability into R2R manufacturing of the solar cell modules. Several studies that have been carried out for such electrodes are discussed below [35, 40, 97–120]. Although technologies for the recycling of the ITO have also been demonstrated, these require the removal of the device layers, which damages the device [98]. One methodology to achieve the recycling of ITO involves the application of the ultrasonication of ITO substrates having fabricated devices for 15 min at 45 °C in order to remove the layers of materials like Al, P3HT:PCBM and PEDOT:PSS deposited on ITO substrates [98]. The morphology of ITO showed a little change as a result of recycling, with slightly larger clusters of small grains and a smoother surface. These small changes were reported to result from contact with PEDOT:PSS. The dispersions of PEDOT:PSS, with a pH of ~ 2, were used for spin coating, and it was reported that these dispersions may initially remove the underlayer of ITO; however, subsequent recycling may not lead to further changes of morphology. These cleaned substrates were then demonstrated to be used again for the manufacturing of solar cells.

Although the application of such technique can also be demonstrated to recover the ITO from the flexible solar cells in the modules, these require the removal of the device layers, which damages the device. Thus, the step of elimination of ITO as an electrode material can not only lead to the simplification of the processes and materials used in the roll-to-roll technology but also to the reduction of the cost involved [35].

For an inverted device geometry, an R2R enabled fabrication of devices has demonstrated such removal of the use of ITO, with many layers of constituent materials deposited on transparent/non-transparent flexible substrates [35]. It was demonstrated that using slot-die coating technique, four layers of materials were deposited. These layers consisted of an ITO-free bottom electrode layer with silver nanoparticles deposited on a 130-micron-thick PEN substrate, an ETL of ZnO nanoparticles, an active layer of P3HT:PCBM and a top HTL of PEDOT:PSS [35]. Further, the top electrode was deposited by screen printing a metallic grid structure with 80% light transmission. The materials used in the devices were patterned into stripes, which allowed the making of individual cell device as well as serially connected modules consisting of 2, 3 and 8 stripes. All the solution-processed layers in the device were reported to be prepared through vacuum free processing in air. However, the study reported a low efficiency of 0.3% due to poor light transmission through the back electrode [35].

The direct printing of semitransparent silver grids onto the flexible PET foil, followed by light sintering of HTL and, printing and slot-die coating of ZnO nanoparticles, has been demonstrated for developing an ITO-free electrode [97]. An electron-accepting semitransparent front electrode, directly applicable in the manufacturing of polymer solar cell modules (Fig. 10c), was shown to be produced using this approach [97]. This front electrode along with a rotary-screen-printed HTL electrode was the used for manufacture of ITO-free solar cell modules [97]. In addition, the ink used for the developing the front electrode was aqueous processed consisting of 20% silver loading. The printing of the silver grids (Fig. 10b, d) onto the PET was done using inkjet printing, followed by R2R light sintering of these inkjet-printed patterns using a flash lamp system, as shown in Fig. 10a.

In the sintering process, the ink particles are annealed to a specific temperature. During this process, the carrier liquid and dispersing materials present in the ink are evaporated from it. Further, an additional heating after evaporation can cause the agglomeration of the nanoparticles. The light sintering improved performance as well as the adhesion of the printed patterns on the PET very significantly. An improvement in the efficiency from 1.5 up to 1.7% after four flashes was reported.

A highly conducting PEDOT:PSS layer, deposited on the top of a pristine PET substrate or a flextrode consisting of a highly conductive metallic grid, a semitransparent conductor and a hole blocking layer, has been demonstrated for the front electrode as an alternative to the ITO [99]. A single machine roll coater (Fig. 11a), which enabled the processing of entire device layers without moving the substrate from one machine to another, was demonstrated. This roll coater was used to manufacture solar cells with the ITO-free front electrodes. Such approach was shown to be readily scalable, using one compact laboratory scale coating/printing machine (Fig. 11a). Such machine was shown to be directly industrially compatible for pilot scale R2R processing. The technique was successfully used for one continuous roll processing of PET substrates. In addition, it was also successfully used for the manufacturing of polymer solar cells by solution processing of five layers using only slot-die coating and flexographic printing. Using a novel and compact flexographic printing roll (Fig. 11c), comprising of a metal cylinder with side registration, the deposition of a back silver electrode by flexographic printing with the same roll coater has been demonstrated [99]. The technique involved the deposition of first four initial layers through slot-die coating along with the use of a transparent front electrode (Fig. 11b) based on PEDOT:PSS as a solution processable alternative to ITO [99].

Similar to the above approach, the application of a highly conductive HTL combined with current collecting metallic grid structures has also been demonstrated as an alternative to eliminate the application of the ITO for electrodes [99]. These grids have been shown to be good alternative to lithographically deposited and evaporated structures. A fast/cost-effective printing method was used for the deposition of such metallic structures or grids. These current collecting grids were deposited by inkjet printing of a silver-based nanoparticle dispersive ink on a 200-micron-thick PEN foil coated with a thin-film barrier. The inkjet printing was done by using a

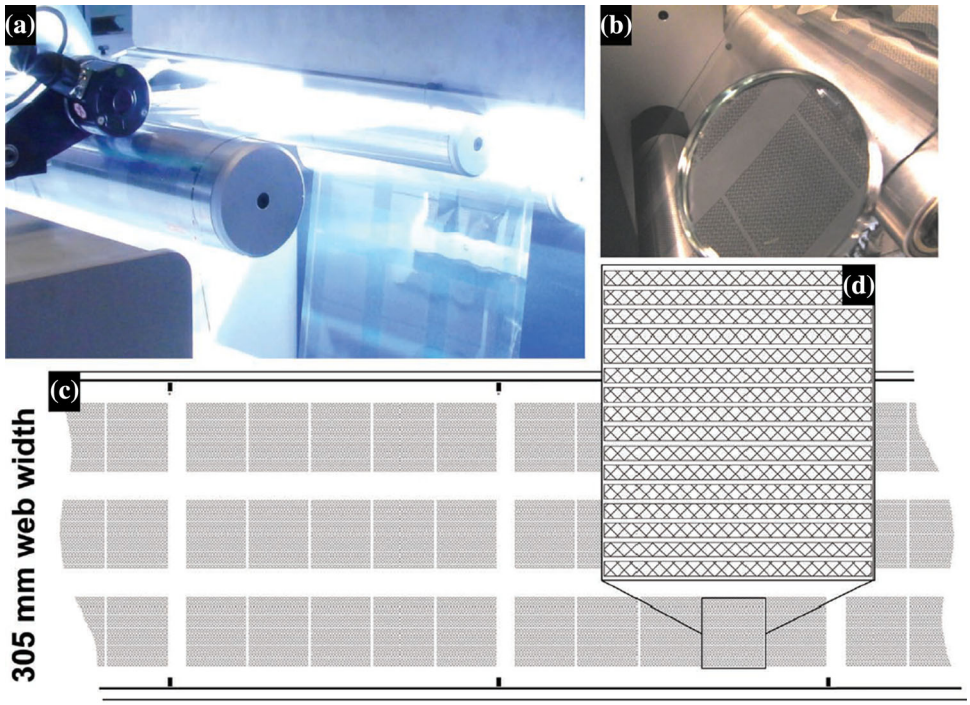

Figure 10 **a** A photograph of roll-to-roll photonic sintering of the inkjet-printed silver-grid structures taken during a flash. **b** A view of the roll-to-roll inkjet-printed pattern after drying, through a magnifying glass. **c** The graphical illustration of the web showing the repeated motif comprising 15 individual modules. **d** The zoom-in on the silver electrode pattern corresponding to one module. Reference [97] Copyright Wiley-VCH Verlag GmbH & Co. KGaA. Reproduced with permission.

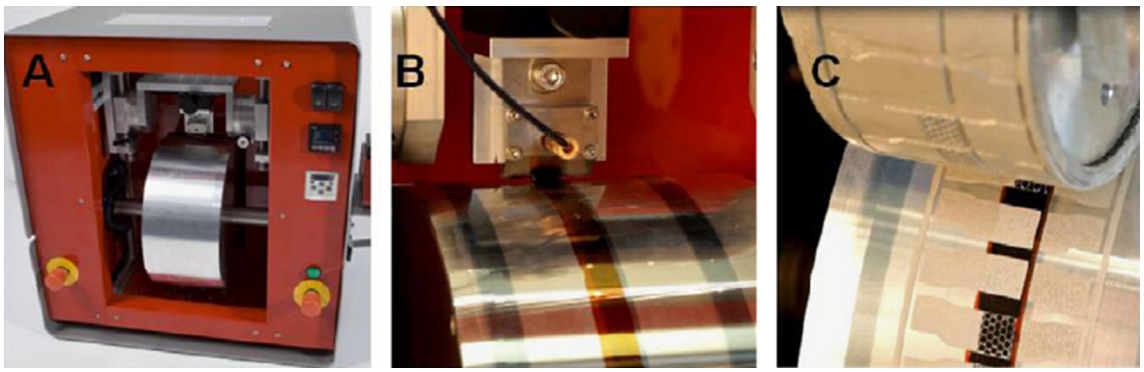

Figure 11 **a** A picture of the small roll coater from the front, **b** slot-die coating of the active layer and **c** flexographic printing of the back silver electrode. Reproduced with permission from Elsevier (Ref. [99]).

piezoelectric drop-on-demand system. For the full front electrode, high-conductivity PEDOT:PSS was then printed on top of the grids. These printed layers were annealed at 130 °C for 10 min, leading to a 100-nm-thick HTL layer with 200 S/cm conductivity and 500 Ohm/sq sheet resistance [100]. However, the problem of these printed structures is the requirement of sintering, e.g., conventional oven sintering or light sintering after deposition, to achieve desired conductivity [100]. The conventional oven sintering is a slow process and does not distinguish between foil and ink heating, while the light sintering results in much high heating rates and is applied only with locally restricted pulses to the ink patterns. With these different processing conditions, the track morphology of the sintered silver structures clearly depends on the type of the applied sintering method. The SEM images of grids are shown in Fig. 12, with different thermal/flash sintering times, respectively. The higher the sintering times, the more improved the contacts between the individual particles, with the deepest contrast between the 10- and 30-min sintered samples (Fig. 12a, b) [100]. Even with this duration, a high residual organic component still remains in the sample even after thermal sintering, where particles do not merge [100]. However, for 30-min sintering, the connectivity between the particles is significantly higher, with an increased average

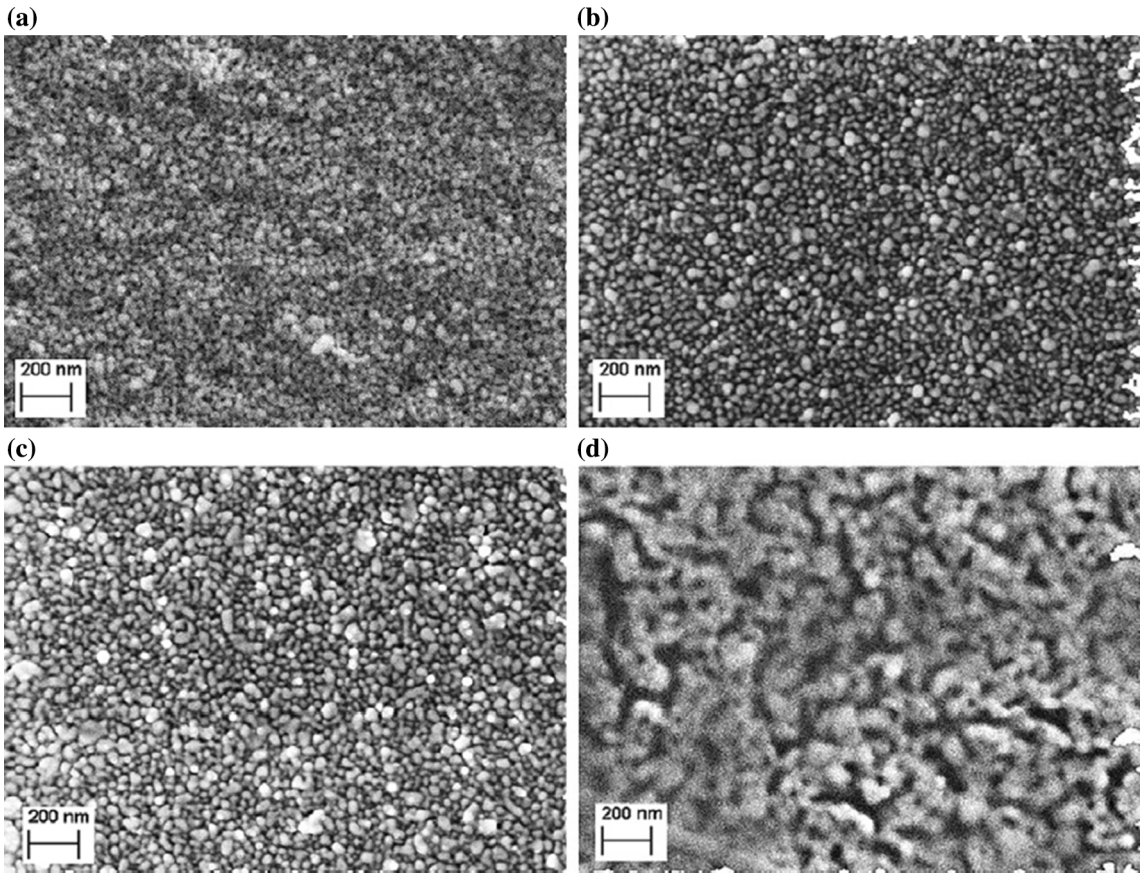

Figure 12 The scanning electron microscopy (SEM) images of an inkjet-printed silver track after **a** 10 min, **b** 30 min and **c** 360 min of thermal sintering at 130 °C in an oven and **d** 5 s of flash sintering. Reproduced with permission from Elsevier (Ref. [100]).

particle size due to partial merging. This effect becomes more pronounced after 360 min of thermal sintering (Fig. 12c). Interestingly, the 5 s of flash sintering (Fig. 12d), however, removes most of the organic materials along with a large merging of the particles [100].

Hosel et al. demonstrated the application of a stack of silver-grid/PEDOT:PSS/ZnO layers as ITO-free, semitransparent, electron-selective front electrode for inverted devices [40]. In order to achieve this, a fast inline R2R printing/coating on PET and barrier foil (Fig. 13a) was done in ambience at web speeds of 10 m per min for the manufacturing of flexible ITO-free devices with multilayer stack [40]. The whole device stack was shown to be completed by the use of rotary-screen-printed HTL and a comb-patterned silver-grid back electrode, both at 2 m min^{-1} (Fig. 13b). The ITO-free flextrode, with potential for large-area devices, was fabricated by flexographic printing of a honeycomb-type grid structure by using an aqueous-based silver nanoparticle ink. The flextrode showed a less sheet resistance with effective optical transmission in the visible range. Subsequently, using rotary screen printing, PEDOT:PSS was deposited on top of silver-grid structure, making one side of it exposed for further direct contacts and thus, for serially interconnected printed modules. The technique was demonstrated to successfully manufacture fully R2R-processed solar cells and modules with higher efficiency of 1.8% on unit cells. The modules with more than 1.6% PCE were also demonstrated.

Kang et al. [101] demonstrated the application of flexible/transparent Cu nanowire mesh electrode as a potential alternative for ITO. A simple metal transfer process using flexible PDMS stamp was used for this, which showed a greater flexibility, efficient light transmittance and electrical conductivity than conventional ITO electrode deposited on plastic substrates. The nanoimprint lithography (NIL) technique using SiO_2 mold (Fig. 14a) [102] was first performed in order to fabricate the resist template of the PDMS

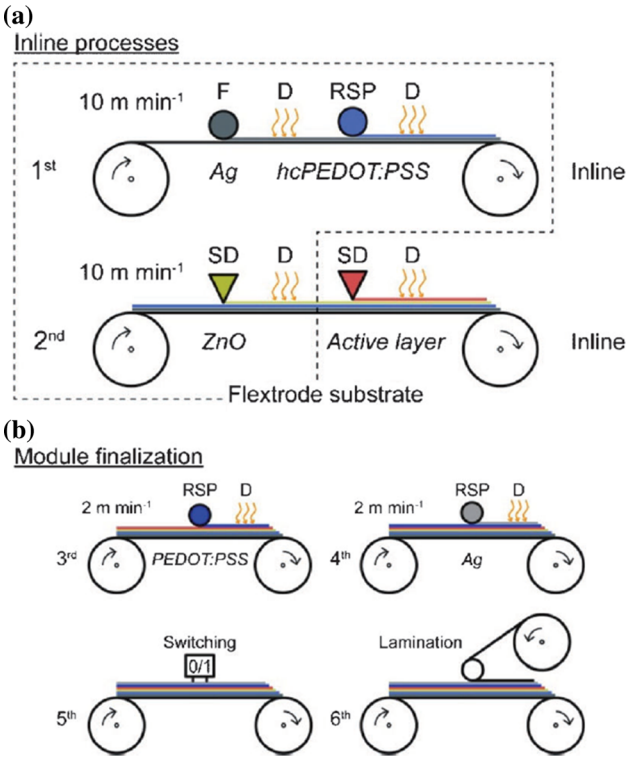

Figure 13 **a** The inline fabrication of the flextrode substrate and **b** the solar cell module finalization. The silver grid together with highly conductive PEDOT:PSS layer, ZnO, and an active layer can be processed inline at 10 m min^{-1}. The illustrated processes are flexo-printing (F), rotary screen printing (RSP), slot-die coating (SD) and drying (D). Reference [40] Copyright Wiley-VCH Verlag GmbH & Co. KGaA. Reproduced with permission.

stamp. It consisted of two sets of 130-nm deep orthogonal grating structures but with different line widths and periods. The stamp (Fig. 14b) was made from the imprinted resist template by drop casting and curing a high modulus/commercial PDMS [103–105] for a flexible and mechanically supported patterned layer. After the removal of the stamp from the template (Fig. 14c), Cu/Ti layers were sequentially deposited on the stamp by electron-beam evaporation. The layers were subsequently treated with O_2 plasma (Fig. 14d), followed by metal deposition (Fig. 14e) and addition of glycerol (Fig. 14f).

This NIL printing technique was demonstrated to be potentially extended to a cost efficient manufacturing of the large-area electrodes with the use of flexible molds [106, 107]. Large-area nanometallic electrodes on flexible substrates were thus demonstrated by using the R2R process [101]. The printing of nanometallic (e.g., Au) gratings on large-area PET substrates was demonstrated through a continuous R2R transfer printing process (Fig. 15a). For this demonstration, a surfactant (1H,1H,2H,2H-perfluorodecyl trichlorosilane)-treated UV-curable epoxy silicone patterns [108] deposited on PET substrate were used as a flexible mold (Fig. 15b). Another flexible mold, made of ETFE, was also fabricated and then was used for the fabrication of the flexible epoxy silicone mold by UV R2RNIL process [106]. After metal deposition, an anti-sticking layer was thermally deposited on the stamp to ensure reduced adhesion of the metallic layer to the mold. Further, the stamp was wrapped on the tensioned belt around rollers (Fig. 15a), and Au nanogratings (Fig. 15b, c) on the stamp were then transferred onto a PET substrates coated with partially cured UV epoxy. This resulted in the large-area flexible substrates (Fig. 15d). A power conversion efficiency of about 2.1% in the device using Cu electrode was reported, comparable to the efficiency of 2.24% for the device using ITO electrode with.

The application of carbon to replace silver and ITO as electrode material, without vacuum steps, has also been demonstrated [109, 110]. This resulted in significantly lower manufacturing cost and made the device modules environmentally safe, with simultaneous retention of their flexibility, efficiency and stability. The carbon electrode was rotary screen printed, and it was used as a back electrode in the flexible solar cell modules. For this, firstly the text pattern and the extraction lines for the electrode were printed at 10 m min^{-1} to obtain a nominal wet thickness of 10 μm, followed by IR drying and then a treatment using the hot air oven set to 140 °C. Subsequently, the interconnections between the cells of the module were rotary-screen-printed to obtain a nominal wet thickness of 40 μm at a web speed of 4 m min^{-1} under the same drying conditions. The modules manufactured using these electrodes were demonstrated to achieve efficiency up to 1.83%. Such substitution of carbon has established that the roll-to-roll manufacturing of the modules can still not be compromised using carbon electrodes, with the same fast printing and coating.

Similarly, low-temperature paintable carbon electrodes have been developed using Cu_2ZnSnS_4 (CZTS) nanoparticles as a potential HTL for perovskite solar cells [111]. The devices with a CZTS HTL showed a power conversion efficiency of 12.53% [111].

In order to extend the application of ITO-free electrodes to the wearable photoelectric devices, FTEs

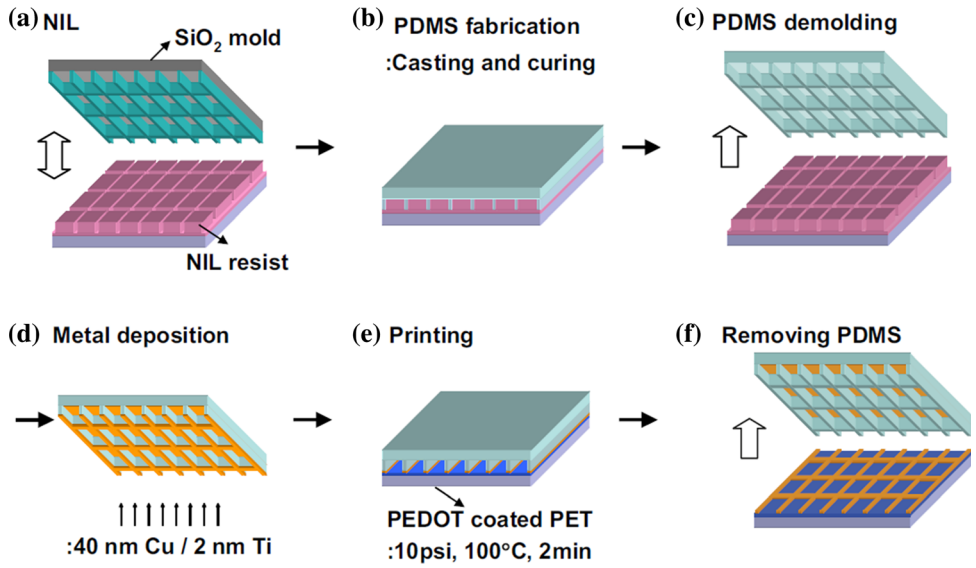

Figure 14 Schematic diagram of the fabrication of the PDMS stamp and the transfer printing of Cu nanowire mesh electrode. **a** The conventional NIL produces the resist template. **b** The PDMSs are drop-casted and cured. High modulus PDMS is first drop-casted and cured at 65 °C for 5 min. The commercial PDMS, Sylgard 184, is then drop-casted and cured at 65 °C for 2 h to mechanically support the first layer. **c** The PDMS is demolded after cooling down to room temperature. **d** 40-nm-thick Cu and 2-nm-thick Ti are sequentially deposited by electron-beam evaporation. **e** The Cu mesh on the PDMS stamp is transferred onto PEDOT:PSS coated PET substrate at 10 psi and 100 °C for 2 min. **f** Lifting up the PDMS stamp leaves the Cu mesh electrode on PEDOT:PSS coated PET substrate. Reproduced with permission from Elsevier (Ref. [101]).

have been shown to be important constituents of the solar cell modules. Although alternatives to ITO for highly flexible transparent electrodes have recently been reported, which include metal oxides, carbon nanomaterials and conductive polymers [112–114], the optoelectronic properties are still limited due to less pristine conductivity [115]. In contrast, materials like metallic nanowires and grids demonstrate high optoelectronic performance with less sheet resistances and efficient transmission, but have limited commercial applications due to poor mechanical properties [116, 117]. In order to fulfill these requirements, a homogeneously oriented PEDOT:PSS:reduced graphene oxide (RGO) composite was formed for its use in the FTEs [118]. This was achieved by using a thin layer of RGO through slot-die printing during roll-to-roll process. In order to fabricate the FTEs, the PEDOT:PSS:RGO composite layers were slot-die coated on the PET substrates. It was demonstrated that a subsequent hydroiodic acid post-treatment of these FTEs removes the insulating content of conductive polymer in PEDOT:PSS:RGO composite, and in addition, reduces the graphene oxide to improve the conductivity and endurance of electrodes. This also reduced the cost due to the use of carbon materials and R2R technologies. The devices based on PEDOT:PSS:RGO electrodes obtained an efficiency of 8.32%, higher than the efficiency of 7.69% obtained with conventional ITO-based PSCs.

Further, transparent conducting electrodes have also been developed through the roll-offset printing of silver-grid mesh patterns for the fabrication of all-solution-processed organic solar cells [119]. The roll-offset printing technique has been demonstrated to achieve higher printing resolution with a smooth thin-film surface roughness, as both the thickness and the surface roughness can be controlled by the coating process, and the line shape of the roll-offset-printed patterns can be controlled by other processes. It was demonstrated that for the devices with the printed Ag-mesh electrodes, a line pitch of 800 μm was achieved by using the roll-offset printing. These devices were shown to achieve an efficiency of 2.81%, higher than the efficiency of 2.76% of the ITO based devices.

Meng et al. [120] demonstrated the fabrication of flexible transparent electrodes composed of PEDOT:PSS and Ag grid/PET. The electrodes were fabricated by low-cost solution printing method in which viscosity, surface energy of PEDOT:PSS ink

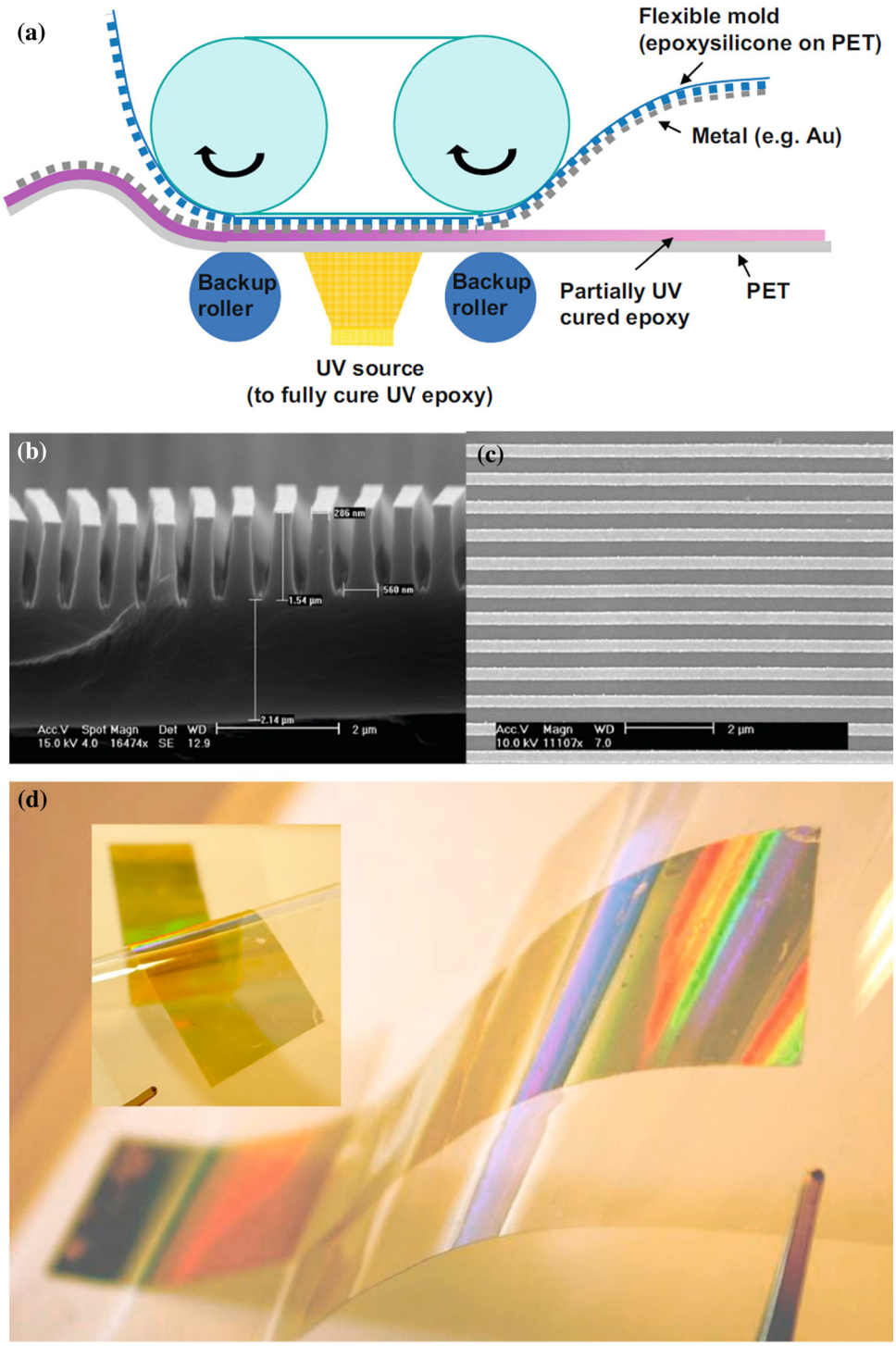

Figure 15 **a** Schematic of the R2R transfer printing process, **b** SEM images of the imprinted epoxysilicon grating structure on the replicated flexible mold, **c** the transferred Au nanograting on UV-cured epoxy coated on a PET substrate, and **d** photograph of large-area (32 mm × 184 mm) Au nanogratings on UV epoxy-coated PET substrate. Inset photograph shows the transparency of the Au nanogratings transferred to PET. Reproduced with permission from Elsevier (Ref. [101]).

and other printing parameters were controlled. An efficiency of 8.08% was achieved in the devices with these flexible transparent electrodes as compared to 7.54% using the ITO–PET transparent electrodes in the PTB7-Th:$PC_{71}BM$ devices.

In addition, flexible devices based on Ag-mesh flexible electrodes with a PCE of 11.5% have been fabricated using an Al-doped ZnO as ETL in PSCs [121].

Further, charge carrier selective electrodes for both electrons and holes have also been demonstrated [122]. This was achieved by using insertion layers of hydrophobically-recovered and contact-printed siloxane oligomers between electrodes and active

material. An insertion layer was used for both electrodes in P3HT:PCBM based solar cells, which makes each electrode more selective for one type of charge carriers, i.e., blocking electrons at anode and holes at cathode, leading to an improvement in the charge carrier extraction and thus, an increased device efficiency. A simple conformal contact of a PDMS stamp on a sample surface leads to the printing of oligomeric siloxane molecules, leading to an ultrathin layer of contact-printed siloxane oligomers on that surface. Thus, the insertion layer was formed at interface by unreacted siloxane oligomers diffused out from a cured PDMS stamp through conformal contacting for less than 100 s. The siloxane oligomer printed devices showed efficiency enhancement when compared to non-printed ones. However, this technique was demonstrated for the devices employing ITO as an electrode, but it may be explored for the flexible large-area devices without ITO. In addition, the contact-printing technique was demonstrated without the use of any vacuum or wet processing steps and, in addition, with its simplicity and large-area applicability, it was reported to be very useful for the R2R manufacturing of the solar cells.

Similar to the polymer solar cells, the roll-to-roll printing technology has been employed for the perovskite solar cells. Although the perovskite-based solar cells have recently emerged as effective extensions to the polymer-based solar cells, there are many challenges to address in the area of these solar cells, including the challenges related to the electrode material, and these challenges are described in brief below. In case of the perovskite solar cells, the scalability of the fabrication process has been reported to be achievable through these key steps—firstly, using the scalable coating or printing techniques in order to form the active perovskite layer, secondly, by processing the solar cells on flexible substrates, which requires lower process temperatures and finally, the printing/coating of the back electrode with efficient contact to the active material without affecting the beneath layers [123]. In case of the first step, for making the perovskite layer, one-step deposition technique (typically using mixture of methylammonium iodide (MAI) and $PbCl_2$ or PbI_2) or two-step deposition technique (typically using sequentially deposited layer of PbI_2, MAI by dip/spin coating) has been demonstrated. In order to achieve the scalability of these deposition steps, the spray coating and slot-die deposition methods have been shown to be compatible. Further, for the second step, the processing of the solar cells on flexible PET substrates at lower process temperatures has been reported, however, using the non-scalable fabrication steps like spin coating and vacuum deposition. Similarly, for the final step, the solution-based deposition or printing of the metal or carbon/silver back electrode in inverted devices using R2R-compatible process technologies has also been demonstrated. The printing of a metal back electrode, like silver electrode, under ambient conditions leads to the full replacement of the evaporated metal electrodes as well as the removal of the vacuum processing required during the use of an evaporated back electrode. Such technique may fully lead to high-throughput and cost-effective devices as envisaged by the R2R technology. In order to achieve this, using step-by-step approach of firstly introducing a screen-printed electrode, then shifting the fabrication from a rigid to a flexible PET substrate, and finally fabricating the device stack on a roll coater with slot-die coating, an upscaling process for the perovskite solar cells has been demonstrated [123]. For this, one/two-step deposition techniques were employed for the fabrication of two types of device geometries—normal one-step (Fig. 16a) and inverted two-step (Fig. 16b). It was reported that each of the fabrication procedures differs in performance for a different geometry, with one-step excellent for the ITO/PEDOT:PSS normal geometry substrate with 9.4% efficiency, while two-step better for the ITO/ZnO/PCBM inverted geometry substrate with 6.2% efficiency (Fig. 16c). With the perovskite material methylammonium lead triiodide ($MAPbI_3$) used as an absorber layer in the solar cell, efficiency up to 21% has been reported [124].

Further, screen printing of the metal electrodes was also demonstrated for both device geometries. In order to achieve the screen printing, a tiny benchtop-scale screen printer (Fig. 17a), made for single device batch processing, was employed. This screen printer has been reported to be similar to a R2R operated large machine to ensure the scalability of the printing process. Further, two different inks, a carbon-based ink and a solvent free UV-curable silver-based ink, were used for the screen printing of the electrodes. However, the carbon ink did not result in proper working devices, in contrast with the Ag-based ink, which resulted in better devices (Fig. 17b). Such difference in the device performances has been

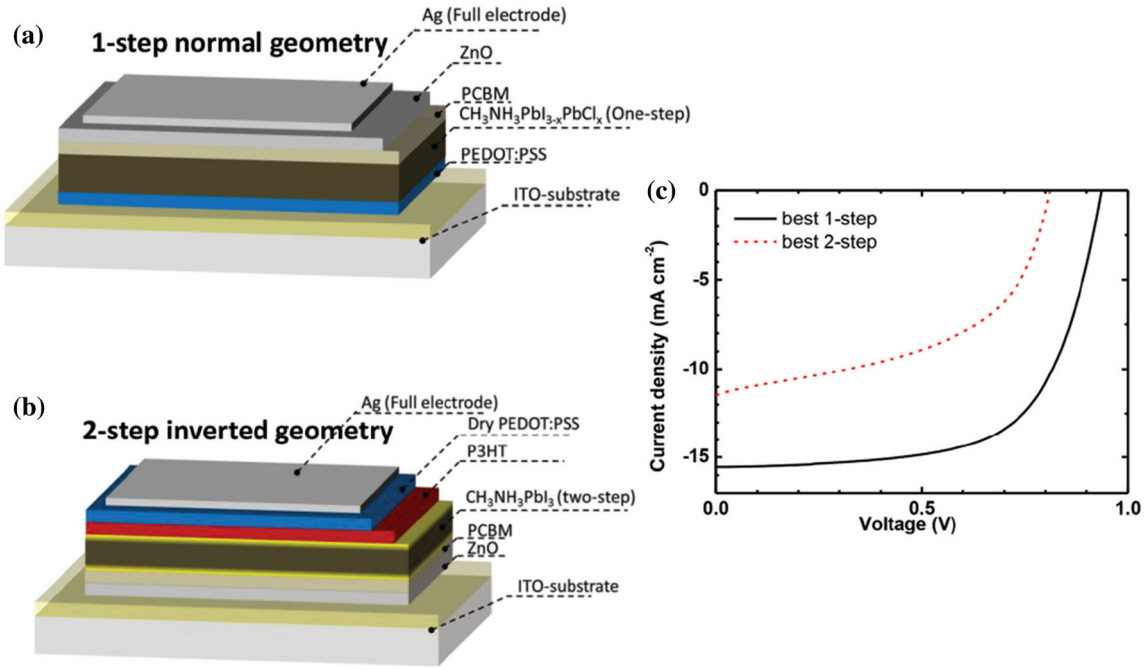

Figure 16 **a**, **b** Perovskite solar cell structures. **c** Best device using either the one-step normal geometry procedure or the two-step inverted geometry procedure. Both devices employ a glass/ITO substrate and an evaporated silver electrode. Reference [123] Copyright Wiley-VCH Verlag GmbH & Co. KGaA. Reproduced with permission.

attributed to the reaction of carbon with iodide/triiodide, leading to contact with perovskite film, or through exposure of carbon to perovskite degraded by materials like gas-phase hydrogen iodide. The screen printing of the metal electrodes was further extended from the ITO-glass to ITO-PET substrates. However, switching from evaporation to the screen printing of the electrodes was shown to reduce the device performance (Fig. 17c, d). Although this technique was demonstrated for the devices using ITO as an electrode, it may be explored for the flexible large-area devices without ITO.

For the full upscaling, the application of slot-die coating of the perovskite layer on the flexible substrates using a mini-roll coater setup (Fig. 18a) for both one/two-step perovskite solar cells was also demonstrated. However, it was found that this upscaling process resulted in 50% performance loss, where the efficiency dropped from 9.4 to 4.9% (Fig. 18b).

Environmental and processing stable materials

The stability of the solar cells manufactured through roll-to-roll processing is an important parameter and depends upon the stability of the constituent materials under the environmental conditions. These conditions are reported to influence the physical properties of the materials of roll-to-roll manufactured devices, which lead to stability issues in these devices. Further, the stability of the constituent materials under the processing conditions is also an important parameter [44, 50, 125–146]. This section includes many reported studies on the influence of the processing conditions on the stability of the constituent materials. Also, the methods to address these issues as well as several environmental and processing stable materials have also been explored in this section.

It is well known that in order to achieve high performance through a set of materials which are used in the manufacturing of the devices, the physical properties of these materials need to be optimized. However, such tuning up of the properties of the materials may also necessitate the compromise or improvement in other important parameters which affect the performance of the devices. One of these important parameters is the stability of the devices, which may be affected by the changes introduced in the physical properties of the materials for improved performance in other parameters like efficiency. For example, one of the ways to improve the V_{OC} is to

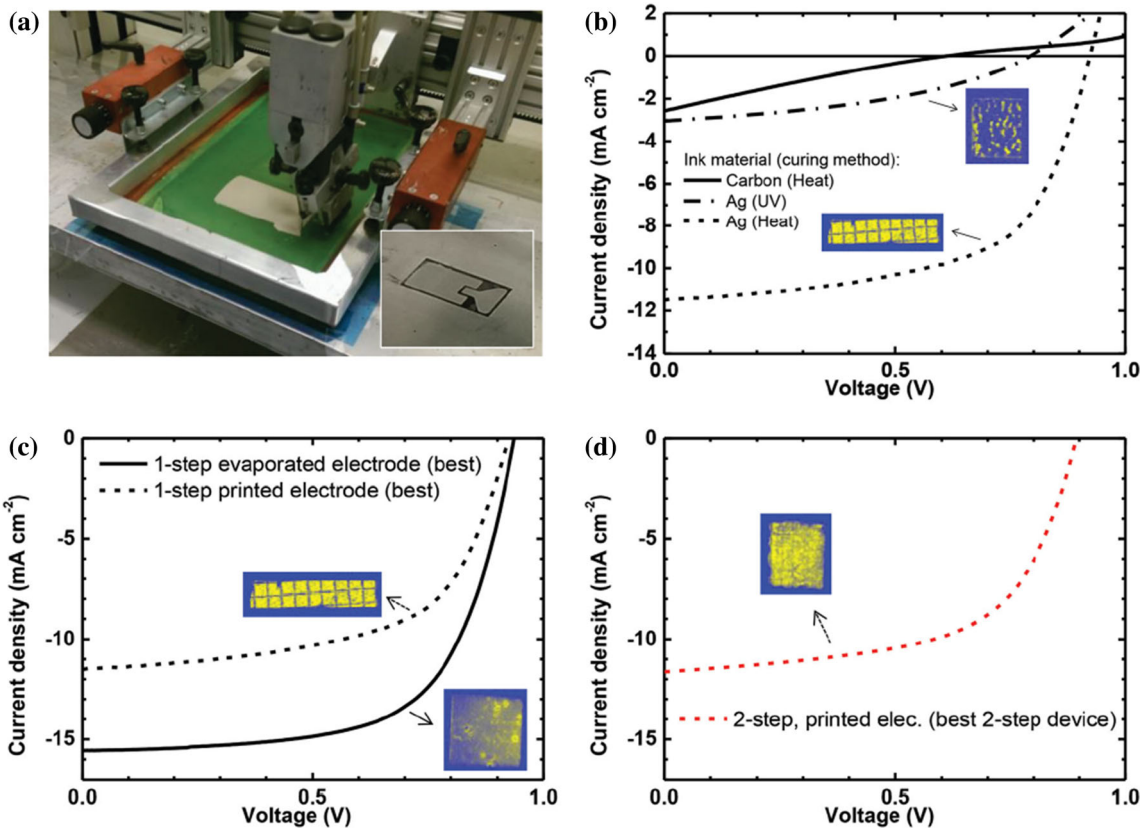

Figure 17 **a** Photograph of the screen printing setup shown during printing of a single device, with the inset showing the 5 × 2.5 cm^2 glass substrate immediately after the screen has lifted. **b** Typical *J*–*V* characteristics of one-step devices comparing three different electrode printing processes using either a heat-curable carbon ink, or a UV- or heat-curable silver ink, where the carbon and UV ink impose damage to the underlying solar cell stack (solid line), the heat curable does not (dashed line). The inset shows the light beam-induced current (LBIC) maps of the respective devices, with signal intensity going from blue to yellow revealing defectuous areas of the device. The heat-cured device LBIC is imposed with a millimeter grid to measure its size. **c**, **d** Comparison of *J*–*V* characteristics of one- and two-step devices, respectively, having either an evaporated (solid line) or a printed electrode (dashed line). Again, the insets show LBIC maps of the devices, with a millimeter grid imposed on the printed device LBICs. All LBIC intensity scales are normalized to the peak intensity for each device and are not intercomparable. Reference [123] Copyright Wiley-VCH Verlag GmbH & Co. KGaA. Reproduced with permission.

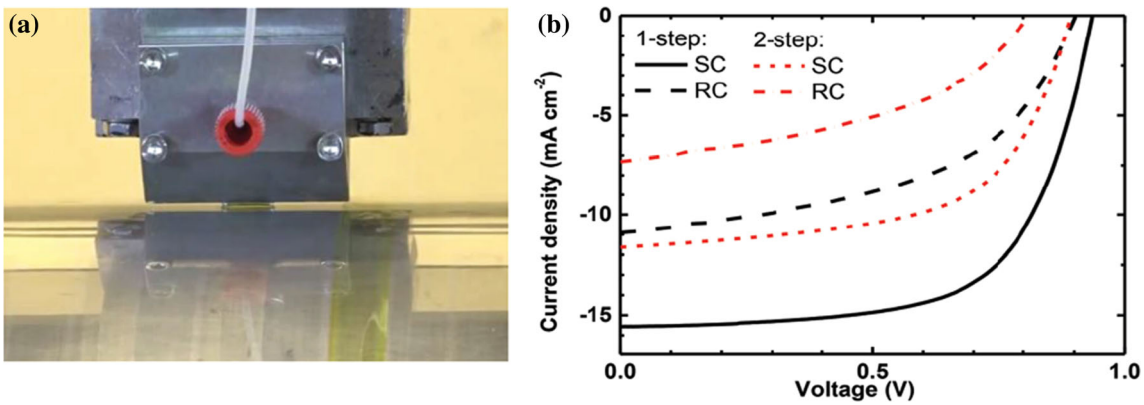

Figure 18 **a** Photograph of the slot-die roll coating process, here of a layer of PbI_2, where an already coated stripe is visible to the right. **b** The *J*–*V* curves of the best one- and two-step devices comparing spin coating (SC) with roll coating (RC). Reference [123] Copyright Wiley-VCH Verlag GmbH & Co. KGaA. Reproduced with permission.

lower the HOMO level of the donor polymer. One strategy employed in order to achieve this has been the use of strong electron taking groups, e.g., fluorine atoms, into the acceptor monomer backbone [125]. The higher electron affinity likely enhances the intermolecular packing and therefore results in higher hole mobility. The use of fluorine into the 5,6-positions of the BT unit and analogs has been explored extensively, leading to new polymer materials with higher efficiency of more than 8% [126, 127]. In addition, many of these polymers have been reported to perform well even with more than 200-nm-thick R2R-compatible active layer. The copolymerization of 5,6-difluorinated BT and BDT with alkylthiophenes has been reported to achieve high efficiency even at higher 300 nm thickness without any application of solvent annealing, additives or post-treatments [126]. The application of combining fluorine and methyl together to enhance charge carrier mobilities and improve the morphology has also been demonstrated to achieve the efficiencies over 11% for devices with an active layer thickness over 400 nm [128]. In addition, the efficiencies of over 14% for the R2R-compatible devices with 300-nm-thick active layers have also been reported [129, 130]. Nevertheless, the fluorine substituents have been shown to affect the stability of the polymers and thereby that of PSC devices [125]. For example, for flexible high-area R2R devices, the application of low-bandgap polymer series based on benzo[1,2-b:4,5-b′]dithiophene (BDT) and dithienylbenzothiadiazole, with different numbers of fluorine substituents on the 2,3,1-benzothiadiazole unit, has been reported in order to study the photochemical degrading of polymer and operating lifetime in these solar cells [125]. For this, two polymer series, (P1–P3) and (P4–P6) (Fig. 19), with different numbers of fluorine atoms on the BT unit and with distinctive side chains on the BDT unit were synthesized. The longer alkyl side chains have been attributed to provide enhanced solubility required in large-scale and high-speed processing of active layer solutions having concentrations above 50 mg/mL. It was revealed that the fluorine improved the photochemical stability. The photochemical stability was shown to enhance with the number of fluorine atoms [125]. In addition, the 2-hexyldecylthiophene (P4–P6) side chains on the BDT unit were also shown to provide better photochemical stability than 2-hexyldecyloxy side chains (P1–P3). Further, the P1–P6 series was also shown to exhibit enhancement in the photochemical stability as compared to P3HT. This was attributed to their relative deficiency of side chains linked to the backbone as compared to P3HT.

In addition to the stability of these polymers, the stability of the roll-to-roll manufactured devices based on these polymers series P1–P6 was also studied [125]. For this, the devices were fabricated on a PET-based material substrate. This material was prepared by R2R coating of silver grid, PEDOT and ZnO. Both active layer and back PEDOT:PSS were slot-die coated, and the back silver electrode was flexographically printed in an inverted geometry: PET substrate/Ag-grid/PEDOT:PSS/ZnO/active layer/PEDOT:PSS/Ag (Fig. 20a). It was found that the incorporation of fluorine atoms leads to an increase in the V_{OC} of the fabricated devices for both polymer series (P1–P3) and (P4–P6) (Fig. 20b). The best device efficiency of 3.8% was achieved for (P4–P6) series for an active area of 1 cm^2 [125]. In addition, the lifetime measurements done on these devices showed an initial faster decay in the performance for (P4–P6), followed by relatively slow decay rate [125].

Similarly, narrow-bandgap copolymers PIDTFPQ and PIDTFTQ based on bulky indacenodithiophene (IDT) and mono-fluorophenanthrenequinoxaline (FPQ) or mono-fluorodithienobenzoquinoxaline (FTQ), possessing a large fused phenanthrene or benzodithiophene ring on top of pyrazine unit, have been synthesized for the application of manufacturing of solar cells through roll-to-roll coating method [131]. These polymers showed better properties in terms of their stability, making them suitable for large-area devices. Both polymers showed a decomposition temperature (T_d, 5% weight loss) exceeding 420 °C, indicating that their thermal stability was sufficiently enough for application in PSCs. Further, no glass transition or melting behavior was observed for both polymers. However, it has also been reported earlier that the processing conditions of post-treatments like solvent additives or thermal annealing, which are used for the improvement in the device performance, are unfavorable for fabricating large-area solar cells, especially for the printing or roll-to-roll manufacturing technology [131]. This requirement makes it important for the polymers to show better properties for better performance in case of the large-area devices, without the application of any solvent additives or thermal annealing. It was

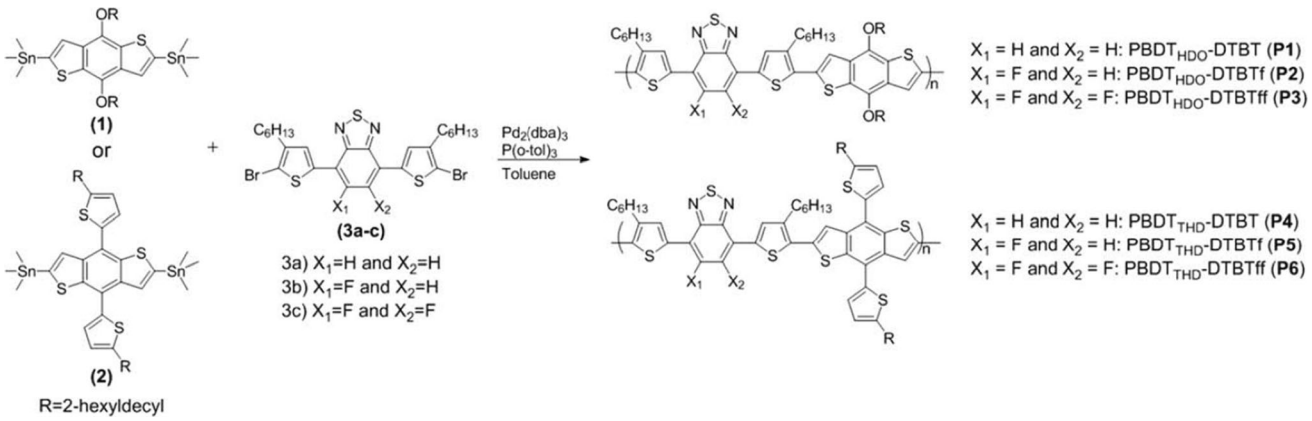

Figure 19 Synthesis of polymers: $PBDT_{OHD}$-DTBT (P1), $PBDT_{OH}$D-DTBTf (P2), $PBDT_{OHD}$-DTBTff (P3), $PBDT_{THD}$-DTBT (P4), $PBDT_{THD}$-DTBTf (P5), and $PBDT_{THD}$-DTBTff (P6). Reference [125] Copyright Wiley-VCH Verlag GmbH & Co. KGaA. Reproduced with permission.

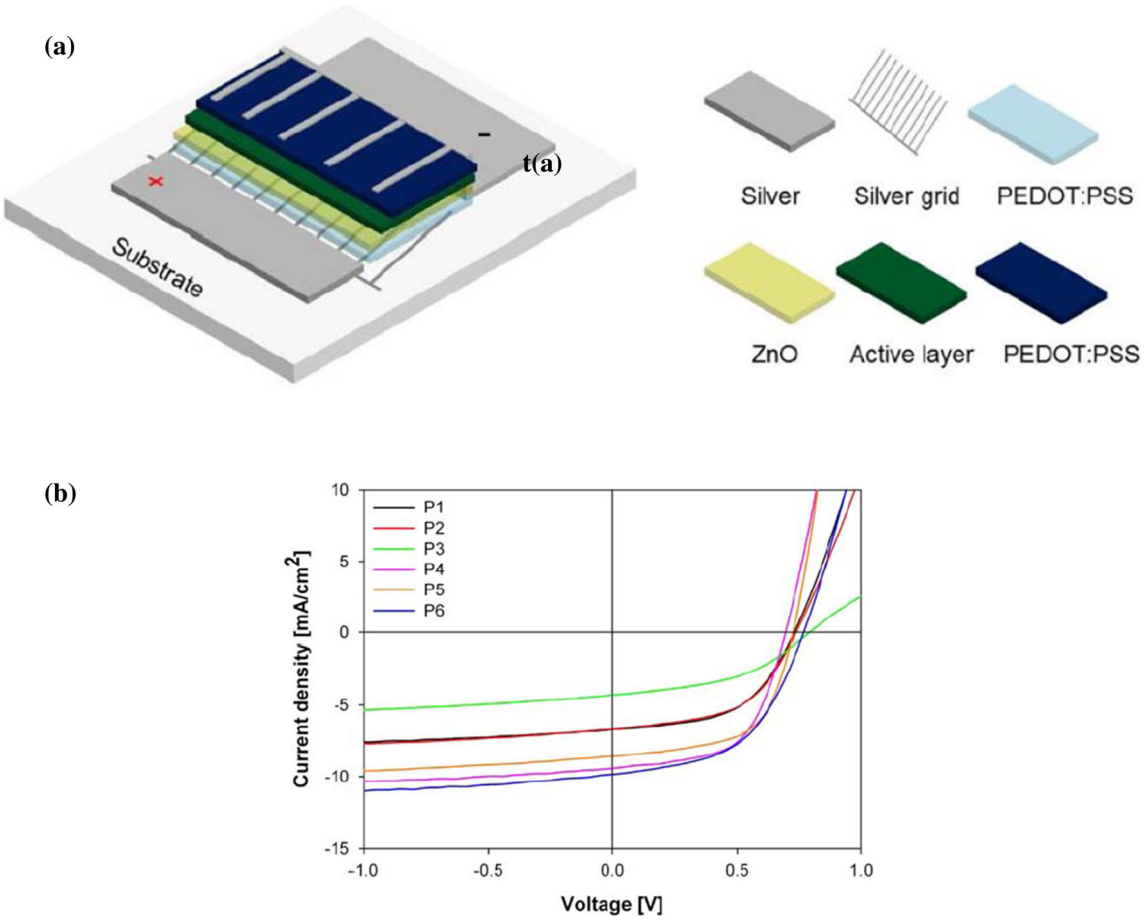

Figure 20 **a** Schematic representation of the PSC devices with an inverted geometry of PET substrate/silver-grid/PEDOT:PSS/ZnO/active layer/PEDOT:PSS/silver. **b** *J–V* characteristics of the best performing flexible and ITO-free PSC devices based on the polymers P1–P6. Reference [125] Copyright Wiley-VCH Verlag GmbH & Co. KGaA. Reproduced with permission.

revealed that the narrow-bandgap copolymers PIDTFPQ and PIDTFTQ showed improved optical properties, electrochemical properties, π–π packing behavior, charge carrier transport, morphology and photovoltaic properties leading to efficiencies of 5.54% and 5.00% of the devices, without using any

solvent additives or thermal annealing, making these materials suitable for the large-area roll-to-roll manufacturing technology [131].

Similarly for the inverted planar solar cells, a simple method to modify interfaces has been developed by using a hybrid ligands interfacial layer, which has been demonstrated to reduce open-circuit voltage loss in solar cells as well as enhance the stability of these devices [132]. In order to transfer ligands, quantum dots were used as intermedia without affecting perovskite, leading to band bending on top surface of perovskite film. This resulted in a 20.6% PCE, and these devices showed enhanced stability after quantum dots modification [132].

Among the donor polymers and acceptor materials used for the solar cells, only some like P3HT:PCBM have shown ability to withstand the difficult conditions of large-area R2R processing [44]. These conditions include all-solution processing, ambient atmospheric conditions and multiple cycled higher temperatures. Further, P3HT:PCBM devices have also been reported to perform better with thick (> 200 nm) active layers [44]. However, as discussed, in order to speed up the research on the higher-area device performance, new better-performing, R2R-compatible and processing stable alternatives to P3HT are also required to be synthesized. Helgesen et al. showed the synthetic optimization of a copolymer PDTSTTz (Fig. 21), based on DTS and TTz, for the device processing [44]. The PDTSTTz:PCBM blend thin films have been reported to undergo less photochemical degradation during accelerated aging conditions [133] and can withstand

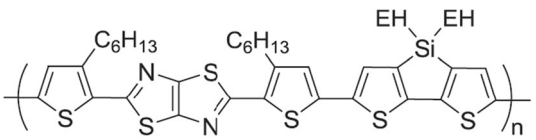

PDTSTTz-3

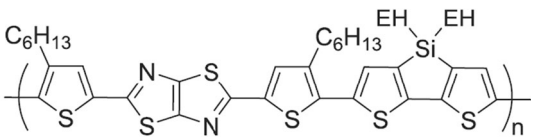

PDTSTTz-4

Figure 21 Molecular structure of the polymers PDTSTTz-3 and PDTSTTz-4. EH = 2-ethylhexyl. Reference [44] Copyright Wiley-VCH Verlag GmbH & Co. KGaA. Reproduced with permission.

thermal annealing without showing any performance loss [134, 135]. Among these properties, the excellent photochemical stability is an essential quality for the materials which are required to undergo R2R processing [44]. The solar cells based on PDTSTTz:PCBM were fabricated using R2R processing, and efficiencies up to 3.5% were reported with roll-coated devices [44]. In addition, better processing control and device performance was also reported with the roll-coated PDTSTTz-4:PCBM devices, making PDTSTTz-4 polymer as a potential material for R2R technology [44].

Some of the widely used donor polymers used in the highest performance devices are BDT-TT donor polymers, PTB7 and PTB7-Th, which have also been studied for their stability [136]. Many other polymers based on the BDT-TT donor polymer backbone have also been used in high-performance devices, but these polymers have been shown to degrade rapidly in the presence of light and oxygen [136, 137]. However, one of the factors which affect the stability of BDT-TT polymers is the widespread use of high boiling point solvent additives, with DIO being the most common [136]. The effect of DIO on stability has been attributed to its rapid photolysis in UV light, which generates reactive iodine and iodooctane radicals that can react with the polymer backbone [136]. However, for polymers like PTB7 having alkoxy side chains, the oxygen atom helps to stabilize the structure toward H-abstraction and subsequent oxidation [136]. The study on the influence of the solvent additives on the stability of the polymers like PTB7 and PTB7-Th has revealed that the option of pendant side chain as well as solvents used significantly influence active layer stability, with alkyl thienyl side chain polymers to be lesser stable than alkoxy side chain polymers [136]. In addition, high-boiling-point additives like DIO are found to significantly enhance photoinduced degradation unless completely removed [136]. This accelerated photooxidation has been reported to be attributed to the enhanced oxygen diffusion in films with residual solvent [136]. The study has also reported the application of the non-halogenated solvent *o*-xylene with 2% *N*-methylpyrrolidone as a method to achieve lesser active layer degradation [136]. This method also results in maintaining the favorable intermixture of morphology, which is otherwise achieved by using halogenated additives with higher boiling points.

Such polymer stability is important to make the better scalable and R2R-compatible polymers [136].

Similarly, the effects of the presence of the high-boiling additives in trace amounts in PEDOT:PSS, after coating/printing of the HTL, on the stability of the fully ambient R2R processed ITO-free modules are also reported [138]. These high-boiling additives are added to HTL for conductivity improvement and remain as residual and therefore may affect the long-term operating lifetime of the device. In order to understand such influence of the additives, different combinations of PEDOT types or formulations were used for both the front/back HTL in the manufacturing of the solar cell modules. These modules were then subjected to different kinds of lifetime studies following well-established protocols (Fig. 22) [138]. For the main stability test under high-humidity/high-temperature conditions, it was found that all the combinations degraded fast and almost no stabilization was found for either combination (Fig. 22). However, during the outdoor operation, the addition of EG, instead of DMSO, as an additive, was found to significantly improve the operational stability of the modules [138]. The roll-to-roll-based drying method is faster as compared to spin coating, and the mechanism accounted to be responsible for the effects of the solvents has been related to the polarity of the solvents, with DMSO being a highly polar ($\varepsilon_r = 48$) high boiling solvent while EG being less polar ($\varepsilon_r = 41$) high boiling solvent [138]. Also, during the drying, the liquid phase of the initial aqueous HTL dispersion has been reported to comprise only the high-boiling solvent to a large extent toward the end of the drying. For DMSO, the exposure of the ionic part of the HTL is favorable giving a higher hydrophilic surface, while for EG, the higher apolar parts of the HTL are exposed [138]. Therefore, the enhanced hydrophilicity of HTL dried with DMSO has been reported to be a likely reason for the observed

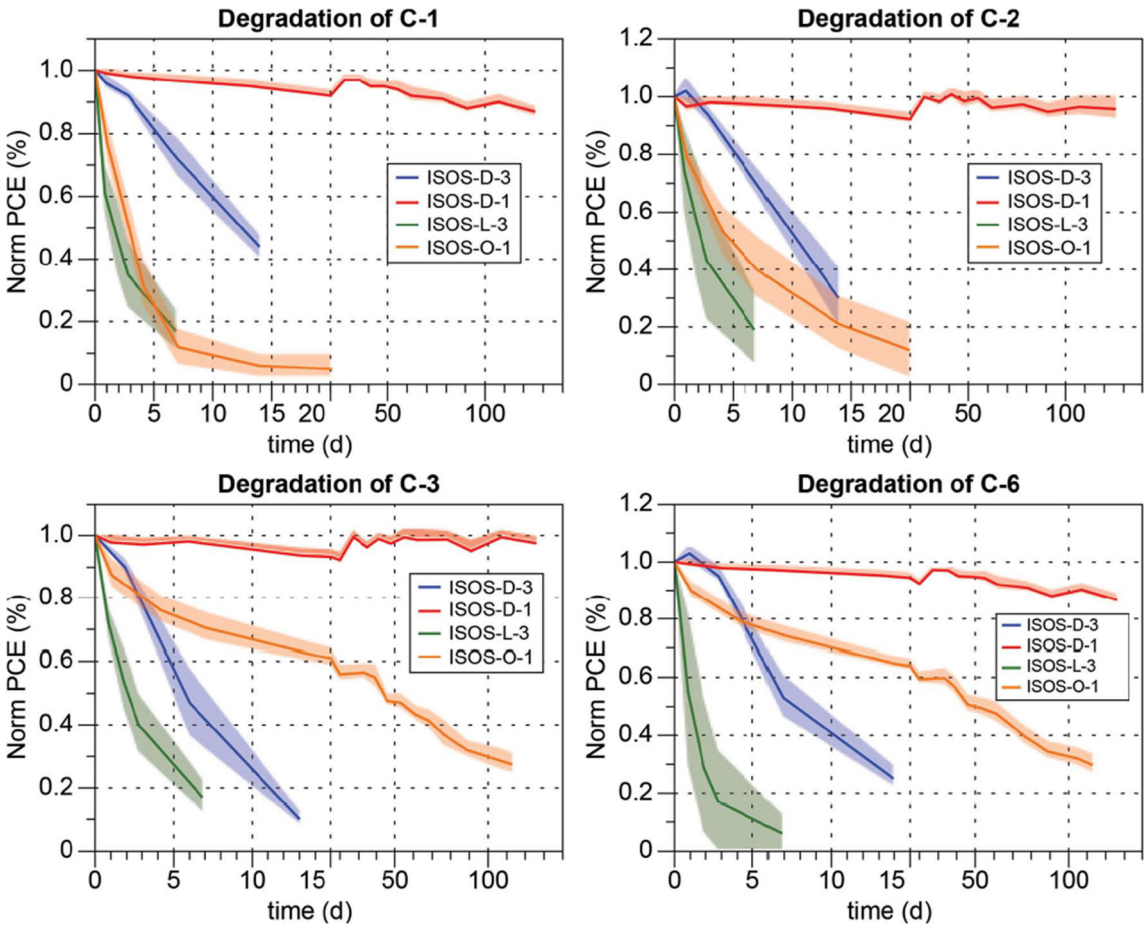

Figure 22 Degradation curves for each ISOS condition for the four chosen PEDOT:PSS combinations. Reference [138] Copyright Wiley-VCH Verlag GmbH & Co. KGaA. Reproduced with permission.

increase in operational degradation for the devices even with no water [138].

One of the issues in BHJs is the generation of the S-shaped curves or S-kinks in the current–voltage characteristics of the solar cells, which leads to low fill factor and thus, poor stability and reduced device efficiency of these devices. This S-shaped curve is often attributed to an energy barrier resulting in inefficient carrier transport in one of the layers/interfaces, thus preventing charge extraction [139]. Further, the S-shaped curve generation has also been reported in case of the large-scale production of devices [139]. The devices were processed under multiple post-production treatments like high-intensity (1000 W m^{-2}) and low-intensity (280 W m^{-2}) illumination, and thermal annealing at temperatures of 65, 85 and 105 °C in an air atmosphere for 90 min in the dark. These multiple post-production treatments were done in order to understand the effects of temperature, illumination and atmosphere on the characteristics of repeated current–voltage scans (photoannealing) of the devices. However, it was shown that after exposure to 1000 W m^{-2} illumination at 85 °C and repeated current–voltage scans, the inflection point or S-shaped curve gradually disappeared with significant improvement in the performance [139]. In addition, the atmosphere also plays important role in the inflection point phenomenon. In order to understand this, encapsulated cells were tested in the atmosphere of air, oxygen and nitrogen at 85 ± 3 °C and under 1000 W m^{-2} illumination, which revealed quite similar behavior in the inflection point phenomenon regardless of atmosphere (Fig. 23d–f). In this test, at the beginning, the curves showed a clear inflection which was removed over the course of 10 min. In addition, experiments with the cells not encapsulated after processing were also done, and distinctly different behavior of these cells in various atmospheres was observed (Fig. 23a–c). No photovoltaic response in air or oxygen regardless of time was observed in this case; however, the photocurrent extracted at − 1.25 V decreased quickly in air and even more rapidly in oxygen. This deterioration of photocurrent was attributed to an oxidative degradation of P3HT accelerated by temperature and illumination.

Further, the experiments on the encapsulated cell, left in an oxygen-rich atmosphere for 14 days and subsequently photoannealed under standard conditions (air, 85 °C, AM 1.5G, 1000 W m^{-2}) were also done (Fig. 24a, b). Using TOF–SIMS and XPS analyses of interfaces and surfaces, the study also reported photooxidation and redistribution of oxygen inside the cell based on ZnO photoconductivity. In this process, ZnO can photocatalyze the degradation of organic species, suggesting the occurring of major chemical processes in the bulk of the nanoporous ZnO and at the ZnO–P3HT:PCBM interface [139].

Roll-to-roll-compatible processing techniques

This section deals with the various processing techniques and parameters used during the manufacturing of the roll-to-roll-processed solar cells, and their impact on the important parameters influencing the device performance, e.g., morphology of the deposited films, is also discussed. The methods used to address these issues are also discussed. In addition to the polymer solar cells, similar studies on the roll-to-roll-processed perovskite solar cells are also discussed in detail in this section.

One of the factors which have been shown to affect the device efficiency is the morphology of the deposited films of the active layer including the large donor/acceptor phase separation in all-polymer BHJs [50, 140]. Depending upon the parameters during the deposition and the type of the deposition technique, the morphology of the coated films can show variation. Hong et al. demonstrated the application of slot-die coating technique using the low-viscosity solutions of the blends of P3HT and PCBM, and reported the influence of the factors like mask shim length, coating speed and substrate temperature on the quality/thickness the deposited films [141]. As discussed earlier, in a slot-die apparatus, the ink to be deposited is forced to the internal of the slot-die head and then forced out through a narrow gap between top and bottom parts of the head (Fig. 25). A shim mask is a thin mask which allows the ink to be deposited on the top of substrate after passing through it (Fig. 25). Several thickness control factors are considered when using shim masks, which determine the quality and thickness of the coated films, such as substrate temperature, shim length, coating speed, pumping rate, gap distance and solution concentrations [141]. The shim length is defined as the length of the protruding part of the mask from the slot-die head and is very important factor for uniform film. The study found that the

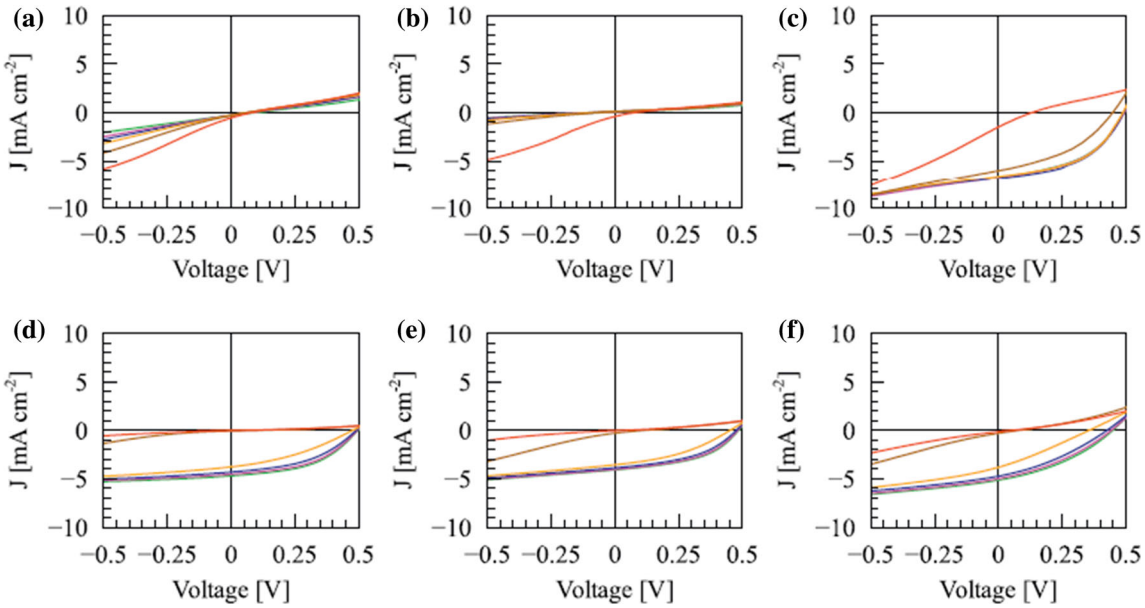

Figure 23 Change of IV curves under photoannealing of unencapsulated and encapsulated cells in different atmospheres **a** unencapsulated in air, **b** unencapsulated in O_2, **c** unencapsulated in N_2, **d** encapsulated in air, **e** encapsulated in O_2 and **f** encapsulated in N_2. Colors of curves correspond to time (red) 1 min, (brown) 5 min, (orange) 10 min, (blue) 15 min, (pink) 20 min and (green) 25 min. Reproduced with permission from Elsevier (Ref. [139]).

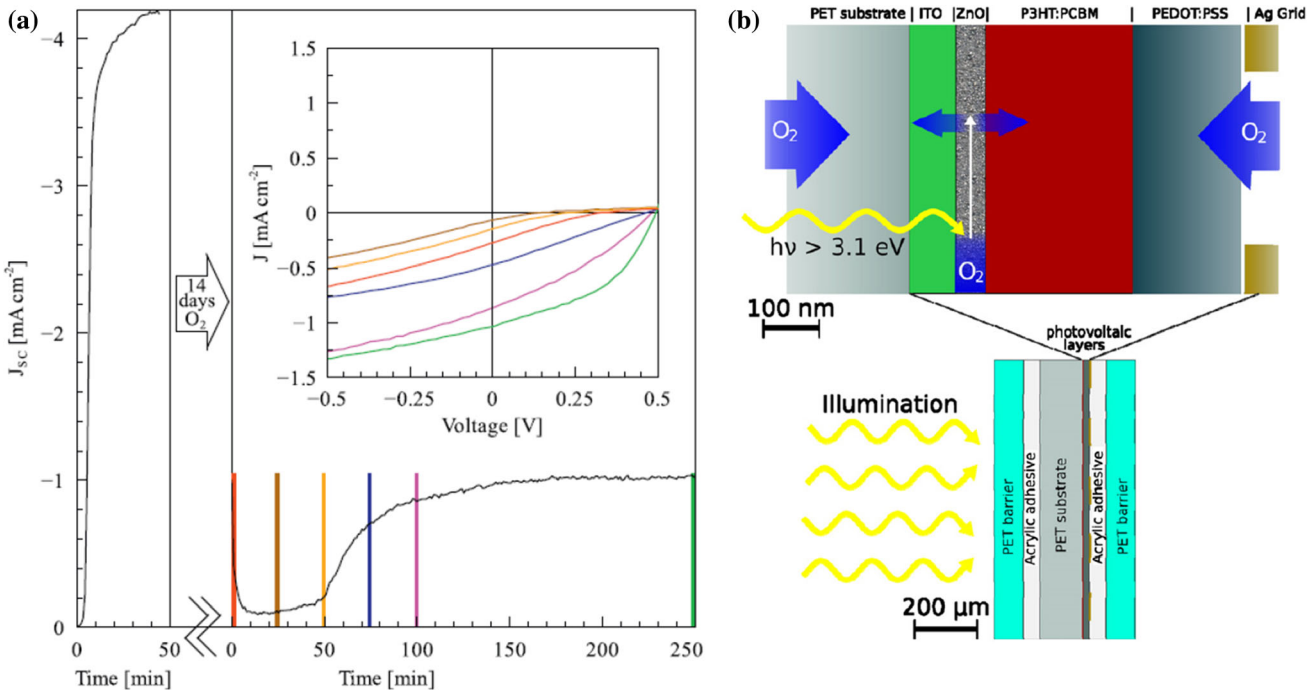

Figure 24 **a** Change in J_{SC} under photoannealing in oxygen atmosphere (before *x*-axis break) and re-annealing after storage in a 95% oxygen atmosphere for 14 days (after *x*-axis break). Inset shows evolution of IV curves at (red) 0 min, (brown) 25 min, (orange) 50 min, (blue) 75 min, (pink) 100 min and (green) 250 min. **b** Schematic of proposed oxygen redistribution upon illumination and heating. Reproduced with permission from Elsevier (Ref. [139]).

thickness of P3HT:PCBM increases with the shim length. Further, the substrate temperature was shown to affect solvent evaporation and thereby the film morphology. It was reported that for high substrate

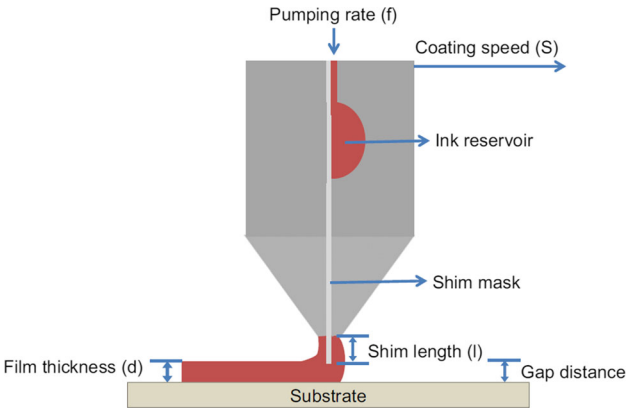

Figure 25 A schematic of the coating parameters used in slot-die coating. Reproduced with permission from Elsevier (Ref. [141]).

temperature, the evaporation of the chlorobenzene solvent was quick as compared to the room temperature evaporation, which decreased the solid content agglomeration time, thereby giving a uniform film. Further, it was found that the thickness of the film is shown to decrease with high coating speed due to low surface tension. Also, large-area spin-coated and slot-die coated devices showed efficiency of 2.67% and 3.07%, with a uniform average efficiency of 2.58% for high-throughput (5.0 m/min) slot-die-coated devices [141].

The donor/acceptor polymer crystallization, leading to large-scale phase separation in all-polymer devices, is also an important factor considered during the roll-to-roll deposition of the materials for the cells [142]. Higher crystallinity has been shown to improve the charge carrier mobility and thereby facilitate the charge collection leading to improved device efficiency [143]. Previous studies have reported that a better optimization between the donor/acceptor phase separation and the crystallinity can be achieved by post-deposition thermal or solvent vapor annealing [144, 145]. However, as discussed earlier, the conditions of post-treatments like solvent additives or thermal annealing have been reported to be unfavorable for fabricating large-area solar cells, especially for the printing or roll-to-roll manufacturing technology [131]. Therefore, it is important to control both phase separation and the crystallinity of the donor and acceptor polymers without any post-treatments like solvent additives or thermal annealing, in order to achieve a better performance of the solar cells compatible for the roll-to-roll manufacturing technology. In order to control the crystallization behavior, a non-regular heavy polymer side chain has been used in the polymer to disrupt the polymer chain packing. This prevented the crystallization and formed amorphous polymer blends (Fig. 26a), which were then used in R2R printing of all-polymer solar cells using a custom-built mini R2R coater (Fig. 26b) [50]. It was shown that the irregular bulky polymer side chain into the backbone prevents the conjugated polymer from crystallizing even when it is given sufficient duration by using a high boiling point solvent. For this, the study employed the application of combinations of two isoindigo-based conjugated polymers as donor polymers—(PII2T), with branched alkyl side chains, and randomly copolymerized (PII2T-PS), with 90% branched alkyl side chains and 10% polystyrene (PS) (Fig. 26c). In addition, two PNDIT- and PPDIT-based acceptor polymers were also used (Fig. 26d) [50]. In case of the donor polymers, depending upon the type of polymer side chain, significant differences in the GIXD diffraction patterns were found, revealing different degree of ordering in these polymers. The polymer PII2T with highly regular branched alkyl side chains showed a high degree of ordering, while with the heavy PS side chains, the ordering of PII2T-PS was severely disrupted. It was found that a high phase separation size is related to a higher relative degree of crystallinity of at least one of the polymers in the blends [50]. Also, these polymers were used for the manufacturing of the all-polymer BHJs, and it was demonstrated that with the combination of the donor and acceptor polymers, both having low crystallinity, a reduction in the phase separation size was achieved leading to better performance of the devices. In addition, large-area all-polymer R2R printed solar cells were also demonstrated, with efficiencies of 5% for cell area up to 10 cm^2 [50]. Similarly, the lower domain sizes and stable coating morphology, obtained with the donor and acceptor polymers having low crystallinity, were attributed to make them suitable for roll-to-roll manufacturing technology regardless of coating speed [50].

The BHJ morphology has also been reported to be highly sensitive to solvent drying dynamics, which are significantly different during and after the spin coating. Therefore, the process parameters optimized for spin coating cannot be directly used for R2R technology [146]. Hence, a detailed understanding of the morphology/crystallization evolution of materials during R2R processing is important from this

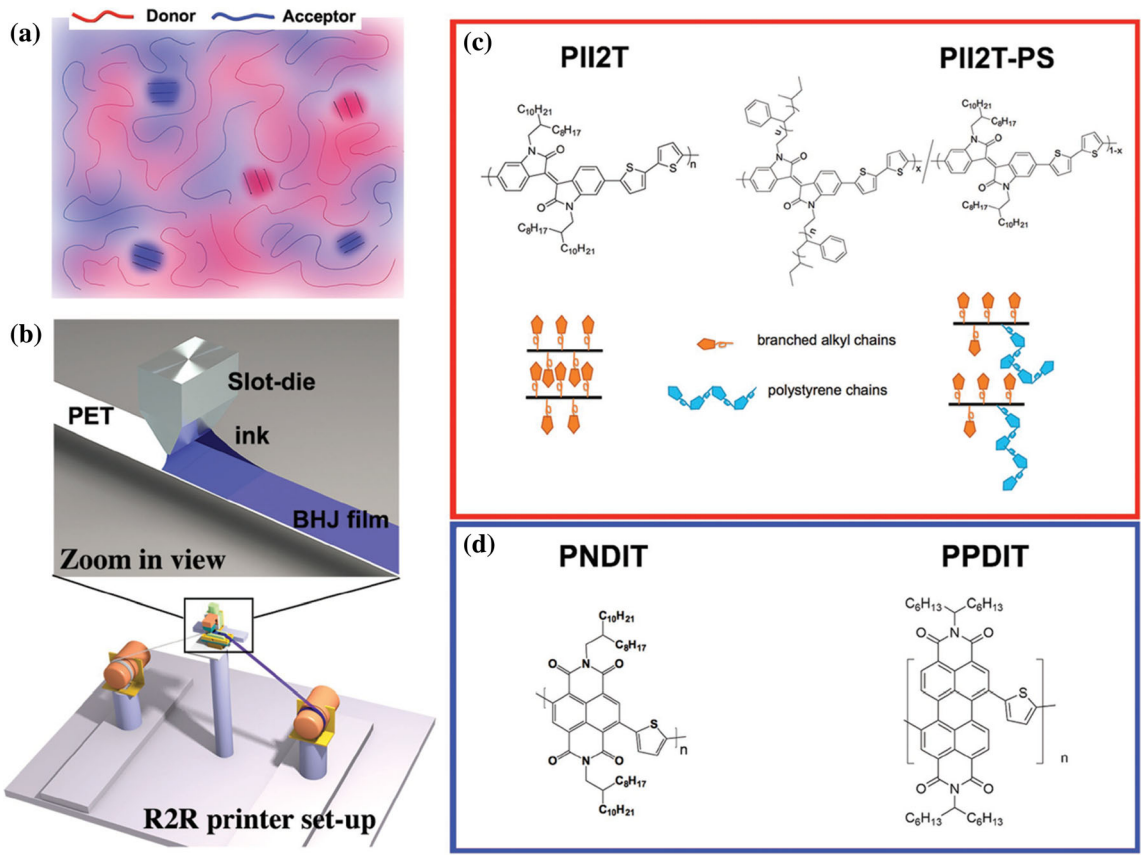

Figure 26 **a** Illustration of BHJ morphology for intermixed donor and polymer chains. Red lines represent the donor chain and blue lines represent the acceptor chain. **b** R2R printing using a slot-die coater setup. Top figure shows the zoom-in view of the slot-die coating process. **c** Chemical structure of two isoindigo-based donor polymers used in this work. In the right plot, the degree of polymerization ratio between $X = 10$ determines the percentage of polystyrene (PS) side chain. Schematic of packing structure with regular branched alkyl side chains, which can form ordered crystalline domains and irregular bulky PS side chains were shown next to it, which inhibit the formation of ordered crystalline domain. **d** Chemical structure of the acceptor polymers PNDIT and PPDIT. Reference [50] Copyright Wiley-VCH Verlag GmbH & Co. KGaA. Reproduced with permission.

point of view. One of the widely used powerful and nondestructive tools for this is X-ray scattering, which is widely applied to study the molecular packing structures of polymers, e.g., molecular orientation, relative crystalline size distribution and degree of crystallinity [146]. However, such facilities lack in situ X-ray scattering during the roll-to-roll coating, in which the speed of coating can be large to replicate high-throughput coating and also can help to study the crystallization dynamics during the solvent evaporation. Therefore, for in situ X-ray scattering, crystallization tracking roll-to-roll coaters have been developed (Fig. 27) [146]. In this setup (Fig. 27), the ink is deposited on a flexible substrate and the corresponding morphology information from the substrate is obtained using the X-ray scattering measurements at the different drying stage (Fig. 28). Also, this technique has potential for direct probing of both polymer chain packing order close to the drying edge as well as orientation in the dried film, in a single in situ printing experiment. A wide range of dry time resolutions, from ms to seconds, was shown to be achieved for the P3HT films. The different drying time resolutions facilitated the studying the crystallization during fast/slow drying as determined by coating parameters [146].

Jeong et al. reported a method of highly ordered nanoscale texturing for altering the material morphology to make it compatible with roll-to-roll process [147]. This method significantly improved many physical and chemical functions like effective broadband antireflection, light trapping effects, the surface properties and light absorption in polymer solar cells. Such nanoscale texturing can be achieved through the

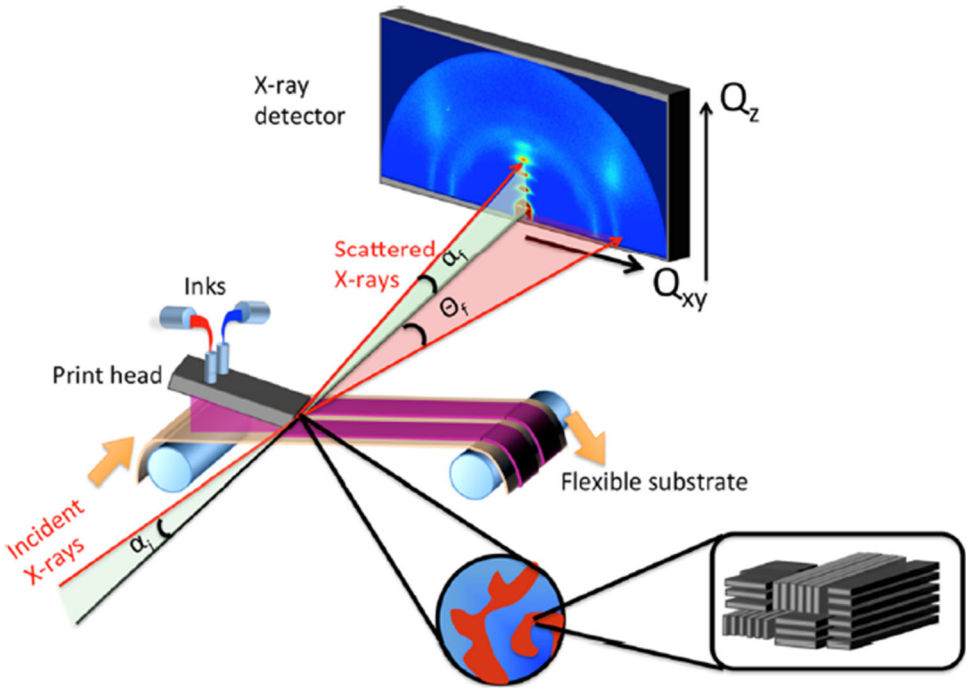

Figure 27 Schematic of the in situ X-ray scattering setup for direct monitoring of the drying dynamics and morphology evolution using a mini-roll-to-roll coater. Grazing incidence X-ray scattering is performed during the printing process, and the diffraction images are collected with a fast area detector. The crystalline structure of polymer and polymer blends are extracted from diffraction data to understand the morphology evolution of the R2R-coated semiconductor film. Reprinted with permission from Ref. [146]. Copyright (2016) American Chemical Society.

application of the nanoparticles [147]. However, such nanostructures making methods are incompatible with large-scale R2R processes. Therefore, a simple scalable and compatible printing method for assembling 2D/3D close-packed nanoparticle arrays on flexible substrates or coating of these arrays on rigid substrates in assembly line has been demonstrated [147]. These results demonstrated the nanoparticle monolayer structure as an effective light trapping template for photovoltaic applications with higher nanoparticle sizes achieving the largest improvements in the wavelength range of 550–800 nm, respectively [147].

In case of R2R all-polymer devices, a key issue that affects the performance of the solar cells is the lower tendency of electron-accepting polymer to form a mixed phase relative to $PC_{71}BM$ during the roll-to-roll-compatible deposition techniques [142]. This issue leads to the worse film morphology and polymer crystallization and therefore has been reported to greatly impact the printed devices performance [142]. One of the reported methods to overcome this is the solvent vapor annealing for long durations [148]. Further, more convenient and economical method of addition of additives has also been reported to optimize the morphology and nanophase separation [149, 150]. However, the solvent vapor annealing method is not widely employed in all-PSCs; therefore, all-polymer devices based on PTB7-Th as electron-donor and PNDI-T10 as electron-acceptor, have been fabricated by R2R-compatible printing techniques using an additive but without any annealing treatment [151]. The study reported the application of varying amounts of additive DIO to optimize the morphology. With the application of 0.4 vol% DIO into the processing solvent, a boost in the fill factor up to 0.71 and PCE up to 8.61% was reported [151]. It was reported that the additive prolongs the drying time of all polymer nanocomposites leading to a better morphology and higher crystallinity, with demonstrated PCE of 6.65% for large-area all-PSCs with a flexible ITO-free structure [151]. Thus, all-PSCs were demonstrated as potential in case of the large-area R2R technology [151].

Similarly, the manufacturing of large-scale R2R based highly efficient polymeric tandem devices also presents some major challenges of less optimized parameters like coating methods, ink composition,

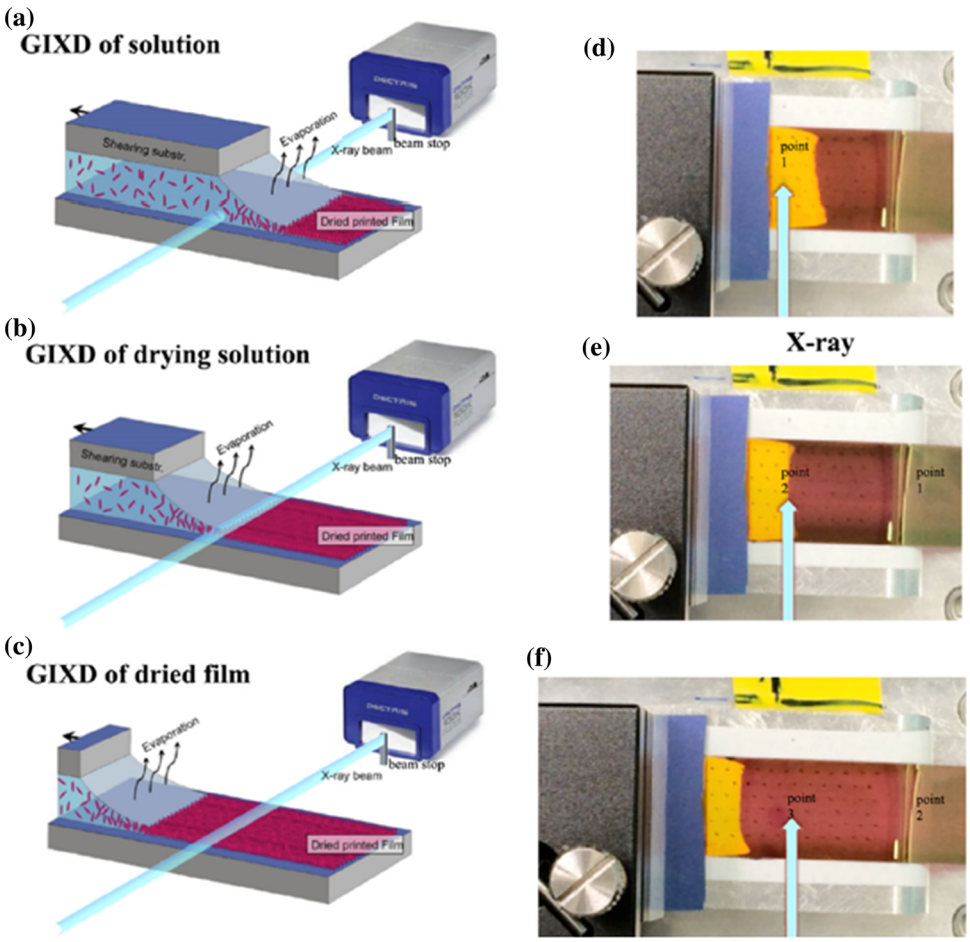

Figure 28 Schematic views (**a**–**c**) and top down photographs (**d**–**f**) for the different drying stages of organic solar cell ink by solution shearing coating. (**a**, **d**) X-ray passes through the wet film, (**b**, **e**) X-ray passes through the drying film, and (**c**, **f**) X-ray passes through the dried film. Reprinted with permission from (Ref. [146]). Copyright (2016) American Chemical Society.

and the commercially unavailability of better performing active materials [152]. All these factors affect the morphology of the deposited films. One study has demonstrated the fabrication of the organic tandem solar cells based on a moderate bandgap polymer GEN-2 and a low bandgap polymer diketopyrrolopyrrole-quinquethiophene (pDPP5T-2), with GEN-2:$PC_{60}BM$ as a front cell and pDPP5T-2:$PC_{70}BM$ as a back cell [152]. The study reported efficiencies of 7.66% and 5.56% on glass and flexible PET substrates, respectively. These solar cells were demonstrated to be fabricated under ambient conditions using coating technique compatible with high-scale production. The application of a low-temperature/solution-processed intermediate layer (IML), based on PEDOT and ZnO nanoparticles, as a transparent charge extraction layer was also demonstrated. The 60–80 nm thick IML was shown to exhibit an excellent transmittance in the range from 400 to 950 nm and was modified by a solution-processed barium hydroxide ($Ba(OH)_2$) thin layer [152]. It was further reported that the modification by the thin $Ba(OH)_2$ layer did not affect the light transmittance in the range from 500 to 950 nm, with an overall transmission of 95% achieved for the $Ba(OH)_2$ modified IML, demonstrating it as a potential IML for polymeric tandem devices [152].

In addition to the polymeric devices, as discussed above, the studies on the manufacturing of the stable perovskite solar cells through roll-to-roll coating have also been explored [52, 153–165]. Recent studies on perovskite-based solar cells have shown efficiencies up to 20% with high stability [154, 155]. Although the perovskite-based devices have recently emerged as effective extensions to the polymer-based solar cells, there are many challenges to address in the area of these solar cells. For example, the planar perovskite cells with conventional architecture have shown long-term stability only in some cases when used with a halide perovskite combination [156], an aqueous-free PEDOT:PSS [157] or a vacuum-based temperature annealing to fully eliminate chloride by-

products [158]. Further, in case of long-term degradation, the inverted planar perovskite cells with aqueous-based PEDOT:PSS as the HTL on the ITO substrate have also been reported to easily degrade due to the hygroscopic/acidic tendency of PEDOT [159], easy PSS diffusion into other layers and unstability of the ITO/polymeric interface [30, 160]. In some cases, in order to address the issues related to the stability, more advantageous architectures based on a metal oxide scaffold showing an improved stability up to 1000 h in the dark [161] and light [162] have been reported. The stability of these architectures was shown to be higher than that of the inverted or non-inverted planar counterparts. However, these are some of the several issues to be addressed in case of the perovskite solar cells, with further challenges in case of the R2R based perovskite solar cells as discussed below. Several studies on the processing techniques and the parameters used in case of the roll-to-roll-processed perovskite solar cells and their influence on the device performance, and the methods to address these issues are also described in detail below.

One of the factors playing major role in the performance of perovskite devices is the perovskite thin-film quality, which in turn is affected by deposition technique used [165]. Similar to the polymer solar cells, the slot-die method is also used for the deposition of lead halide-based perovskite layers in case of the roll-to-roll-processed perovskite solar cells [153]. The application of technique of slot-die coating has been demonstrated to address the problem of scalability of these solar cells [52]. In fact, the device efficiency up to 9.2%, comparable to spin-coated devices, has been achieved for the slot-die coated perovskite devices [153]. The importance of slot-die coating technique is that it offers the production of stripe pattern and thickness control in comparison with other conventional techniques [52]. Although slot-die coating method is a R2R-compatible technique, earlier studies have shown that as compared to slot-die method, the spin coating offers the advantage of the dynamic drying of the solvent [153]. This results in excess solvent in case of the slot-die coating method, which further affects the crystallization dynamics [153]. Such poorly controlled crystallization dynamics can lead to vertically grown crystals, causing a rough and inefficient surface covering perovskite layer and therefore, a less photocurrent [153]. Further, several advanced deposition methodologies, using slot-die coating, have been developed to make perovskite-based thin films, which include one-step/two-step solution deposition techniques [163, 164] and vacuum-based thermal vapor deposition technique [167]. The one-step method is simple and cost effective; however, the non-homogeneous perovskite thin film deposited with this method further usually needs controlled solvent/thermal treatments in order to obtain efficient PSC devices [168]. The two-step method has been widely used in polymeric devices with better performance and therefore, it acts as a better and less-cost method to fabricate devices [164]. However, the lower performance may also result in case of two-step sequential deposition due to the development of inefficient thin film and an incomplete surface covering of perovskite layer [168]. Therefore, for a better quality of perovskite layer with complete surface covering, other material processing methods have also been explored for their compatibility with high-scale and large-output R2R printing techniques [165]. One study has reported exploring an intramolecular exchange technology through a low-temperature/two-step process to deposit better-quality uniform $CH_3NH_3PbI_3$ film with better coverage [165]. The study reported additive less two-step deposition of PbI_2 based complex at room temperature, and then the deposition of CH_3NH_3I solution subsequently. An efficiency of 14.26% for the perovskite devices with a buffer less inverted structure was reported [165]. Similarly, a two-step process has been shown to be employed for better surface covering of perovskite deposited onto a mesoporous titania scaffold, in which first lead iodide is deposited from solution and then converted into perovskite by MAI immersion [153]. The slot-die coating was used for the deposition, which allowed patterned layers to be produced, and thereby, eliminated the complex removal steps related to unpatterned deposition. Also, the air quenching of the deposited films during the deposition by slot-die coating of PbI_2 was also enabled. However, for further converting the lead iodide into perovskite, a second coating step was employed which added to the complexity of the processing. The crystallization dynamics was thus shown to be controlled through the application of the cold air knife over the deposited layers, along with a preheated substrate to control the temperature gradient [153]. Further, as the manufacturing of the perovskite solar cells requires the application of the perovskite precursor solutions, it has been shown

that the small ions in perovskite precursors have rapid crystal forming tendency and are prone to pinhole formation during wet film formation [52]. Although approaches like the application of additives and solvent/gas backed coating have been developed to make pinhole-less uniform perovskite layers, the challenge of single deposition process has also been addressed [52]. This challenge was overcome by firstly forming a layer of PbI_2 and then transferring it to perovskite through exposure to CH_3NH_3I solution, followed by the application of small amount of MAI, which acts as an additive and effectively decreases PbI_2 crystallization in deposition step [52]. An efficiency up to 11% was reported using actual R2R machine in air for the production of flexible perovskite solar cells [52].

Similarly, flexible planar heterojunction perovskite solar cells based on polyethylene-2,6-naphthalate/indium tin oxide/SnO_2/perovskite/spiro-OMeTAD/Ag have also been developed using R2R microgravure printing [166]. The devices showed PCE up to 10.56% and an average PCE of 9.97% [166].

Similar to the polymeric devices, one of the factors which affect the morphology of the slot-die coated films in the R2R processed solar cells is the drying mechanism of the films [47]. It is well known that many coating/printing methods make a wet film first, followed by natural or hot air-dried films. However, in a slow drying step, the deposited solution may have tendency to flow and therefore, uniformity of the film may be lost depending on the material. Further, additional problems have been reported to be encountered with the deposition processes with different materials. For example, as the lead iodide (PbI_2) coating process in the R2R processed perovskite solar cells consists of only small ions that rapidly form crystals, certain morphology problems are reported to occur due to drying step of the deposition process [47]. It was found that during a slow drying step, there is a formation of pinholes when the easy migration of PbI_2 small ions and formation of overgrown crystals occur, leading to the formation of some areas on substrates that lack material. In order to counter this, an external quenching to replicate the spin coating was introduced (Fig. 29), in which different forms of PbI_2 films, cloudy and glassy forms, were formed from one form to other. The UV–visible absorption (Fig. 30a) shows the differences in the conversion degree for different forms [47].

A significant enhancement in the absorption intensity over the full spectral range of 400–800 nm for the perovskite film converted from a cloudy form was observed. Further, for slot-die coated PbI_2 layers, the glassy PbI_2-based devices showed poor performance with 0.6% efficiency (Fig. 30b). However, the cloudy PbI_2-based devices showed a better performance with 11.94% efficiency, indicating the strong dependence of the device performance on the PbI_2 morphology.

Further, the effect of processing-temperatures on device performance can be observed (Fig. 31b). Although the upscaling of the perovskite solar cells to the roll-to-roll printing is also limited by the sintering at high temperatures, which prevents the application of flexible substrates in R2R processing [167, 168], these devices showed a gradual improvement in the performances as temperature was increased, with 11.96% efficiency at 70 °C [47]. Using the similar techniques, planar perovskite solar cells have also been developed, and an efficiency up to 10.14% has been demonstrated for these R2R-compatible planar perovskite devices [47, 167, 168].

As discussed earlier, the films deposited through slot-die have more tendency to develop defects rather than spin-coated films, which have an internal drying process [169]. Also, slot-die deposition has tendency to develop less coverage perovskite layers with overgrown crystals than spin coating. Further, as described earlier that in order to address this issue, a gas-quenching step was introduced along with a sequential deposition [47]. However, this resulted in the introduction of an unwanted additional step and also made a prolonged soaking step essential before the second step, resulting in the R2R-incompatible developed process, as it is not suitable to be used for frequently moving substrates. In order to address these issues, a one-step slot-die deposition has been demonstrated, in which a combined gas quenching/substrate heating was used produce a defect-less layer [169]. Further, the blowing/heating steps were also used for faster solvent evaporation [169]. It was shown that such films showed significantly improved surface coverage with an efficiency of 9.8%, as compared to the films prepared at room temperature with an efficiency of 4.3% [169].

One of the issues with scaling up the manufacturing of the perovskite devices is the less number of scalable HTL materials that can give required morphology during the printing [170]. In order to

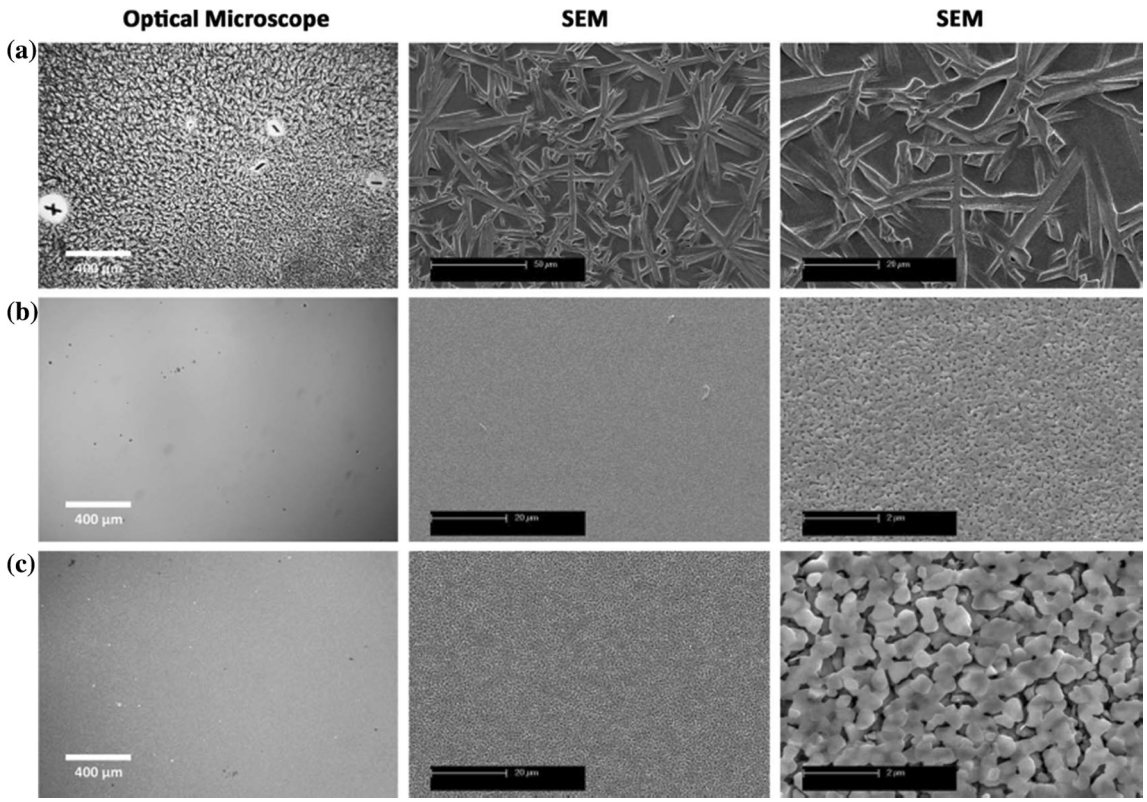

Figure 29 Optical microscopy and SEM images of the slot-die coated PbI_2 films under various coating conditions. **a** The naturally dried PbI_2 film. **b** The gas-quenched glassy PbI_2 film stored in air. **c** The gas-quenched cloudy PbI_2 film stored in enclosed space. Reference [47] Copyright Wiley-VCH Verlag GmbH & Co. KGaA. Reproduced with permission.

overcome this issue, a printing-friendly hole transport layer of Bifluo-OMeTAD, with much more tolerance to defects even due to a small chemical modification, has been introduced [170]. This material has been reported as a high-performing HTL which maintains favorable optoelectronic properties, thus making it very suitable for large-area applications. A device efficiency up to 12.7% with the devices based on this HTL has been reported [169]. Further, the application of a twisted but fully π-conjugated Bifluo-OMeTAD into slot-die coated devices, achieved via molecular design and exhibiting excellent film forming properties, has also been reported [170]. It was reported that the chemical structure of Bifluo-OMeTAD effectively suppressed the crystallization during printing, resulting in essentially an amorphous layer of Bifluo-OMeTAD and a smooth surface with very few aggregating lumps. Such an amorphous layer of Bifluo-OMeTAD with a smooth surface resulted in the efficiency of 14.7%, showing it to be an effective scalable hole transport material [170].

Further, the degradation of the roll-to-roll compatible perovskite solar cells also results from the metal electrode-related degradation that has been found to significantly affect the stability of the devices [173]. It has been shown that the silver layer, used as an electrode, suffers from severe corrosion, and the formation of silver halides (such as AgCl, AgI) in humid environments has been reported to occur mainly due to the undesirable contact and reaction between Ag electrode and the mobile halide ions from the perovskite light absorber [171, 172]. Further, it has also been reported that an exposure of the solar cells to a certain temperature induces the metal migration through the organic hole transporting layer into the perovskite material, significantly affecting the device performance, which makes it crucial to prevent the metal contacts from reacting with the perovskite material [173]. In order to address this issue, the manufacturing of roll-to-roll-compatible, semitransparent/self-encapsulated perovskite devices has been demonstrated by simply laminating two separated perovskite-based substrates, the front sub-

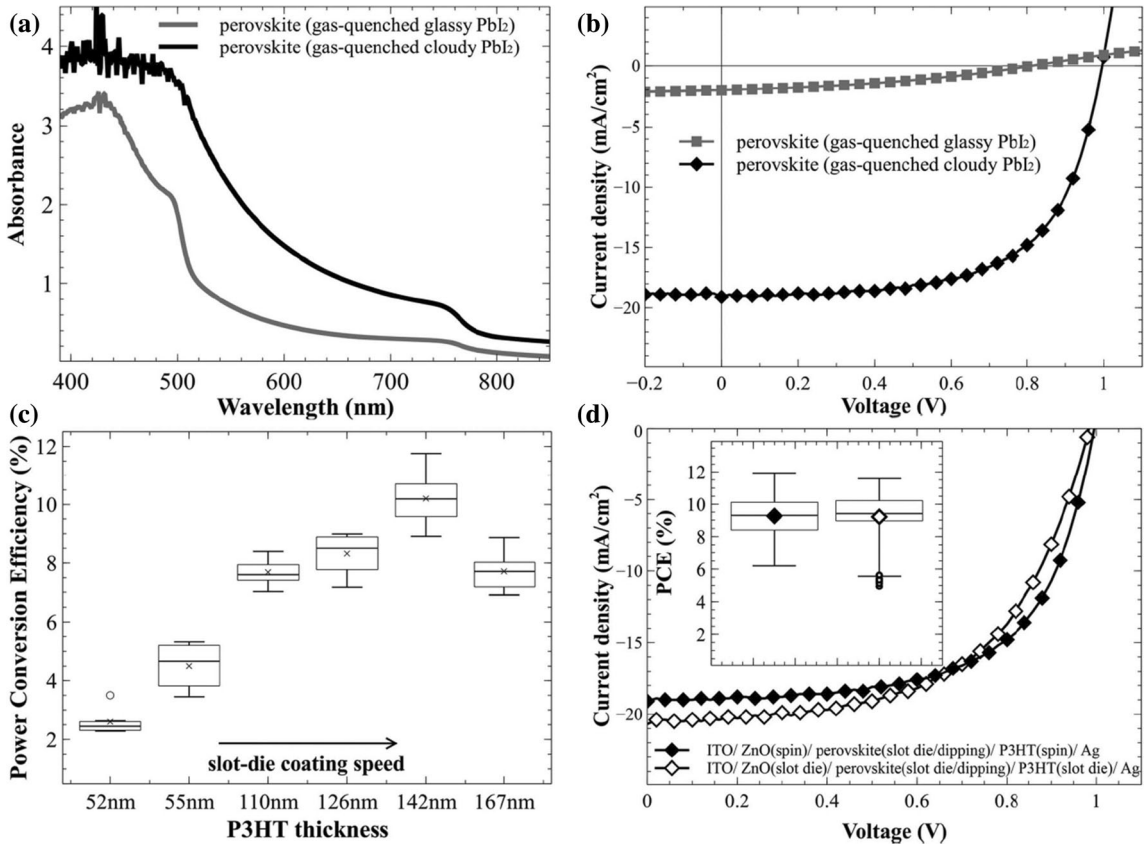

Figure 30 **a** UV–visible absorption of perovskite layers processed with slot-die coated PbI_2 and MAI dipping. **b** *J–V* characteristics for the highest performing devices with structure of ITO/ZnO(spin)/perovskite (slot die/dipping)/P3HT(spin)/Ag(evaporation). **c** Power conversion efficiency distributions of 10 devices with various thicknesses of slot-die coated P3HT. **d** *J–V* characteristics for the highest performing devices and the power conversion efficiency distributions of 20 devices with the spin-coated ZnO and P3HT layers and the slot-die coated ZnO and P3HT layers. Reference [47] Copyright Wiley-VCH Verlag GmbH & Co. KGaA. Reproduced with permission.

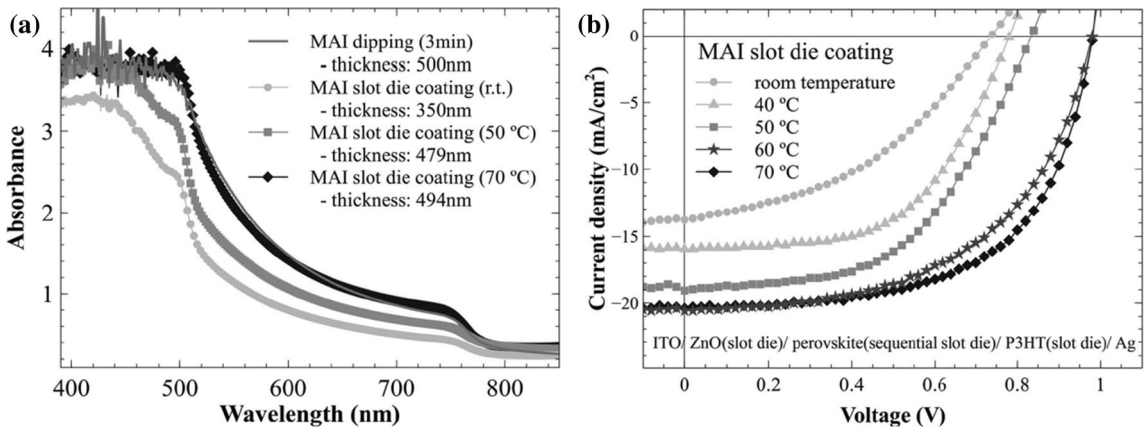

Figure 31 **a** UV–visible absorption graphs of the sequentially slot-die-coated perovskite layers with processing at room temperature, 50 °C and 70 °C. **b** *J–V* characteristics for the highest performing devices with processing at room temperature, 40 °C, 50 °C, 60 °C and 70 °C. Reference [47] Copyright Wiley-VCH Verlag GmbH & Co. KGaA. Reproduced with permission.

cell (ITO/PEDOT:PSS/$CH_3NH_3PbI_3$) and back sub-cell (compact-TiO_2/mesoporous-TiO_2/$CH_3NH_3PbI_3$), without vacuum evaporation of metal electrode [173]. Further, it was shown that the addition of

chlorobenzene between two perovskite layers significantly increases the perovskite crystals interfusion, which has been attributed to contribute to perovskite film with more crystallinity and light absorption in laminated cells. An efficiency of 6.9% for the self-encapsulated perovskite device with a device area of 0.39 cm^2 and an excellent stability for the solar cell even after being soaked in water for 24 h was reported to be achieved [173].

Printing modules

The scaling of the printing technology to develop the large-area polymeric or perovskite device modules is the ultimate step in the commercialization of the roll-to-roll printing technology of these solar cells. This section deals with the several demonstrations of such printed modules that have been developed as well as the various developments in the architectures and techniques used for such printed modules.

As discussed earlier, in order to step up the development of the solar cells using laboratory-scale techniques to high-throughput technology, the techniques involved in the various steps of fabrication must also be upgraded to roll-to-roll processing compatible techniques. One of the promising fabrication methods, as discussed earlier in detail, for depositing active layers/interlayers on large-area polymer solar cell modules is the slot-die coating technique. Most reported polymer solar cell modules have been developed by this method using several serially connected solar cells with identical wide stripes of one dimensional patterning [45, 69, 141, 181]. However, this module architecture also consists of blank shifts of each layer, which are used to avoid unwanted coating and an interconnected area between the unit cells. This results in lower geometric fill factors, i.e., the ratio of photoactive to total area, with significant aperture loss [45]. The geometric fill factors can be increased using wider stripes; however, it results in large efficiency loss due to low conducting electrodes [45, 174, 175]. Therefore, the large-area printed modules in such cases will have lower efficiencies than those of the laboratory-scale devices [45]. In order to improve the module geometric fill factors, an effective module architecture (Fig. 32a) was developed for device modules with serially connected alternating interlayers for opposite charge polarity [45]. The module consisted of alternating regular and inverted subcells that were serially connected with common top and/or bottom electrodes between the nearby subcells. Such module architecture offered advantages, such as printing the active layers in large-areas without any patterning and minimizing the aperture losses with the blank offset coating [45]. Further, to replace vacuum deposition process, required for the interlayer used in these modules, a solution-based method was used. With such new module architecture, a reported 90% geometric fill factor with 4.24% module efficiency was achieved, corresponding to 82% of the efficiency of laboratory-scale polymer solar cells [45]. The reported module efficiencies of 4.28% and 4.09% for the glass and PET substrates, respectively, were also achieved [45].

In addition, the photovoltaic modules based on small molecule benzodithiophene terthiophene rhodanine (BTR) have also been successfully developed using R2R-compatible method [177]. It has been reported that in contrast to the polymers, small molecules are potential candidate for industrial applications due to their well-defined molecular structure, relatively higher purity and less batch-to-batch variation [176, 177]. However, as in case of some polymer solar cells, many efficient small molecule devices require the prolonged R2R-incompatible thermal/solvent vapor annealing [177]. Heo et al. reported the fabrication of small molecule based large-area modules using BTR and $PC_{71}BM$ blends [177]. The fabrication of the modules involved a slot-die scalable method and the use of a halogen-free solvent. The study also employed the application of the non-halogenated diphenyl ether (DPE) additive for the processing of the blend films, resulting in the significant improvement of performance of the devices, with increment in the efficiency from 3.81 up to 6.56% [177]. The study also reported the fabrication of 10 cm^2 high area modules with efficiency of 4.83% using the small molecules blends [177].

Further, flexible photovoltaic modules based on P3HT and PCBM blend films printed on the PET substrates, with 15.45 cm^2 area and prepared by R2R-compatible gravure method, have also been demonstrated [39]. The study has reported modules with eight serially connected solar cells in same substrate. For this, the layout of modules was kept monolithic with the purpose to cover the power output for specified applications and to make them integrable with an inline production process [39]. The study reported the modules comprising 5, 7 and 8 serially

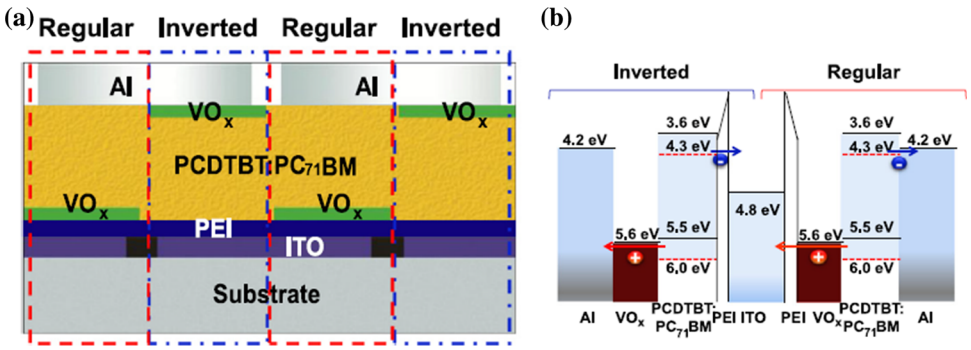

Figure 32 **a** The module architecture. **b** Energy band diagram. Reproduced with permission from Elsevier (Ref. [45]).

connected cells, with the active area efficiencies of 1.92, 1.79 and 1.68%, respectively [39].

Similar effort to manufacture complete R2R processed high-area flexible polymeric device modules have been demonstrated in laboratory scale in an ambient atmosphere [178]. This was enabled by wet processing and vacuum less steps. In addition, additive printing/coating methods without the application of lithographic or subtractive methods were used. It was demonstrated that a crucial inline coating of intermediate layer leads to a better technical output. The complete module consisted of a multilayered tandem stack of different materials like front PEDOT:PSS (20 m min^{-1}), ZnO ink, PFN ink (2.4 m min^{-1}), MH301:PCBM inks (1.5 m min^{-1}), MH306:PCBM inks (1.2 m min^{-1}), silver back electrode (rotary-screen-printed at 2 m min^{-1}) and carbon contacts (rotary-screen-printed at 2 m min^{-1}) with different wet thicknesses and dried at different temperatures [178]. An efficiency of 1.76% for an active area of 52.2 cm^2 for an eight tandemly connected cell module was also demonstrated [178].

As discussed, the manufacturing of the R2R-printed modules has been demonstrated by employing two different principles, either a serial connection of stripe modules in order to reduce the Ohmic losses or using monolithic modules for higher geometric fill factor and flexibility of the process [38]. Using the second concept, one study demonstrated the manufacturing of the inverted devices on a Kapton foil with top illumination, and using an aluminum/chromium bi-layer system as electron contact [38]. The Kapton foil was chosen due to its better thermal/mechanical stability. The layer structure used for the manufacturing of the encapsulated solar cells was Kapton/Al/Cr/P3HT:PCBM/PEDOT:PSS/printed Ag (Fig. 33). Both stripe modules (Fig. 33) and monolithic modules were manufactured. Firstly, small-area cells (3 cm^2 active area) were carefully optimized and then, these devices were transferred to a complete R2R-compatible slot-die coating and screen printing of all-solution-processed layers under ambient conditions. It was demonstrated that the modules comprising of 16 serially connected cells produced total area efficiencies up to 0.5%, with 0.35% efficiency for the best monolithic modules [38].

Similarly, flexible micro-groove back-contact solar cells and modules based on $MAPbI_3$ are fabricated through the serial connection of adjacent grooves, with such modules achieving open-circuit voltages up to nearly 15 V and a PCE of 4.4% [179].

Further, high-area flexible P3HT:PCBM modules, with performance similar to R2R commercial devices, have been successfully demonstrated by employing ambient gravure printing using an industrial scale printing proofer [43]. Both HTL of PEDOT:PSS and the active layer of P3HT:PCBM were successively printed on ITO-coated polyethylene terephthalate (ITO/PET) substrates, with evaporated Al top electrodes. The modules of 45 cm^2, composed of 5 cells connected in series, were manufactured and showed a power conversion efficiency of over 1.0%.

Similarly, a high-area (10 cm^2) module with an efficiency of 8.3% has been demonstrated by employing the technique of 3D printer-based slot-die coating [56]. A mixture of $PbAc_2$- and $PbCl_2$-based lead precursors for an inverted structure of ITO/PEDOT:PSS/$CH_3NH_3PbI_3$/C_{60}/PCBM/bathocuproine(BCP)/Ag was used to develop the devices. These perovskite films were shown to have a better-grown uniform morphology, with devices showing better performance and reproducibility than single $PbAc_2$. Also, $PbAc_2$ was helpful for a completely covered perovskite film through quick crystallizing process, and a small $PbCl_2$ was shown to lead to a better grain

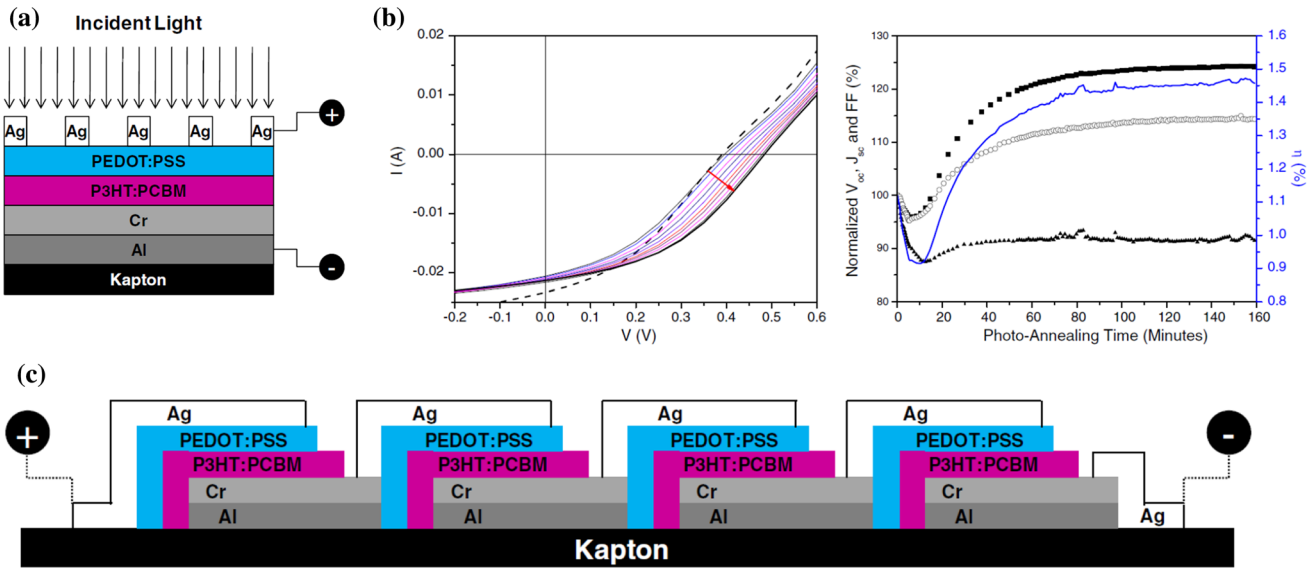

Figure 33 **a** Illustration of the device architecture. **b** (Left) IV curve typical evolution during photoannealing of an encapsulated model device at 1000 Wm^{-2}, 72 ± 2 °C (dotted) as-produced (solid) after photoannealing; (right) evolution of the photovoltaic parameters versus photoannealing time (top) V_{OC}, (bottom) J_{SC}, (dotted) FF and (solid) efficiency. Device was processed using foil B and PEDOT:PSS was spin-coated at 1250 rpm. **c** Schematic cross section of the device showing the layers stacking and their position (view along the stripes). Reproduced with permission from Elsevier (Ref. [38]).

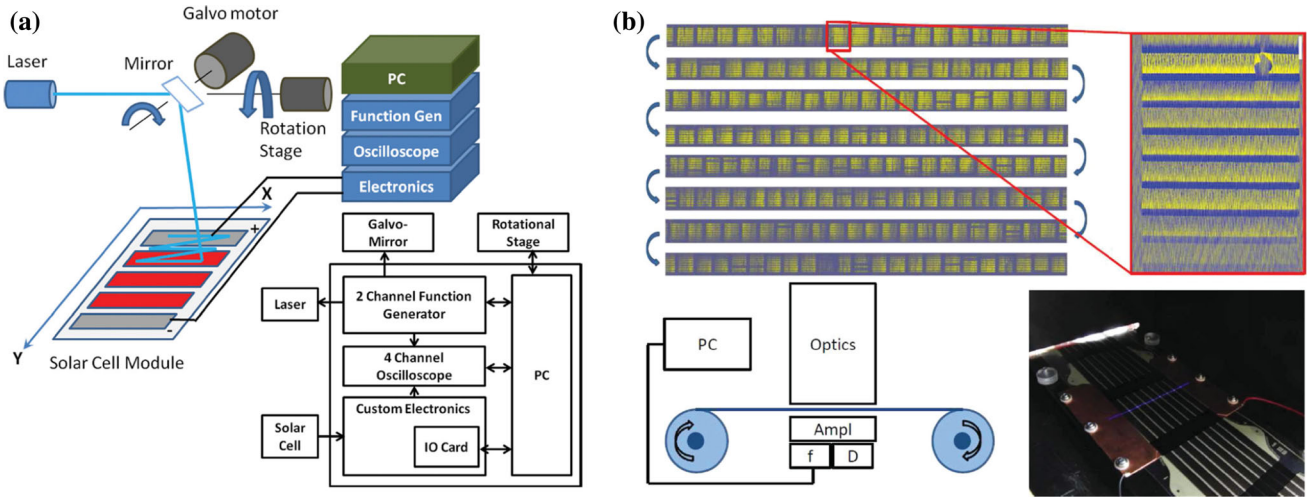

Figure 34 **a** Schematic drawing of the new LBIC setup and communications diagram. **b** Results from a 15-m-long roll of free OPV presenting a significant amount of printing errors characterized using roll-to-roll contactless LBIC with FFT processing (30-kHz sine-wave-modulated pulsed laser). Defect stripes and weaker signals are clearly seen. One cell with a large open-circuit defect is highlighted. The setup is shown below (lower left) and a photograph of the free OPV modules passing the electrodes and the laser beam are shown (lower right). Reference [186] Copyright Wiley-VCH Verlag GmbH & Co. KGaA. Reproduced with permission.

size and morphology. These precursors also decreased the prolonged $PbCl_2$ post-treatment [56].

In addition, other techniques, like spray coating utilizing partial overlapping, have been developed to deposit uniform film over large area and were used to demonstrate the fabrication of device modules [180]. The laboratory-scale devices with area of 0.09 cm^2 based on PBTI3T/PCBM have been demonstrated to produce an efficiency of 6.63% using this technique. The technique was then used to

manufacture module with 38.5 cm^2 photoactive area, with efficiency up to 5.27% [180].

Further, complete R2R vacuum-free all-solution-processed based module in the ambient atmosphere has also been demonstrated [181]. For this, five active layers were deposited on an ITO-coated PET substrate [181]. Firstly, a layer of ZnO nanoparticles was deposited by either knife-over edge or slot-die coating [181]. Further, the subsequent layers using less viscous and low-surface-tension ink compositions of a mixture of P3MHOCT and ZnO-nps were deposited at slow coating speeds. A screen-printed or slot-die-coated PEDOT:PSS layer and a silver electrode layer were then subsequently deposited [181]. The study has demonstrated a polymer solar cell module with dimensions 28 cm × 32 cm along with serially connected modules [181]. Further, the processing speeds used for the R2R processed layers were reported in the range of 40–50 mh^{-1} [181]. The study also reported the solar cell device efficiency of 0.84% and 0.375% [181]. Similarly, scalable small photovoltaic modules based on metal halide perovskite solar cells have also been demonstrated to produce the efficiency up to 24.2% [182]. The application of 2D materials and self-assembled nanocolloid materials has also been used to achieve efficiencies up to 15.3% for high-area modules [183, 184].

In addition to the fabrication of the photovoltaic modules, characterization tools have also been developed in order to characterize these modules for their performance over duration [185–187]. Such characterization of the modules is important to analyze and understand the change in the performance of these modules under the ambient conditions. An important recently developed contactless characterization tool is the light beam-induced current (LBIC) 2D mapping system (Fig. 34) with a faster acquisition rate, which is used for the characterization of the spatial distribution of the device degradation [186]. It involves the measurement of the current output from the solar cell with the movement of a laser light source over the device area. For each point, a current value corresponding to the incident light is measured and converted into a different color hue scale [186]. Due to layer-by-layer printing/coating feature of the roll-to-roll printed photovoltaics, several types of defects like layer thickness variations, misalignment, dewetting spots, delamination, particle contamination, etc., are generated, making LBIC mapping relevant for R2R photovoltaics [37, 96, 186]. The LBIC

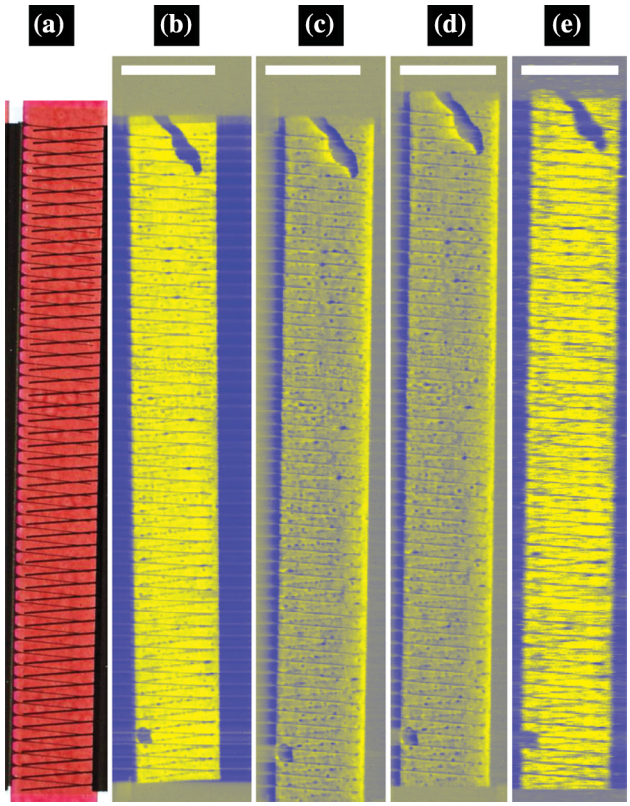

Figure 35 **a** A photograph of a solar cell is shown to the left. The corresponding LBIC images are shown recorded using the different methods: **b** Contact mode CW laser, **c** contactless mode, CW laser, contactless mode, **d** 100 kHz square wave (90% duty) pulsed laser and contactless mode, **e** 30 kHz sine wave modulated laser with FFT filtering. Reference [186] Copyright Wiley-VCH Verlag GmbH & Co. KGaA. Reproduced with permission.

images (Fig. 35) show a number of visible defects that are not visible in the photographic image.

Further, optoelectronic probing of the single junctions and interfacial charge transport in fully printed/coated tandem devices, using a combination of light beam-induced current mapping and monochromatic current–voltage characterization, has also been reported to enable the identification of the efficiency limiting printing/coating defects in the printed modules [187].

Conclusion and perspectives

The review describes in detail the various efforts undertaken to achieve the current state of the art of the roll-to-roll printing technology as well as the gaps that exist in this technology, and the methods that

have been developed to try to overcome these gaps. The processing of the polymer as well as perovskite thin films employing the R2R techniques has been demonstrated in several studies, which clearly shows that this technology holds a promising outcome. Further, the progress in this area also ensures that the realization of fast, low-cost and environmental-friendly manufacturing of the solar cells at commercial scale lies within reach of several technologies within this area. Several important issues that have been effectively addressed include the development and application of environmentally compatible materials, application of inexpensive materials, e.g., for electrodes with the replacement of ITO as transparent electrode, avoiding the use of vacuum processing and the development of the environmental and processing stable materials. However, the full integration of these new initiatives and subsequent developments needs to be performed at higher scale and faster pace if this technology has to be commercialized. In the long term, one of the key features for the high-throughput production will be that it will be environmental friendly technology. This feature can only be realized at a large-scale production through processing from water, and therefore, more research in this area is required in order to make it possible to be achieved at commercial scale. Further, the application of the different types of ink compositions, for example, dissolved solutions, emulsions and dispersed nanoparticles as the replacements to the typical orthogonal solvents for the processing of multilayer devices, can prove to be an alternative to achieve this. However, it is clear that for the realization of the large-area processing of the polymer thin films, the application of the generally used toxic and chlorinated solvents must be replaced by environmental-friendly materials. In addition to the solvent substitutions, more effective processing techniques also need to be developed along with the new environmental and processing stable materials that can sustain ambient processing conditions. For example, the technique of in-line processing of the materials in which several layers are processed sequentially during the same run is one of the techniques to improve the effectiveness of the processing. In case of the materials, various strategies should be ideally developed in tandem with the solvent substitutions, thus making it possible to approach the two issues simultaneously. Further, in case of perovskite solar cells, the large-area devices have lower efficiencies as compared to the devices produced on the laboratory scale. This is due to the important challenges of the replication of laboratory conditions and the cost of large-area manufacturing of the devices. In addition, in order to optimize the factors such as solubility, crystallization rate and device efficiency, appropriate solvents and perovskite precursor formulations are needed to be considered. The parameters such as solvent viscosity, boiling point, toxicity of the perovskite solution and environmental compatibility of the materials must be considered for better device performance and production efficiency. Also, the processing factors such as coating temperature and ambient humidity level, which affect perovskite film quality, must be optimized. The techniques of hot casting and N_2/air blow drying for the perovskite layer preparation also significantly affect the perovskite morphology, crystallization, defects and grain size and, therefore, affect the PSC performance. Therefore, the uniform and highly crystalline perovskite films prepared through R2R techniques are important for better device performance. It is with the ingenious introduction of new materials together with the incorporation of the new techniques that can reserve a promising outcome of the technology.

Acknowledgements

Abhay Gusain is awarded FAPESP Postdoctoral fellowship grant (2017/07635-2) by FAPESP, Brazil. Prof. Paulo B. Miranda, IFSC, USP Sao Paulo, Brazil is acknowledged for his support.

Compliance with ethical standards

Conflict of interest The authors hereby declare no conflict of interest in publication of this article.

References

[1] Winder C, Sariciftci NS (2004) Low bandgap polymers for photon harvesting in bulk heterojunction solar cells. J Mater Chem 14:1077–1086

[2] He Z, Zhong C, Su S, Xu M, Wu H, Cao Y (2012) Enhanced power-conversion efficiency in polymer solar cells using an inverted device structure. Nat Photonics 6:591–595

[3] He Z, Xiao B, Liu F, Wu H, Yang Y, Xiao S, Wang C, Russell TP, Cao Y (2015) Single-junction polymer solar cells with high efficiency and photovoltage. Nat Photonics 9:174–179

[4] You J, Dou L, Yoshimura K, Kato T, Ohya K, Moriarty T, Emery K, Chen CC, Gao J, Li G, Yang Y (2013) A polymer tandem solar cell with 10.6% power conversion efficiency. Nat Commun 4:1–10

[5] Zhou H, Zhang Y, Mai CK, Collins SD, Bazan GC, Nguyen TQ, Heeger AJ (2015) Polymer homo-tandem solar cells with best efficiency of 11.3%. Adv Mater 27:1767–1773

[6] Liu S, You P, Li J, Li J, Lee CS, Ong BS, Sury C, Yan F (2015) Enhanced efficiency of polymer solar cells by adding a high-mobility conjugated polymer. Energy Environ Sci 8:1463–1470

[7] Liu J, Liang Q, Wang H, Li M, Han Y, Xie Z, Wang L (2014) Improving the morphology of PCDTBT:$PC_{70}BM$ bulk heterojunction by mixed-solvent vapor-assisted imprinting: inhibiting intercalation, optimizing vertical phase separation, and enhancing photon absorption. J Phys Chem C 9(118):4585–4595

[8] Chu TY, Alem S, Tsang SW, Tse SC, Wakim S, Lu J, Dennler G, Waller D, Gaudiana R, Tao Y (2011) Morphology control in polycarbazole based bulk heterojunction solar cells and its impact on device performance. Appl Phys Lett 25:98

[9] Chi D, Qu S, Wang Z, Wang J (2014) High efficiency P3HT:PCBM solar cells with an inserted PCBM layer. J Mater Chem C 2:4383–4387

[10] Lu L, Luo Z, Xu T, Yu L (2013) Cooperative plasmonic effect of Ag and Au nanoparticles on enhancing performance of polymer solar cells. NanoLetter 13(1):59–64

[11] Zhang M, Gu Y, Guo X, Liu F, Zhang S, Huo L, Russell TP, Hou J (2013) Efficient polymer solar cells based on benzothiadiazole and alkylphenyl substituted benzodithiophene with a power conversion efficiency over 8%. Adv Mater 25:4944–4949

[12] Zhou H, Zhang Y, Seifter J, Collins SD, Luo C, Bazan GC, Nguyen TQ, Heeger AJ (2013) High-efficiency polymer solar cells enhanced by solvent treatment. Adv Mater 25:1646–1652

[13] Tsai JH, Lai YC, Higashihara T, Lin CJ, Ueda M, Chen WC (2010) Enhancement of P3HT/PCBM photovoltaic efficiency using the surfactant of triblock copolymer containing poly(3-hexylthiophene) and poly(4-vinyltriphenylamine) segments. Macromolecules 43(14):6085–6091

[14] Mühlbacher D, Scharber M, Morana M, Zhu Z, Waller D, Gaudiana R, Brabec C (2006) High photovoltaic performance of a low-bandgap polymer. Adv Mater 18:2884–2889

[15] Vanlaeke P, Vanhoyland G, Aernouts T, Cheyns D, Deibel C, Manc J, Heremans P, Poortmans J (2006) Polythiophene based bulk heterojunction solar cells: morphology and its implications. Thin Solid Films 511–512:358–361

[16] Albrecht S, Janietz S, Schindler W, Frisch J, Kurpiers J, Kniepert J, Inal S, Pingel P, Fostiropoulos K, Koch N, Neher D (2012) Fluorinated copolymer PCPDTBT with enhanced open-circuit voltage and reduced recombination for highly efficient polymer solar cells. J Am Chem Soc 134(36):14932–14944

[17] Hou J, Chen HY, Zhang S, Li G, Yang Y (2008) Synthesis, characterization, and photovoltaic properties of a low band gap polymer based on silole-containing polythiophenes and 2,1,3-benzothiadiazole. J Am Chem Soc 130(48):16144–16145

[18] Li XH, Sha WE, Choy WC, Fung DD, Xie FX (2012) Efficient inverted polymer solar cells with directly patterned active layer and silver back grating. J Phys Chem C 116(12):7200–7206

[19] Park SH, Roy A, Beaupré S, Cho S, Coates N, Moon JS, Moses D, Leclerc M, Lee K, Heeger AJ (2009) Bulk heterojunction solar cells with internal quantum efficiency approaching 100%. Nat Photonics 3:297–302

[20] Jørgensen M, Norrman K, Krebs FC (2008) Stability/degradation of polymer solar cells. Sol Energy Mater Sol Cells 92:686–714

[21] Norrman K, Madsen MV, Gevorgyan SA, Krebs FC (2010) Degradation patterns in water and oxygen of an inverted polymer solar cell. J Am Chem Soc 132:16883–16892

[22] Dam N, Scurlock RD, Wang B, Ma L, Sundahl M, Ogilby PR (1999) Singlet oxygen as a reactive intermediate in the photodegradation of phenylenevinylene oligomers. Chem Mater 11:1302–1305

[23] Zhang M et al (2016) Highly efficient ternary polymer solar cells by optimizing photon harvesting and charge carrier transport. Nano Energy 22:241–254

[24] Ma X et al (2020) Highly efficient quaternary organic photovoltaics by optimizing photogenerated exciton distribution and active layer morphology. Nano Energy 70:104496

[25] Hu Z et al (2019) Semitransparent polymer solar cells with 9.06% efficiency and 27.1% average visible transmittance obtained by employing a smart strategy. J Mater Chem A 7:7025–7032

[26] Ma X et al (2020) Efficient ternary organic photovoltaics with two polymer donors by minimizing energy loss. J Mater Chem A 8:1265–1272

[27] Matturro MG, Reynolds RP, Kastrup RV, Pictroski CF (1986) Thioozonide decomposition. Sulfur and oxygen

atom transfer. Evidence for the formation of a carbonyl O-sulfide intermediate. J Am Chem Soc 108:2775–2776

[28] Norrman K, Larsen NB, Krebs FC (2006) Lifetimes of organic photovoltaics: combining chemical and physical characterisation techniques to study degradation mechanisms. Sol Energy Mater Sol Cells 90:2793–2814

[29] Lögdlund M, Brédas JL (1994) Theoretical studies of the interaction between aluminum and poly(p-phenylenevinylene) and derivatives. J Chem Phys 101:4357–4364

[30] de Jong MP, van Ijzendoorn LJ, de Voigt MJA (2000) Stability of the interface between indium-tin-oxide and poly(3,4-ethylenedioxythiophene)/poly(styrenesulfonate) in polymer light-emitting diodes. Appl Phys Lett 77:2255–2257

[31] Hu HL et al (2020) Nucleation and crystal growth control for scalable solution-processed organic-inorganic hybrid perovskite solar cells. J Mater Chem A 8(4):1578–1603

[32] Krebs FC, Espinosa N, Hosel M, Søndergaard RR, Jørgensen M (2014) 25th anniversary article: rise to power—OPV-based solar parks. Adv Mater 26:29–39

[33] Green MA et al (2011) Solar cell efficiency tables (version 38). Prog Photovolt Res Appl 19:565–572

[34] Service RF (2011) Outlook brightens for plastic solar cells. Science 332:293

[35] Krebs FC (2009) All solution roll-to-roll processed polymer solar cells free from indium-tin-oxide and vacuum coating steps. Sol Energy Mater Sol Cells 10:761–768

[36] Kopola P, Aernouts T, Guillerez S, Jin H, Tuomikoski M, Maaninen A, Hast J (2010) High efficient plastic solar cells fabricated with a high-throughput gravure printing method. Sol Energy Mater Sol Cells 94:1673–1680

[37] Andersen TR, Larsen-Olsen TT, Andreasen B, Bottiger APL, Carle JE, Helgesen M, Bundgaard E, Norrman K, Andreasen JW, Jørgensen M, Krebs FC (2011) Aqueous processing of low-band-gap polymer solar cells using roll-to-roll methods. ACS Nano 5(5):4188–4196

[38] Manceau M, Angmo D, Jørgensen M, Krebs FC (2011) ITO-free flexible polymer solar cells: from small model devices to roll-to-roll processed large modules. Org Electron 12:566–574

[39] Kopola P, Aernouts T, Sliz R, Guillerez S, Ylikunnari M, Cheyns D, Valimaki M, Tuomikoski M, Hast J, Jabbour G, Myllyl R, Maaninen A (2011) Gravure printed flexible organic photovoltaic modules. Sol Energy Mater Sol Cells 95:1344–1347

[40] Hosel M, Søndergaard RR, Jørgensen M, Krebs FC (2013) Fast inline roll-to-roll printing for indium-tin-oxide-free polymer solar cells using automatic registration. Energy Technol 1:102–107

[41] Andersen TR, Dam HF, Andreasen B, Hösel M, Madsen MV, Gevorgyan SA, Søndergaard RR, Jørgensen M, Krebs FC (2013) A rational method for developing and testing stable flexible indium- and vacuum-free multilayer tandem polymer solar cells comprising up to twelve roll processed layers. Sol Energy Mater Sol Cells 120:735–743

[42] Angmo D, Sweelssen J, Andriessen R, Galagan Y, Krebs FC (2013) Inkjet printing of back electrodes for inverted polymer solar cells. Adv Energy Mater 3:1230–1237

[43] Yang J, Vak D, Clark N, Subbiah J, Wong WWH, Jones DJ, Watkins SE, Wilson G (2013) Organic photovoltaic modules fabricated by an industrial gravure printing proofer. Sol Energy Mater Sol Cells 109:47–55

[44] Helgesen M, Carlé JE, Krebs FC (2013) Slot-die coating of a high performance copolymer in a readily scalable roll process for polymer solar cells. Adv Energy Mater 3:1664–1669

[45] Back H, Kong J, Kang H, Kim J, Kim J, Lee K (2014) Flexible polymer solar cell modules with patterned vanadium suboxide layers deposited by an electro-spray printing method. Sol Energy Mater Sol Cells 130:555–560

[46] Eggenhuisen TM et al (2015) Digital fabrication of organic solar cells by Inkjet printing using non-halogenated solvents. Sol Energy Mater Sol Cells 134:364–372

[47] Hwang K, Jung YS, Heo YJ, Scholes FH, Watkins SE, Subbiah J, Jones DJ, Kim DY, Vak D (2015) Toward large scale roll-to-roll production of fully printed perovskite solar cells. Adv Mater 27:1241–1247

[48] Iannaccone G, Välimäki M, Jansson E, Sunnari A, Corso G, Bernardi A, Levi M, Turri S, Hast J, Griffini G (2015) Roll-to-roll compatible flexible polymer solar cells incorporating a water-based solution-processable silver back electrode with low annealing temperature. Sol Energy Mater Sol Cells 143:227–235

[49] Angmo D, Andersen TR, Bentzen JJ, Helgesen M, Søndergaard RR, Jørgensen M, Carlé JE, Bundgaard E, Krebs FC (2015) Roll-to-roll printed silver nanowire semitransparent electrodes for fully ambient solution-processed tandem polymer solar cells. Adv Funct Mater 25:4539–4547

[50] Gu X, Zhou Y, Gu K, Kurosawa T, Guo Y, Li Y, Lin H, Schroeder BC, Yan H, Lopez FM, Tassone CJ, Wang C, Mannsfeld SCB, Yan H, Zhao D, Toney MF, Bao Z (2017) Roll-to-roll printed large-area all-polymer solar cells with 5% efficiency based on a low crystallinity conjugated polymer blend. Adv Energy Mater 7:1602742

[51] Jung YS, Hwang K, Heo YJ, Kim JE, Lee D, Lee CH, Joh HI, Yeo JS, Kim DY (2017) One-step printable perovskite films fabricated under ambient conditions for efficient and

reproducible solar cells. ACS Appl Mater Interfaces 9:27832–27838
[52] Heo YJ et al (2017) Printing-friendly sequential deposition via intra-additive approach for roll-to-roll process of perovskite solar cells. Nano Energy 41:443–451
[53] Zhang C, Luo Q, Wu H, Li H, Lai J, Ji G, Yan L, Wang X, Zhang D, Lin J, Chen L, Yang J, Ma C (2017) Roll-to-roll micro-gravure printed large-area zinc oxide thin film as the electron transport layer for solution-processed polymer solar cells. Org Electron 45:190–197
[54] Dou B et al (2018) Roll-to-roll printing of perovskite solar cells. ACS Energy Lett. 3:2558–2565
[55] Wu W et al (2018) Molecular doping enabled scalable blading of efficient hole-transport-layer-free perovskite solar cells. Nat Commun 9:1625
[56] Lee D, Jung YS, Heo YJ, Lee S, Hwang K, Jeon YJ, Kim JE, Park J, Jung GY, Kim DY (2018) Slot-die coated perovskite films using mixed lead precursors for highly reproducible and large-area solar cells. ACS Appl Mater Interfaces 10:16133–16139
[57] Wang P et al (2019) Solution-processable perovskite solar cells toward commercialization: progress and challenges. Adv Funct Mater 29:1807661
[58] Amollo TA et al (2019) Organic solar cells: materials and prospects of graphene for active and interfacial layers. Crit Rev Solid State Mater Sci. https://doi.org/10.1080/10408436.2019.1632791
[59] Wentao Y et al (2019) Recent progress in inkjet-printed solar cells. J Mater Chem A 23(7):13873–13902
[60] Haixia X et al (2019) Recent Progress of flexible perovskite solar cells. Phys Status Solidi R 13(5):1800566
[61] Jiankui C et al (2019) Review of wound roll stress in roll-to-roll manufacturing of flexible electronics. Sci Bull 64(5–6):555–565
[62] Brunetti F et al (2019) Printed solar cells and energy storage devices on paper substrates. Adv Funct Mater 29(21):1806798
[63] Abbel R et al (2018) Roll-to-roll fabrication of solution processed electronics. Adv Eng Mater 20(8):1701190
[64] Zhang Y et al (2018) Current status of outdoor lifetime testing of organic photovoltaics. Adv Sci 5(8):1800434
[65] Wei Z et al (2018) Flexible perovskite solar cells based on green, continuous roll-to-roll printing technology. J Energy Chem 27(4):971–989
[66] Yen-Sook J et al (2018) Progress in scalable coating and roll-to-roll compatible printing processes of perovskite solar cells toward realization of commercialization. Adv Opt Mater 6(9):1701182
[67] Luca L et al (2015) Guidelines for closing the efficiency gap between hero solar cells and roll-to-roll printed modules. Energy Technol 3(4):373–384
[68] Søndergaard R, Hösel M, Angmo D, Larsen-Olsen TT, Krebs FC (2012) Roll-to-roll fabrication of polymer solar cells. Mater Today 15:36–49
[69] Søndergaard RR, Hösel M, Krebs FC (2013) Roll-to-roll fabrication of large area functional organic materials. J Polym Sci B Polym Phys 51:16–34
[70] Kim YY, Yang TY, Suhonen R, Välimäki M, Maaninen T, Kemppainen A, Jeon NJ, Seo J (2019) Gravure-printed flexible perovskite solar cells: toward roll-to-roll manufacturing. Adv Sci 6:1802094
[71] Lim GH et al (2014) A transition solvent strategy to print polymer: fullerene films using halogen-free solvents for solar cell applications. Org Electron 15(2):449–460
[72] van Franeker JJ et al (2013) All-solution-processed organic solar cells with conventional architecture. Sol Energy Mater Sol Cells 117:267–272
[73] de Gans BJ et al (2004) Inkjet printing of polymers: state of the art and future developments. Adv Mater 16:203–213
[74] Peng X et al (2017) Perovskite and organic solar cells fabricated by inkjet printing: progress and prospects. Adv Mater 41:1703704
[75] Lee J et al (2019) Slot-die and roll-to-roll processed single junction organic photovoltaic cells with the highest efficiency. Adv Eng Mater 9(36):1901805
[76] Tait JG, Rand BP, Heremans P (2013) Concurrently pumped ultrasonic spray coating for donor: acceptor and thickness optimization of organic solar cells. Org Electron 14(3):1002–1008
[77] Girotto C, Moia D, Rand BP, Heremans P (2011) High-performance organic solar cells with spray-coated hole-transport and active layers. Adv Funct Mater 21:64–72
[78] Tait JG, Worfolk BJ, Maloney SA, Hauger TC, Elias AL, Buriak JM, Harris KD (2013) Spray coated high-conductivity PEDOT:PSS transparent electrodes for stretchable and mechanically-robust organic solar cells. Sol Energy Mater Sol Cells 110:98–106
[79] Steirer KX, Berry JJ, Reese MO, van Hest MFAM, Miedaner A, Liberatore MW, Collins RT, Ginley DS (2009) Ultrasonically sprayed and inkjet printed thin film electrodes for organic solar cells. Thin Solid Films 517:2781–2786
[80] Girotto C, Rand BP, Steudel S, Genoe J, Heremans P (2009) Nanoparticle-based, spray-coated silver top contacts for efficient polymer solar cells. Org Electron 10:735–740
[81] Espinosa N et al (2012) Solar cells with one-day energy payback for the factories of the future. Energy Environ Sci 5:5117–5132

[82] Krebs FC, Gevorgyan SA, Alstrup J (2009) A roll-to-roll process to flexible polymer solar cells: model studies, manufacture and operational stability studies. J Mater Chem 19(30):5442–5451

[83] Espinosa N, Valverde RG, Urbina A, Krebs FC (2011) A life cycle analysis of polymer solar cell modules prepared using roll-to-roll methods under ambient conditions. Sol Energy Mater Sol Cells 95(5):1293–1302

[84] Zhang X et al (2017) Polymer solar cells employing water-soluble polypyrrole nanoparticles as dopants of PEDOT:PSS with enhanced efficiency and stability. J Phys Chem C 121:18378–18384

[85] Ogawa M et al (2009) Fabrication and photovoltaic properties of multilayered thin films designed by layer-by-layer assembly of poly(p-phenylenevinylene)s. Sol Energy Mater Sol Cells 93:369–374

[86] Rider DA et al (2010) Stable inverted polymer/fullerene solar cells using a cationic polythiophene modified PEDOT:PSS cathodic interface. Adv Funct Mater 20:2404–2415

[87] Li HM et al (2003) Photocurrent generation in multilayer self-assembly films fabricated from water-soluble poly(-phenylene vinylene). Chem Eur J 9:6031–6038

[88] Søndergaard R, Helgesen M, Jørgensen M, Krebs FC (2011) Fabrication of polymer solar cells using aqueous processing for all layers including the metal back electrode. Adv Eng Mater 1:68–71

[89] Kietzke T, Neher D, Landfester K, Montenegro R, Guntner R, Scherf U (2003) Novel approaches to polymer blends based on polymer nanoparticles. Nat Mater 2:408–412

[90] Landfester K (2001) The generation of nanoparticles in miniemulsions. Adv Mater 13:765–768

[91] Larsen-Olsen TT, Andersen TR, Andreasen B, Bottiger APL, Bundgaard E, Norrman K, Andreasen JW, Jørgensen M, Krebs FC (2012) Roll-to-roll processed polymer tandem solar cells partially processed from water. Sol Energy Mater Sol Cells 97:43–49

[92] Zhan T, Zhao X, Yang D, Yang X (2018) Efficient polymer solar cells spray-coated from non-halogenated solvents towards practical fabrication. Energy Technol 6:171–177

[93] Wu Y, Zou Y, Yang H, Li Y, Li H, Cui C, Li Y (2017) Achieving over 9.8% efficiency in nonfullerene polymer solar cells by environmentally friendly solvent processing. ACS Appl Mater Interfaces 9(42):37078–37086

[94] Lamont CA, Eggenhuisen TM, Coenen MJJ, Slaats TWL, Andriessen R, Groen P (2015) Tuning the viscosity of halogen free bulk heterojunction inks for inkjet printed organic solar cells. Org Electron 17:107–114

[95] Kuwabara T, Nakashima T, Yamaguchi T, Takahashi K (2012) Flexible inverted polymer solar cells on polyethylene terephthalate substrate containing zinc oxide electron-collection-layer prepared by novel sol–gel method and low-temperature treatments. Org Electron 13:1136–1140

[96] Krebs FC, Søndergaard R, Jørgensen M (2011) Printed metal back electrodes for R2R fabricated polymer solar cells studied using the LBIC technique. Sol Energy Mater Sol Cells 95:1348–1353

[97] Angmo D, Larsen-Olsen TT, Jørgensen M, Søndergaard RR, Krebs FC (2013) Roll-to-roll inkjet printing and photonic sintering of electrodes for ITO free polymer solar cell modules and facile product integration. Adv Energy Mater 3:172–175

[98] Dang MT, Brunner PLM, Wuest JD (2014) A green approach to organic thin-film electronic devices: recycling electrodes composed of indium tin oxide (ITO). ACS Sustain Chem Eng 2:2715–2721

[99] Carle JE, Andersen TR, Helgesen M, Bundgaard E, Jørgensen M, Krebs FC (2013) A laboratory scale approach to polymer solar cells using one coating/printing machine, flexible substrates, no ITO, no vacuum and no spin coating. Sol Energy Mater Sol Cells 108:126–128

[100] Galagan Y, Coenen EWC, Abbel R, van Lammeren TJ, Sabik S, Barink M, Meinders ER, Andriessen R, Blom PWM (2013) Photonic sintering of inkjet printed current collecting grids for organic solar cell applications. Org Electron 14:38–46

[101] Kang MG, Park HJ, Ahn SH, Guo LJ (2010) Transparent Cu nanowire mesh electrode on flexible substrates fabricated by transfer printing and its application in organic solar cells. Sol Energy Mater Sol Cells 94:1179–1184

[102] Guo LJ (2007) Nanoimprint lithography: methods and material requirements. Adv Mater 19:495–513

[103] Kang MG, Kim MS, Kim J, Guo LJ (2008) Organic solar cells using nanoimprinted transparent metal electrodes. Adv Mater 20:4408–4413

[104] Kang MG, Guo LJ (2008) Metal transfer assisted nanolithography on rigid and flexible substrates. J Vac Sci Technol B 26:2421–2425

[105] Pina Hernandez C, Kim JS, Guo LJ, Fu PF (2007) High-throughput and etch-selective nanoimprinting and stamping based on fast-thermal-curing poly(dimethylsiloxane)s. Adv Mater 2007(19):1222–1227

[106] Ahn SH, Guo LJ (2008) High-speed roll-to-roll nanoimprint lithography on flexible plastic substrates. Adv Mater 20:2044–2049

[107] Ahn SH, Guo LJ (2009) Large-area roll-to-roll and roll-to-plate nanoimprint lithography and analytical models for predicting residual layer thickness. ACS Nano 3:2304–2310

[108] Cheng X, Guo LJ, Fu PF (2005) Room-temperature, low-pressure nanoimprinting based on cationic photo polymerization of novel epoxy silicone monomers. Adv Mater 17:1419–1424

[109] dos Reis Benatto GA, Roth B, Madsen MV, Hösel M, Søndergaard RR, Jørgensen M, Krebs FC (2014) Carbon: the ultimate electrode choice for widely distributed polymer solar cells. Adv Energy Mater 4:1400732

[110] He S et al (2019) Carbon-based electrode engineering boosts the efficiency of all low-temperature-processed perovskite solar cells. ACS Energy Lett 4(9):2032–2039

[111] Cao Y et al (2020) Cu_2ZnSnS_4 as an efficient hole transporting material for low temperature paintable carbon electrode based perovskite solar cells. Org Electron 76:105455

[112] Choi H, Kim HB, Ko SJ, Kim JY, Heeger AJ (2015) An organic surface modifier to produce a high work function transparent electrode for high performance polymer solar cells. Adv Mater 27:892–896

[113] Zhang W, Zhao B, He Z, Zhao X, Wang H, Yang S, Wu H, Cao Y (2013) High-efficiency ITO-free polymer solar cells using highly conductive PEDOT:PSS/surfactant bilayer transparent anodes. Energy Environ Sci 6:1956–1964

[114] Li Z, Qin F, Liu T, Ge R, Meng W, Tong J, Xiong S, Zhou Y (2015) Optical properties and conductivity of PEDOT:PSS films treated by polyethylenimine solution for organic solar cells. Org Electron 21:144–148

[115] Sun K, Li P, Xia Y, Chang J, Ouyang J (2015) Transparent conductive oxide-free perovskite solar cells with PEDOT:PSS as transparent electrode. ACS Appl Mater Interfaces 7(28):15314–15320

[116] Kang H, Jung S, Jeong S, Kim G, Lee K (2015) Polymer-metal hybrid transparent electrodes for flexible electronics. Nat Commun 6:6503

[117] Kim N, Kee S, Lee SH, Lee BH, Kahng YH, Jo YR, Kim BJ, Lee K (2014) Highly conductive PEDOT:PSS nanofibrils induced by solution-processed crystallization. Adv Mater 26:2268–2272

[118] Hu X, Meng X, Xiong J, Huang Z, Yang X, Tan L, Chen Y (2017) Roll-to-roll fabrication of flexible orientated graphene transparent electrodes by shear force and one-step reducing post-treatment. Adv Mater Technol 2:1700138

[119] Kim I, Kwak SW, Ju Y, Park GY, Lee TM, Jang Y, Choi YM, Kang D (2015) Roll-offset printed transparent conducting electrode for organic solar cells. Thin Solid Films 580:21–28

[120] Meng X, Hu X, Yang X, Yin J, Wang Q, Huang L, Yu Z, Hu T, Tan L, Zhou W, Chen Y (2018) Roll-to-roll printing of meter-scale composite transparent electrodes with optimized mechanical and optical properties for photoelectronics. ACS Appl Mater Interfaces 10:8917–8925

[121] Tan LC et al (2019) Highly efficient flexible polymer solar cells with robust mechanical stability. Adv Sci 6:1801180

[122] Hwang HS, Khang DY (2015) Charge-carrier selective electrodes for organic bulk heterojunction solar cell by contact-printed siloxane oligomers. Thin Solid Films 589:125–132

[123] Schmidt TM, Larsen-Olsen TT, Carlé JE, Angmo D, Krebs FC (2015) Upscaling of perovskite solar cells: fully ambient roll processing of flexible perovskite solar cells with printed back electrodes. Adv Energy Mater 5:1500569

[124] Chen Z et al (2019) Single-crystal $MAPbI_3$ perovskite solar cells exceeding 21% power conversion efficiency. ACS Energy Lett 4(6):1258–1259

[125] Carle JE, Helgesen M, Zawacka NK, Madsen MV, Bundgaard E, Krebs FC (2014) A comparative study of fluorine substituents for enhanced stability of flexible and ITO-free high-performance polymer solar cells. J Polym Sci B Polym Phys 52:893–899

[126] Wang N, Chen Z, Wei W, Jiang Z (2013) Fluorinated benzothiadiazole-based conjugated polymers for high-performance polymer solar cells without any processing additives or post-treatments. J Am Chem Soc 135(45):17060–17068

[127] Li K, Li Z, Feng K, Xu X, Wang L, Peng Q (2013) Development of large band-gap conjugated copolymers for efficient regular single and tandem organic solar cells. J Am Chem Soc 135(36):13549–13557

[128] Gao W et al (2013) Thick-film organic solar cells achieving over 11% efficiency and nearly 70% fill factor at thickness over 400 nm. Adv Funct Mater 2020:1908336

[129] Zhan L et al (2020) Over 17% efficiency ternary organic solar cells enabled by two non-fullerene acceptors working in an alloy-like model. Energy Environ Sci 13:635–645

[130] Gao J et al (2020) Over 14.5% efficiency and 71.6% fill factor of ternary organic solar cells with 300 nm thick active layers. Energy Environ Sci 13:958–967

[131] Gao Y, An C, Wang Z, Sun Y, Wei Z, Guo F, Yang Y, Zhao L, Zhang Y (2018) Efficient post-treatment-free polymer solar cells from indacenodithiophene and fluorinated quinoxaline-based conjugated polymers. Dyes Pigm 154:164–171

[132] Wang H et al (2020) Reducing photovoltage loss in inverted perovskite solar cells by quantum dots alloying modification at cathode contact. Sol RRL 4:1900468

[133] Helgesen M, Madsen MV, Andreasen B, Tromholt T, Andreasen JW, Krebs FC (2011) Thermally reactive Thiazolo[5,4-d]thiazole based copolymers for high

photochemical stability in polymer solar cells. Polym Chem 2:2536–2542

[134] Zhang ZG, Min J, Zhang S, Zhang J, Zhang M, Li Y (2011) Alkyl chain engineering on a dithieno[3,2-b:2′,3′-d]silole-alt-dithienylthiazolo[5,4-d]thiazole copolymer toward high performance bulk heterojunction solar cells. Chem Commun 47:9474–9476

[135] Zhang M, Guo X, Li Y (2011) Synthesis and characterization of a copolymer based on thiazolothiazole and dithienosilole for polymer solar cells. Adv Energy Mater 1:557

[136] Holliday S, Luscombe CK (2017) Low boiling point solvent additives for improved photooxidative stability in organic photovoltaics. Adv Electron Mater 4:1700416

[137] Hollis JR, Wade J, Tsoi WC, Soon Y, Durrant J, Kim JS (2014) Photochemical stability of high efficiency PTB7:$PC_{70}BM$ solar cell blends. J Mater Chem A 2:20189–20195

[138] Roth B, dos Reis Benatto GA, Corazza M, Søndergaard RR, Gevorgyan SA, Jørgensen M, Krebs FC (2015) The critical choice of PEDOT:PSS additives for long term stability of roll-to-roll processed OPVs. Adv Energy Mater 5:1401912

[139] Lilliedal MR, Medford AJ, Madsen MV, Norrman K, Krebs FC (2010) The effect of post-processing treatments on inflection points in current–voltage curves of roll-to-roll processed polymer photovoltaics. Sol Energy Mater Sol Cells 94:2018–2031

[140] Yan H, Collins BA, Gann E, Wang C, Ade H, McNeill CR (2012) Correlating the efficiency and nanomorphology of polymer blend solar cells utilizing resonant soft X-ray scattering. ACS Nano 6:677–688

[141] Hong S, Lee J, Kang H, Lee K (2013) Slot-die coating parameters of the low-viscosity bulk-heterojunction materials used for polymer solar cells. Sol Energy Mater Sol Cells 112:27–35

[142] Gu X, Yan H, Kurosawa T, Schroeder BC, Gu KL, Zhou Y, To JWF, Oosterhout SD, Savikhin V, Lopez FM, Tassone CJ, Mannsfeld SCB, Wang C, Toney MF, Bao Z (2016) Comparison of the morphology development of polymer-fullerene and polymer-polymer solar cells during solution-shearing blade coating. Adv Energy Mater 6:1601225

[143] Liu Y, Zhao J, Li Z, Mu C, Ma W, Hu H, Jiang K, Lin H, Ade H, Yan H (2014) Aggregation and morphology control enables multiple cases of high-efficiency polymer solar cells. Nat Commun 5:5293

[144] Verploegen E, Miller CE, Schmidt K, Bao Z, Toney MF (2012) Manipulating the morphology of P3HT:PCBM bulk heterojunction blends with solvent vapor annealing. Chem Mater 24:3923–3931

[145] Li G, Yao Y, Yang H, Shrotriya V, Yang G, Yang Y (2007) "Solvent annealing" effect in polymer solar cells based on poly(3-hexylthiophene) and methanofullerenes. Adv Funct Mater 17:1636

[146] Gu X, Reinspach J, Worfolk BJ, Diao Y, Zhou Y, Yan H, Gu K, Mannsfeld S, Toney MF, Bao Z (2016) Compact roll-to-roll coater for in situ X-ray diffraction characterization of organic electronics printing. ACS Appl Mater Interfaces 8:1687–1694

[147] Jeong S, Hu L, Lee HR, Garnett E, Choi JW, Cui Y (2010) Fast and scalable printing of large area monolayer nanoparticles for nanotexturing applications. NanoLetter 10:2989–2994

[148] Li Z, Xu X, Zhang W, Meng X, Ma W, Yartsev A, Inganas O, Andersson MR, Janssen RA, Wang E (2016) High performance all-polymer solar cells by synergistic effects of fine-tuned crystallinity and solvent annealing. J Am Chem Soc 138:10935–10944

[149] Kang H, Lee W, Oh J, Kim T, Lee C, Kim BJ (2016) From fullerene-polymer to all-polymer solar cells: the importance of molecular packing, orientation, and morphology control. Acc Chem Res 49:2424–2434

[150] Kang H, Kim K, Choi J, Lee C, Kim BJ (2014) High-performance all-polymer solar cells based on face-on stacked polymer blends with low interfacial tension. ACS Macro Lett 3:1009–1014

[151] Lin Y, Dong S, Li Z, Zheng W, Yang J, Liu A, Cai W, Liu F, Jiang Y, Russell TP, Huang F, Wang E, Hou L (2018) Energy-effectively printed all-polymer solar cells exceeding 8.61% efficiency. Nano Energy 46:428–435

[152] Li N, Baran D, Spyropoulos GD, Zhang H, Berny S, Turbiez M, Ameri T, Krebs FC, Brabec CJ (2014) Environmentally printing efficient organic tandem solar cells with high fill factors: a guideline towards 20% power conversion efficiency. Adv Energy Mater 4:1400084

[153] Cotella G, Baker J, Worsley D, De Rossi F, Pleydell-Pearce C, Carnie M, Watson T (2017) One-step deposition by slot-die coating of mixed lead halide perovskite for photovoltaic applications. Sol Energy Mater Sol Cells 159:362–369

[154] Chen YC et al (2020) Triphenylamine dibenzofulvene–derived dopant-free hole transporting layer induces micrometer-sized perovskite grains for highly efficient near 20% for p-i-n perovskite solar cells. Prog Photovolt Res Appl 28(1):49–59

[155] Ding C et al (2020) Photoexcited hot and cold electron and hole dynamics at $FAPbI_3$ perovskite quantum dots/metal oxide heterojunctions used for stable perovskite quantum dot solar cells. Nano Energy 67:104267

[156] Suarez B, Gonzalez-Pedro V, Ripolles TS, Sanchez RS, Otero L, Mora-Sero I (2014) Recombination study of

combined halides (Cl, Br, I) perovskite solar cells. J Phys Chem Lett 5(10):1628–1635

[157] Hou Y, Zhang H, Chen W, Chen S, Quiroz COR, Azimi H, Osvet A, Matt GJ, Zeira E, Seuring J, Kausch-Busies N, Lövenich W, Brabec CJ (2015) Inverted, environmentally stable perovskite solar cell with a novel low-cost and water-free PEDOT hole-extraction layer. Adv Energy Mater 5(15):1500543

[158] Xie FX, Zhang D, Su H, Ren X, Wong KS, Grätzel M, Choy WCH (2015) Vacuum-assisted thermal annealing of $CH_3NH_3PbI_3$ for highly stable and efficient perovskite solar cells. ACS Nano 9(1):639–646

[159] You J, Meng L, Song TB, Guo TF, Yang YM, Chang WH, Hong Z, Chen H, Zhou H, Chen Q, Liu Y, De Marco N, Yang Y (2015) Improved air stability of perovskite solar cells via solution-processed metal oxide transport layers. Nat Nanotechnol 11(1):75–81

[160] Berhe TA, Su WN, Chen CH, Pan CJ, Cheng J, Chen HM, Tsai MC, Chen LY, Dubale AA, Hwang BJ (2016) Organometal halide perovskite solar cells: degradation and stability. Energy Environ Sci 9:323–356

[161] Kwon YS, Lim J, Yun HJ, Kim YH, Park T (2014) A diketopyrrolopyrrole-containing hole transporting conjugated polymer for use in efficient stable organic-inorganic hybrid solar cells based on a perovskite. Energy Environ Sci 7(4):1454

[162] Fu Q, Tang X, Huang B, Licheng TH, Chen TL, Chen Y (2018) Recent progress on the long-term stability of perovskite solar cells. Adv Sci 5:1700387

[163] Cao C, Zhang C, Yang J, Sun J, Pang S, Wu H, Wu R, Gao Y, Liu C (2016) Iodine and chlorine element evolution in $CH_3NH_3PbI_{3-x}Cl_x$ thin films for highly efficient planar heterojunction perovskite solar cells. Chem Mater 28:2742–2749

[164] Xiao Z, Bi C, Shao Y, Dong Q, Wang Q, Yuan Y, Wang C, Gao Y, Huang J (2014) Efficient, high yield perovskite photovoltaic devices grown by interdiffusion of solution-processed precursor stacking layer. Energy Environ Sci 8:2619–2623

[165] Li S, Yang B, Wu R, Zhang C, Zhang C, Tang XF, Liu G, Liu P, Zhou C, Gao Y, Meng JQ, Yang J (2016) High-quality $CH_3NH_3PbI_3$ thin film fabricated via intramolecular exchange for efficient planar heterojunction perovskite solar cells. Org Electron 39:304–310

[166] Gong CD et al (2020) Flexible planar heterojunction perovskite solar cells fabricated via sequential roll-to-roll microgravure printing and slot-die coating deposition. Sol RRL 4:1900204

[167] Liu M, Johnston MB, Snaith HJ (2013) Efficient planar heterojunction perovskite solar cells by vapour deposition. Nature 501:395

[168] Eperon GE, Burlakov VM, Docampo P, Goriely A, Snaith HJ (2014) Morphological control for high performance, solution-processed planar heterojunction perovskite solar cells. Adv Funct Mater 24:151

[169] Kim JE, Jung YS, Heo YJ, Hwang K, Qin T, Kim DY, Vak D (2018) Slot die coated planar perovskite solar cells via blowing and heating assisted one step deposition. Sol Energy Mater Sol Cells 179:80–86

[170] Qin T, Huang W, Kim JE, Vak D, Forsyth C, McNeill CR, Cheng YB (2017) Amorphous hole-transporting layer in slot-die coated perovskite solar cells. Nano Energy 31:210–217

[171] Yuan YB, Huang JS (2016) Ion migration in organometal trihalide perovskite and its impact on photovoltaic efficiency and stability. Acc Chem Res 49:286–293

[172] Back H, Kim G, Kim J, Kong J, Kim TK, Kang H, Kim H, Lee J, Lee S, Lee K (2016) Achieving long-term stable perovskite solar cells via ion neutralization. Energy Environ Sci 9:1258–1263

[173] Tan L, Liu C, Huang Z, Zhang Y, Chen L, Chen Y (2017) Self-encapsulated semi-transparent perovskite solar cells with water-soaked stability and metal-free electrode. Org Electron 48:308–313

[174] Krebs FC, Tromholt T, Jørgensen M (2010) A new architecture for printable photovoltaics overcoming conventional module limits. Nanoscale 2:873–886

[175] Kang H, Hong S, Back H, Lee K (2014) A new architecture for printable photovoltaics overcoming conventional module limits. Adv Mater 26:1602–1606

[176] Collins SD, Ran NA, Heiber MC, Nguyen TQ (2017) Small is powerful: recent progress in solution-processed small molecule solar cells. Adv Energy Mater 7(10):1602242

[177] Heo YJ, Jung YS, Hwang K, Kim JE, Yeo JS, Lee S, Jeon YJ, Lee D, Kim DY (2017) Small-molecule organic photovoltaic modules fabricated via halogen-free solvent system with roll-to-roll compatible scalable printing method. ACS Appl Mater Interfaces 9:39519–39525

[178] Anderson TR et al (2014) Scalable, ambient atmosphere roll-to-roll manufacture of encapsulated large area, flexible organic tandem solar cell modules. Energy Environ Sci 7:2925–2933

[179] Stringer MW et al (2019) A flexible back-contact perovskite solar micro-module. Adv Sci 12:1928–1937

[180] Zhang T, Chen Z, Yang D, Wu F, Zhao X, Yang X (2016) Fabricating high performance polymer photovoltaic modules by creating large-scale uniform films. Org Electron 32:126–133

[181] Krebs FC (2009) Polymer solar cell modules prepared using roll-to-roll methods: knife-over-edge coating, slot-die coating and screen printing. Sol Energy Mater Sol Cells 93:465–475

[182] Qiu L et al (2019) Scalable fabrication of metal halide perovskite solar cells and modules. ACS Energy Lett 4(9):2147–2167

[183] Agresti A et al (2019) Two-dimensional material interface engineering for efficient perovskite large-area modules. ACS Energy Lett 4(8):1862–1871

[184] Han GS et al (2019) Spin-coating process for 10 cm × 10 cm perovskite solar modules enabled by self-assembly of SnO_2 nanocolloids. ACS Energy Lett 4(8):1845–1851

[185] Matteocci F et al (2019) Fabrication and morphological characterization of high-efficiency blade-coated perovskite solar modules. ACS Appl Mater Interfaces 11(28):25195–25204

[186] Krebs FC, Jørgensen M (2014) 2D characterization of OPV from single and tandem cells to fully roll-to-roll processed modules with and without electrical contact. Adv Opt Mater 2:465–477

[187] Larsen-Olsen TT, Andersen TR, Dam HF, Jørgensen M, Krebs FC (2015) Probing individual subcells of fully printed and coated polymer tandem solar cells using multichromatic opto-electronic characterization methods. Sol Energy Mater Sol Cells 137:154–163